# NONLINEAR VIBRATION BASED MODELING FOR DAMAGE DETECTION OF REINFORCED CONCRETE BEAMS

MUHAMMAD USMAN HANIF

FACULTY OF ENGINEERING
UNIVERSITY OF MALAYA
KUALA LUMPUR

2018

# NONLINEAR VIBRATION BASED MODELING FOR DAMAGE DETECTION OF REINFORCED CONCRETE BEAMS

MUHAMMAD USMAN HANIF

THESIS SUBMITTED IN FULFILMENT OF THE REQUIREMENTS FOR THE DEGREE OF DOCTOR OF PHILOSOPHY

FACULTY OF ENGINEERING
UNIVERSITY OF MALAYA
KUALA LUMPUR

2018

**UNIVERSITY OF MALAYA**

**ORIGINAL LITERARY WORK DECLARATION**

Name of Candidate: **Muhammad Usman Hanif**

Matric No: **KHA130121**

Name of Degree: **Doctor of Philosophy**

Title of Thesis: **Nonlinear vibration based modeling for damage detection of reinforced concrete beams**

Field of Study: **Structural Engineering and Materials**

I do solemnly and sincerely declare that:

(1) I am the sole author/writer of this Work;
(2) This Work is original;
(3) Any use of any work in which copyright exists was done by way of fair dealing and for permitted purposes and any excerpt or extract from, or reference to or reproduction of any copyright work has been disclosed expressly and sufficiently and the title of the Work and its authorship have been acknowledged in this Work;
(4) I do not have any actual knowledge nor do I ought reasonably to know that the making of this work constitutes an infringement of any copyright work;
(5) I hereby assign all and every rights in the copyright to this Work to the University of Malaya ("UM"), who henceforth shall be owner of the copyright in this Work and that any reproduction or use in any form or by any means whatsoever is prohibited without the written consent of UM having been first had and obtained;
(6) I am fully aware that if in the course of making this Work I have infringed any copyright whether intentionally or otherwise, I may be subject to legal action or any other action as may be determined by UM.

Candidate's Signature Date:

Subscribed and solemnly declared before,

Witness's Signature Date:

Name:

Designation:

# NONLINEAR VIBRATION BASED MODELING FOR DAMAGE DETECTION OF REINFORCED CONCRETE BEAMS


## ABSTRACT

Civil engineering structures, especially the bridge structures, are continuously exposed to dynamic loading, thereby deteriorating before their prescribed design life. The demographics of the civil infrastructure majorly consist of reinforced concrete structures. Out of these existing structures, one-third of these structures are structurally deficient. The conventional damage assessment techniques are time consuming and resource intensive, and cannot cater the current bridge inventory to be monitored. Therefore, the structural health monitoring paradigm in civil engineering is in need of an efficient, economical, generally applicable and a realistic global damage detection method. The research on damage detection methods carried out in the past uses vibration characteristics for damage detection. Most of the work assumes the vibrations to be linear i.e. the natural frequencies of the structures are not dependent on the amplitude of vibration. These methods are efficient and attractive for field testing, but they need the baseline data for structural condition assessment. These baseline data are usually obtained through model updating by calibrating the stiffness to match natural frequency, which ignores the intrinsic nonlinearity of the structures. The aim of this research is to propose a damage detection procedure which incorporates the mechanical behavior of concrete in modeling the nonlinearities in a realistic and efficient way. This study presents a concrete modeling framework using concrete damaged plasticity approach. This modeling framework reproduced the vibration behavior of damaged RC beams. The nonlinear behavior, in the form of nonlinear vibration characteristics, was used in proposing a damage detection algorithm which doesn't rely on the baseline data of the structure. The model was implemented in modeling an RC beam using FE modeling software

ABAQUS. An incremental static loading was applied on the beam in 10 cycles of constant intervals to induce damage up to the ultimate load capacity of the beam. Harmonic excitation was applied on the FE model to obtain changes in modal stiffness and changes in nonlinear behavior by the appearance of super-harmonics in frequency domain. It was found that the change in modal stiffness and the nonlinearity coefficients, obtained from super-harmonics, is more sensitive to damage as compared to the natural frequency reduction. These results were validated experimentally. Furthermore, the nonlinear characteristics were developed and used in proposing a damage detection method which does not rely on the baseline data of the structure. Based on the finite element model, a 3-parameters relation was proposed. The parameters of damage, nonlinearity coefficient and exciting force can be used to detect unknown damage from the known values of the excitation force and the nonlinearity coefficients from the actual structure. Therefore, the proposed methodology presents more realistic structural mechanisms, efficient modeling and sensitive damage detection approach in reinforced concrete structures.

**Keywords:** Nonlinear damage detection, RC beams, Concrete constitutive modeling, plastic damage model, inverse engineering problem.

**PEMODELAN BERASASKAN GETARAN TIDAK LINEAR UNTUK MENGESAN KEROSAKAN BAGI RASUK KONKRIT BERTETULANG**

# ABSTRAK

Struktur-struktur kejuruteraan awam, terutamanya struktur-struktur jambatan, didedahkan secara berterusan kepada beban dinamik, dengan itu ia mengalami kemerosotan sebelum mencapai hayat reka bentuk yang ditetapkan. Demografi bagi infrastruktur awam kebanyakannya terdiri daripada struktur-struktur konkrit bertetulang. Daripada struktur-struktur sedia ada ini, satu pertiga daripada struktur-struktur ini mengalami kerosakan struktur. Teknik pengawasan secara konvensional memerlukan masa yang panjang dan sumber yang banyak dan ianya tidak dapat mengendalikan inventori sedia ada yang sebegitu banyak untuk dipantau. Paradigma pemantauan kesihatan struktur bagi kejuruteraan awam memerlukan kaedah pengesanan kerosakan global yang cekap, ekonomi, terpakai secara amnya dan realistik. Penyelidikan mengenai kaedah pengesanan kerosakan yang dijalankan pada masa lalu menggunakan ciri-ciri getaran untuk pengesanan kerosakan. Kebanyakan kerja ini menganggap getaran adalah linear iaitu frekuensi semula jadi struktur tidak bergantung kepada amplitud getaran. Kaedah-kaedah ini adalah cekap dan menarik untuk ujian lapangan, tetapi ianya memerlukan data garis-asas untuk penilaian keadaan struktur. Data garis-asas ini biasanya diperolehi melalui pengemaskinian model dengan menentukur kekakuan untuk dipadankan dengan frekuensi semula jadi, dimana sifat linear intrinsik bagi struktur di abaikan. Tujuan penyelidikan ini adalah untuk mencadangkan prosedur pengesanan kerosakan yang menggabungkan kelakuan mekanikal konkrit dalam pemodelan bukan linear dengan cara yang realistik dan cekap. Kajian ini menunjukkan rangka kerja pemodelan konkrit menggunakan pendekatan keplastikan konkrit rosak. Rangka kerja pemodelan ini menggabungkan sifat tidak linear dalam mereplikasi perubahan dalam ciri-ciri getaran bagi rasuk RC yang rosak. Ciri-ciri getaran tidak linear ini telah digunakan dalam mencadangkan satu algoritma pengesanan kerosakan yang tidak bergantung pada data garis-asas bagi struktur. Model ini telah digunapakai dalam pemodelan sebuah rasuk RC menggunakan perisian pemodelan FE ABAQUS. Penambahan pembebanan secara statik telah digunakan pada rasuk dalam 10 kitaran secara selang tetap untuk menyebabkan kerosakan sehingga sampai kepada kapasiti beban muktamad bagi rasuk. Daya harmonik dikenakan pada model FE untuk mendapatkan perubahan dalam kekakuan modal dan perubahan dalam kelakuan tak linear dengan kemunculan super-harmonik dalam domain frekuensi. Difahamkan bahawa perubahan kekukuhan modal dan pekali bukan linear, yang diperolehi daripada super-harmonik, lebih sensitif terhadap kerosakan berbanding pengurangan frekuensi semula jadi. Keputusan ini telah disahkan secara eksperimen. Tambahan pula, ciri-ciri tidak linear telah digunakan dalam mencadangkan kaedah pengesanan kerosakan yang tidak bergantung pada data garis-asas struktur. Satu hubungan 3-parameter dicadangkan pada model elemen terhingga. Parameter kerosakan, pekali bukan linear dan daya merangsang boleh digunakan untuk mengesan kerosakan yang tidak diketahui, dari nilai-nilai daya perangsang yang diketahui dan pekali tidak linear dari struktur sebenar. Oleh itu, metodologi yang dicadangkan memberikan tingkah laku struktur yang lebih realistik, pemodelan yang cekap dan pendekatan pengesanan kerosakan yang sensitif dalam struktur konkrit bertetulang.

**Katakunci:** Pengesanan kerosakan bukan linear, rasuk RC, pemodelan konstitutif konkrit, model keplastikan kerosakan, masalah kejuruteraan terbalik.

# ACKNOWLEDGEMENTS

I am thankful to Allah Almighty for blessing me with an opportunity to be worthy of such an honorable degree. I wish to thank my supervisors, Associate Professor Dr. Zainah Ibrahim and Professor Dr. Mohammed Jameel for their unconditional support and believing in me throughout the research.

I would further like to thank Mr. Khaled Ghaedi for helping me in the computational modeling and Mr. Hussain Kazmi and Mr. Atif Ahmed for imparting the concepts of signal processing. I really appreciate help by Mr. Faisal from Invicom for helping me in vibration testing, and Mr. Aszlan and Ms. Bija for helping in translation.

I also would like to thank all the staff of Civil engineering department, especially Mr. Sree, for being helpful. I am thankful Mr. Ahad, Mr. Kashif, Dr. Huzaifa, Mr. Hang, Ms. Lim and Mr. Farooq, for their energetic help in the laboratory testing. It wouldn’t have been possible without their help.

I would further like extend my thanks to my family for staying patient and constantly praying for me (Ammi, Abu, Raisa, Chanda, Munna, Asadullah, Guria). I would further thank UM Rimba (Mr. Benjamin, Ms. Fitrah, and Ms. Vanessa) and Water Warriors (Mr. Affan) for making me feel at home and giving me opportunity in making my leisure time more productive in university activities. I am also thankful to Nowmi, Jubayer, Khaled and his missus, Taher, Sina, Boppy, Chaudhry Saab, Dr. Adenine, Zoe, Huzaifa, Jahangir, Sarmad, Imran and many more for being there. This research would not have been possible without their help.

## TABLE OF CONTENTS

Abstract .....iii

Abstrak ..... v

Acknowledgements .....vii

Table of Contents .....viii

List of Figures .....xiii

List of Tables.....xvii

List of Symbols and Abbreviations.....xviii

List of Appendices .....xxii

**CHAPTER 1: INTRODUCTION ..... 1**

1.1 General..... 1

1.2 Problem Statement..... 3

1.3 Research Objectives..... 4

1.4 Scope of Research..... 4

1.5 Significance of the study ..... 5

1.6 Thesis structure..... 6

**CHAPTER 2: LITERATURE REVIEW ..... 8**

2.1 Introduction..... 8

2.2 Background and importance of study..... 8

2.3 Damage assessment of RC structures ..... 13

2.4 Vibration methods ..... 15

2.4.1 Linear vibrations..... 18

2.4.2 Nonlinear vibrations ..... 24

2.4.2.1 Nonlinearity characterization procedures..... 27

2.5 Concrete constitutive modeling .......... 31
2.5.1 Plasticity approach .......... 32
2.5.2 Multiaxial compressive stress-strain behavior .......... 35
2.5.3 Fictitious crack model .......... 36
2.6 Modeling of cracked beam vibration .......... 38
2.6.1.1 Open crack models .......... 38
2.6.1.2 Breathing crack models .......... 39
2.6.1.3 Nonlinear crack models (Cohesive crack models) .......... 40
2.7 Uncertainties in damage assessment of constructed systems .......... 41
2.7.1 Environmental influences .......... 41
2.7.2 Progressive damage .......... 42
2.7.3 Sensitivity to damage .......... 44
2.7.4 Inverse engineering problem .......... 45
2.8 Summary .......... 47

**CHAPTER 3: IDENTIFYING NONLINEAR BEHAVIOR .......... 49**
3.1 Introduction .......... 49
3.2 Identifying Nonlinear behavior .......... 49
3.3 Nonlinear behavior characterization (Preliminary Study) .......... 51
3.3.1 Description of reference model and material properties .......... 51
3.3.2 Constitutive Law and FE modeling .......... 52
3.3.3 Simulation results .......... 54
3.3.3.1 Load-Deflection results .......... 54
3.3.3.2 Crack propagation .......... 55
3.3.3.3 Modal frequency deterioration .......... 56
3.3.3.4 Linear and Nonlinear dynamic analysis .......... 57

3.4 Initial findings and proceeding further ... 59

**CHAPTER 4: MODELING OF REINFORCED CONCRETE ... 61**

4.1 Introduction plasticity approach ... 61

4.2 Uniaxial constitutive relations ... 62

4.2.1 Concrete in uniaxial compression ... 63

4.2.2 Concrete in uniaxial tension ... 67

4.2.3 Reinforcing Steel ... 71

4.3 Concrete damaged plasticity model (CDPM) ... 72

4.3.1 The plasticity Theory ... 72

4.3.2 Yield Function ... 73

4.3.3 Hardening rule ... 76

4.3.4 Flow rule ... 77

4.3.5 Continuum damage mechanics (CDM) ... 78

4.4 Calibration of CDPM ... 80

4.4.1 Compressive constitutive relations (Carreira's model) ... 80

4.4.2 Tensile constitutive relations (fictitious crack model) ... 81

4.4.3 Dilation angle ($\psi$) ... 82

4.4.4 Flow potential eccentricity ($\epsilon$) ... 85

4.4.5 Initial equi-biaxial compressive yield stress to initial uniaxial compressive yield stress ratio ($f_{b0}/f_{c0}$) ... 85

4.4.6 Ratio of the second stress invariant on the tensile meridian to that on the compressive meridian ($K_c$) ... 85

4.4.7 Viscosity parameter or Relaxation time ($\mu$) ... 86

4.5 Model comparison with the past research ... 86

4.5.1 Uniaxial cyclic response ... 87

4.5.2 Biaxial stress-strain response ........ 88

4.6 Summary ........ 91

**CHAPTER 5: IMPLEMENTATION OF MODEL ........ 93**

5.1 Finite Element Modeling of RC beams ........ 95

5.1.1 Solution procedures ........ 98

5.1.1.1 Solution procedure for static loading ........ 98

5.1.1.2 Solution procedure for dynamic loading ........ 100

5.1.2 Steps for FE analysis ........ 103

5.2 Experimental Investigation ........ 104

5.2.1 Casting of Beam specimens ........ 104

5.2.2 Test setup ........ 107

5.2.2.1 Static Testing ........ 108

5.2.2.2 Dynamic Testing ........ 109

5.3 Summary ........ 113

**CHAPTER 6: RESULTS AND DISCUSSION ........ 115**

6.1 Overview ........ 115

6.2 Environmental influences ........ 115

6.3 Static Response ........ 117

6.3.1 Load-Deflection Response ........ 117

6.3.2 Crack Formation ........ 118

6.4 Dynamic Response ........ 121

6.4.1 Modal analysis ........ 121

6.4.2 Restoring Force surfaces ........ 126

6.4.3 Formation of Super-harmonics ........ 129

6.5 Baseline for damage detection .......... 133

**CHAPTER 7: CONCLUSIONS .......... 142**

7.1 Summary of the work .......... 142

7.2 Conclusions drawn .......... 142

7.3 Recommendation for future research .......... 144

References .......... 146

List of Publications and Papers Presented .......... 162

Appendices .......... 163

## LIST OF FIGURES

Figure 2.1: Types of cracking in RC bridges (Transport and Main Roads, 2016) .......... 13

Figure 2.2: General model updating scheme (Cao et al., 2013) .......... 17

Figure 2.3: Frequency response of cracked and un-cracked bar (Hiwarkar, 2010) .......... 27

Figure 2.4: Superharmonics at different exciting frequencies (Nandi & Neogy, 2002) . 28

Figure 2.5: Restoring force-modal displacement curves (Hamad et al., 2011a) .......... 31

Figure 2.6: Comparison of linear and non-linear unloading (Andriotis et al., 2016) ..... 34

Figure 2.7: Hierarchy of various fracture models of concrete (Elices & Planas, 1996) . 37

Figure 2.8: Bilinear breathing crack model (Chondros et al., 2001) .......... 39

Figure 2.9: Natural frequency degradation with damage for past research .......... 45

Figure 2.10: Components of plastic damage model (CDPM) .......... 47

Figure 3.1: Summary of preliminary methodology for identifying nonlinear behavior . 50

Figure 3.2: Reference test setup for detecting nonlinearities (Hamad et al., 2015) .......... 52

Figure 3.3: Constitutive relations using CDPM (Aslani & Jowkarmeimandi, 2012) ..... 53

Figure 3.4: Flow chart for finite element simulation for detecting nonlinear behavior .. 54

Figure 3.5: Static load-deflection plot comparison with Hamad et al., (2015) .......... 55

Figure 3.6: Comparison of cracking (below) with Hamad et al., (2015), (above) .......... 56

Figure 3.7: Reduction in normalized frequency against the percentage of damage ....... 57

Figure 3.8: Comparison of response to harmonic analysis (a) linear (b) non-linear ....... 58

Figure 3.9: Nonlinear trend (super-harmonics) against damage .......... 59

Figure 3.10: Summary of steps involved in proposing damage assessment method ...... 60

Figure 4.1: Plastic and damage behavior of concrete (Tao & Phillips, 2005) .......... 62

Figure 4.2: Parts of uniaxial compressive stress-strain curve .......... 63

Figure 4.3: Complete stress strain curves, reproduced from (Wischers, 1978) .......... 64

Figure 4.4: Experimental compressive stress-strain curves (peak picking method) ....... 64

Figure 4.5: Concrete compressive stress-strain models ................................................ 66

Figure 4.6: Carreira & Chu (1985) model comparison with experimental data ............ 67

Figure 4.7: Cracks in interfacial transition zone (ITZ) (Nemati & Monteiro, 1997) ...... 68

Figure 4.8: Tensile stress-displacement relation .......................................................... 69

Figure 4.9: Tensile stress ($f_{ct}$) vs crack width *(w)* Relationship, from Hordijk (1991) ... 70

Figure 4.10: Stress-strain cyclic response of reinforcing steel ...................................... 71

Figure 4.11: Schematic yield surfaces, from Chen (2007) ............................................ 74

Figure 4.12: Hardening models in biaxial stress field (Zait et al., 2010) ........................ 76

Figure 4.13: Example of yield criteria (CDPM) in the meridional (p-q) plane ............. 78

Figure 4.14: (a) Simulated Cylinder (b) selected elements for stress-strain behavior .... 84

Figure 4.15: Effect of dilation angle ($\psi$) on stress-strain relation of concrete ............... 85

Figure 4.16: Effect of viscosity parameter ($\mu$) on stress-strain relation of concrete ....... 86

Figure 4.17: Comparison of proposed model in cyclic compression with test data ....... 87

Figure 4.18: Comparison of proposed model in cyclic tension with test data ............... 88

Figure 4.19: FE model for studying biaxial behavior (82.6x82.6mm$^2$) ......................... 89

Figure 4.20: Model comparison with biaxial compression tests (Kupfer et al., 1969) ... 90

Figure 4.21: Model comparison with compression-tension tests (Kupfer et al., 1969) .. 90

Figure 4.22: Model comparison with Biaxial tension tests (Kupfer et al., 1969) ........... 91

Figure 5.1: Detailed Flow chart of the methodology .................................................... 94

Figure 5.2: Design of RC Beam for investigation (all units are in mm) ........................ 95

Figure 5.3: Different Mesh sizes for sensitivity analysis .............................................. 97

Figure 5.4: Load-Deflection Comparison for different meshing sizes .......................... 97

Figure 5.5: Beam sketch for computational Model (25mm mesh size) ......................... 98

Figure 5.6: Linear perturbation procedure explained (Dassault Systèmes, 2013) ........ 100

Figure 5.7: Preparation of reinforcing steel ........ 106

Figure 5.8: Fixing of strain gauges on rebars ........ 106

Figure 5.9: Casting of RC beam specimens ........ 106

Figure 5.10: Normalized average compressive strength during the testing regime ...... 107

Figure 5.11: Beam test setup for static and dynamic testing ........ 108

Figure 5.12: Incremental Static loading profile for beam testing ........ 109

Figure 5.13: Modal testing equipment ........ 110

Figure 5.14: Schematic diagram of impact hammer testing ........ 111

Figure 5.15: Schematic diagram of harmonic excitation test setup ........ 111

Figure 5.16: Non-linear vibration testing equipment ........ 112

Figure 5.17: Schematic diagram of harmonic excitation testing procedure ........ 113

Figure 6.1: Environmental effects (a) temperature (b) relative humidity ........ 116

Figure 6.2: Experimental and computation load-deflection response of 5 cycles ........ 117

Figure 6.3: Monotonic Load-deflection response (peak picking) ........ 118

Figure 6.4: Crack formation comparison of simulation and experimental setup ........ 119

Figure 6.5: Comparison of Load and average crack height ........ 120

Figure 6.6: Experimental evolution of Crack widths with increasing load ........ 121

Figure 6.7: Typical response of Impact hammer test at location IHL3 ........ 122

Figure 6.8: Computational (left) and Experimental (right) mode shapes ........ 123

Figure 6.9: Experimental and computational values of first four modal frequencies ... 124

Figure 6.10: Normalized frequency degradation for first four modes ........ 124

Figure 6.11: Natural frequency comparison with damage and crack height ........ 125

Figure 6.12: Typical response of the beam to a harmonic excitation ........ 126

Figure 6.13: Curve fit for restoring force vs displacement plot .................................. 127

Figure 6.14: Restoring force vs displacement (response) at different damage levels... 128

Figure 6.15: Simulated modal stiffness response to damage ....................................... 128

Figure 6.16: (a) Formation of super-harmonics at 150N force, (b) magnified view .... 130

Figure 6.17: (a) Formation of super-harmonics at 300N force, (b) magnified view .... 130

Figure 6.18: (a) Formation of super-harmonics at 750N force, (b) magnified view .... 131

Figure 6.19: (a) Formation of super-harmonics at 1500N force, (b) magnified view .. 131

Figure 6.20: Experimental Super-harmonics at different damage levels ...................... 132

Figure 6.21: Effect of damage on nonlinearity coefficient (Simulation) ...................... 133

Figure 6.22: Effect of damage on nonlinearity coefficient (Experiment) ..................... 134

Figure 6.23: Waterfall plot of the simulated parameters ............................................. 135

Figure 6.24: Interpolated surface for known parameters from simulation .................... 135

Figure 6.25: Calculating the unknown value from other two unknown values ............ 136

Figure 6.26: Interpolated surface values for data from Hamad et al. (2015) ................ 138

Figure 6.27: Predicted excitation force (2N) from Hamad et al. (2015) ....................... 139

# LIST OF TABLES

Table 2.1: Design service life specified by different design codes .................................. 9

Table 2.2: Demographics of existing bridge inventory .................................................. 11

Table 2.3: Summary of damage assessment for constructed systems for last 3 decades 20

Table 2.4: Investigations on modeling techniques with nonlinear behavior .................. 25

Table 3.1: Mechanical properties of concrete (Hamad et al., 2015) ............................... 51

Table 3.2: Mechanical properties of steel reinforcement (Hamad et al., 2015) ............. 52

Table 4.1: Summary of usage of $\psi$ in different studies .................................................. 83

Table 4.2: Biaxial data from Kupfer et al., (1969) ........................................................ 89

Table 5.1: Experimental mechanical properties of concrete .......................................... 96

Table 5.2: Calculated mechanical properties of concrete for FE modeling .................... 96

Table 5.3: Properties of Ready-mix concrete ............................................................... 105

Table 6.1: Estimation of excitation force ..................................................................... 136

Table 6.2: Estimated excitation force from Hamad et al. (2015) ................................. 140

## LIST OF SYMBOLS AND ABBREVIATIONS

| | | |
|---|---|---|
| $C1, C2$ | : | Coefficients in fictitious crack model equation |
| $E_o$ | : | Initial modulus of elasticity of concrete |
| $E_{it}$ | : | Initial Tangent modulus of concrete |
| $E_{cm}$ | : | Modulus of elasticity of concrete |
| $F$ | : | Generalized yield function |
| $F(t)$ | : | Excitation force |
| $G_{ch}$ | : | Crushing energy per unit area |
| $G_F$ | : | Fracture energy per unit area |
| $G_{ij}$ | : | Function for stresses or hardening parameters |
| $I_1$ | : | First effective stress invariant |
| $K_c$ | : | Ratio of second stress invariant in tensile meridian to that of compressive meridian |
| | | |
| $a_c, a_t$ | : | Dimensionless coefficients for damage variable calculation |
| $b_c, b_t$ | | |
| $c$ | : | Damping |
| $d_c, d_t$ | : | Damage variables for compression and tension |
| $f_{bo}/f_{co}$ | : | Ration of biaxial compressive yield stress to uniaxial compressive yield stress |
| $f_{cm}$ | : | Mean value of concrete cylinder compressive strength |
| $f_{co}, f_{to}$ | : | Uniaxial yield stress in compression and tension |
| $f_{ctm}$ | : | Mean value of axial tensile strength of concrete |
| $f_{ctm1}, f_{ctm2}$ | : | Tensile strength in orthogonal principal directions |
| $f_{cu}$ | : | Ultimate compressive strength |

| | | |
|---|---|---|
| $g$ | : | Plastic potential function |
| $k$ | : | stiffness |
| $k_1$, $k_2$ | : | Correction factors for coarse aggregates and mineral admixtures |
| $l_{eq}$ | : | Characteristic length or mesh size |
| $p$ | : | Effective hydrostatic pressure |
| $q$ | : | Von Mises equivalent effective stress |
| $s_{ij}$ | : | Principal deviatoric stresses |
| $\bar{s}$ | : | Effective stress deviator |
| $w$ | : | Crack width |
| $w_c$ | : | Critical crack width |

| | | |
|---|---|---|
| $\alpha$, $\beta$, $\gamma$ | : | Dimensionless constants in yield function |
| $\beta_c$ | : | Parameter for shape of stress-strain curve in compression |
| $\varepsilon_c$ | : | Total strain |
| $\varepsilon_{co}$ | : | Elastic strain |
| $\varepsilon_c^{pl}\varepsilon_t^{pl}$ | : | Plastic compressive strain, plastic tensile strain |
| $\varepsilon_c^{in}\varepsilon_t^{in}$ | : | Inelastic compressive strain, cracking strain |
| $\varepsilon_t, \varepsilon_{ctm}$ | : | Equivalent tensile strain, maximum tensile strain |
| $d\varepsilon^{el}$ | : | Elastic incremental strain |
| $d\varepsilon^{pl}$ | : | Plastic incremental strain |
| $\epsilon$ | : | Flow potential eccentricity |
| $\mu$ | : | Viscosity parameter or relaxation time |
| $\rho_c$ | : | Density of concrete |
| $\sigma_1$, $\sigma_2$ | : | Stress point components on yield curve |
| $\sigma_c$ | : | Yield value in compression |

| | | |
|---|---|---|
| $\sigma_t$ | | Yield value in tension |
| $\bar{\sigma}_c$, $\bar{\sigma}_t$ | : | Effective cohesive stresses in compression and tension |
| $\sigma_{t1}$, $\sigma_{t2}$ | : | Yield values in tension in respective orthogonal principal directions |
| $\sigma_{max}$ | | Maximum principal effective stresss |
| $\bar{\sigma}$ | : | Effective stresses |
| $\psi$ | : | Dilation angle |
| | | |
| *AV* | : | Ambient vibrations |
| *CDM* | : | Continuum Mechanics Damage |
| *CDPM* | : | Concrete damaged plasticity model |
| *CMOD* | : | Crack mouth opening displacement |
| *CSA* | : | Cement Sand Aggregate ratio |
| *CWT* | : | Continuous Wavelet Transform |
| *CZM* | : | Cohesive Zone Model |
| *DFT* | : | Discrete Fourier Transform |
| *DIC* | : | Digital Image Correlation |
| *DWT* | : | Discrete Wavelet Transform |
| *EMA* | : | Experimental Modal Analysis |
| *FC* | : | Forced vibrations |
| *FCM* | : | Fictitious Crack Model |
| *FFT* | : | Fast Fourier Transform |
| *FR* | : | Free vibrations |
| *IH* | : | Impact hammer |
| *IHL* | : | Impact hammer location (marked on the top of beam) |
| *LEFM* | : | Linear elastic fracture mechanics |
| *MDOF* | : | Multi degree of freedom |

| | | |
|---|---|---|
| *MU* | : | Model updating |
| *NLEFM* | : | Nonlinear elastic fracture mechanics |
| *PSD* | : | Power spectral density |
| *RC* | : | Reinforced concrete |
| *RSF* | : | Restoring force surfaces |
| *SDOF* | : | Single degree of freedom |
| *SHM* | : | Structural health monitoring |
| *SL* | : | Static loading |
| *St* | : | Structural Steel |
| *w/c* | : | Water to cement ratio |

# LIST OF APPENDICES

Appendix A: Computational and experimental crack formation ………………. 164

Appendix B: Crack width measurements…………..…………………………… 168

Appendix C: MATLAB code for estimating damage…………………………… 170

# CHAPTER 1: INTRODUCTION

## 1.1 General

Structures, in general, are designed as a combination of simpler members - beams responsible for the lateral forces and columns catering the axial forces. These structural members are designed based on the procedures developed from mechanical properties of materials. The most commonly used construction materials are structural steel and reinforced concrete (RC). RC construction is more popular because of easier availability of materials, convenient construction, stability and more serviceable life. RC design is a combination of concrete and reinforcing steel, with their capabilities utilized in compression and tension, respectively. RC construction is a preferred construction to date because of the advantages of strength, stability and serviceability.

Existing RC structures, especially bridges, are deteriorating before their specified design life. The reasons are environmental effects, unprecedented seismic activity or changes in the loading conditions – like the increase in density of traffic with the course of time. Due to these effects, structures are degrading before their serviceability life. It may be a general statement, but steel structures are easy to repair, the members can be replaced. However, damage in RC structures is a complex problem. Therefore, it is desirable to have a generally applicable damage detection procedure that can give information about current condition of the structure while it is in serviceable state. The branch of engineering, which deals with damage detection and condition assessment, is termed as structural health monitoring. For structural health monitoring of civil infrastructure, the structures are monitored through visual inspections initially. If there are indications of damage, the subsequent damage detection methods are either specifically designed for particular structure or they are localized methods which require the damaged location known prior to employing damage detection technique.

For existing infrastructure, the existing demographics show that 41 percent of the bridges in US bridge inventory, 50 percent in UK and 88 percent of the bridges in Malaysia are reinforced concrete bridges (King, 1999; Neild, 2001; Transport and Main Roads, 2016). And with this immense infrastructure available, the damage detection method is expected to be generally applicable, not reliant on the data from undamaged structure (baseline data) and exhibit the damage mechanisms of the structures replicable by the model (phenomenological models). While efforts have been made by the respective transportation departments to document the current condition of the bridges, it is biggest challenge in coming up with a generalized, globally applicable health monitoring procedure to be useful in the diverse inventory of the existing infrastructure. Vibration methods are attractive because of their convenience in field testing and ability to produce global response of the structure with a few key measurements. The models which reproduce the vibration characteristics of the structures are being researched for almost half a century.

Vibration methods have been popular most methods in structural health monitoring. With the aid of a few measuring devices, the response of the structure can be estimated. This convenience in taking field measurements suits well with the solution requirement of the structural health monitoring problem in civil infrastructure. While a significant effort has been put into studying these methods, they have not been successfully implemented in damage detection of RC structures. Most of these investigations assume the vibrations to be linear i.e. there is no effect of the amplitude of vibration on the response of the structure. Resultantly, the nonlinear behavior of the model is ignored. Furthermore, the cracked structure vibrations are modeled as open or breathing crack models which lack the inherent transition between crack opening and closing during the vibration cycle. Also, the baseline data of the structure are obtained using model updating which involves calibration of local stiffness reduction. There are key studies which suggest that the damage detection using natural frequency degradation is not sensitive and can be influenced by the environmental conditions. The nonlinear behavior, concrete law and a more understanding of cracked concrete vibrations need to be incorporated in the damage detection mechanisms.

## 1.2 Problem Statement

As mentioned before, linearization of the model ignores the inherent nonlinear behavior of concrete. The cracked vibrations are modeled as open or breathing crack models which do not represent the inherent nonlinear behavior in concrete. The nonlinear behavior of concrete needs to be incorporated in modeling the dynamic behavior of cracked concrete.

The damage modeling involves local stiffness reduction, which represents the formation of a crack. Plasticity approach combined with fracture mechanics represent the concrete damage more realistically. Despite their versatility in phenomenological representation of concrete behavior, these approaches have not been investigated in reproducing the nonlinear behavior of concrete.

Another problem is the inverse problem solving which is, not relying on the baseline data of the structure while detecting damage. The baseline data are the data that give information about the structure in its intact or undamaged state. To obtain these data, numerous model-updating schemes are incorporated to identify the system using model updating. The use of local stiffness reduction for damage representation leads to a ‘grey system’ which has partial knowledge of some of the parameters. The modal methods, which incorporate the grey system, are not sensitive enough to simply deploy in the field testing. The environmental effects may drastically influence the behavior of the structure. Therefore, a methodology with least possible dependence on the baseline data, is required to be adopted in structural health monitoring of RC structures.

As the inventory of civil infrastructure available is immense, a generally applicable, global damage detection technique is required for damage detection in RC structures, which utilizes the damage mechanisms of concrete more precisely and can act as a baseline for the nonlinear methods in structural health monitoring.

## 1.3 Research Objectives

The aim of this research is to produce a model which is capable of replicating the mechanical behavior of concrete and reasonably reproduces the nonlinear vibration behavior.

To achieve the aim of this research, following are the objectives proposed in this study:

1. To develop a concrete model based on plasticity and fracture mechanics approaches which represents the mechanical behavior of concrete more accurately in cyclic and multiaxial stress states.
2. To implement the concrete model in modeling reinforced concrete beam and simulate the vibration behavior of cracked RC beams.
3. To evaluate the sensitivity of nonlinear vibration behavior as compared to the conventional linear vibration methods.
4. Experimentally validate the presented model with vibrational response of reinforced concrete beams.
5. To propose a damage detection method which utilizes nonlinear characteristics and does not rely on baseline data of the structure.

## 1.4 Scope of Research

This study is based on developing a constitutive model and implementing it in modeling of an RC beam. The damage will be introduced incrementally and, after each damage increment, nonlinear behavior will be evaluated simulating the harmonic excitation. The nonlinear behavior will be then characterized to propose a damage assessment method without depending on baseline data. The investigation is limited to normal strength, simply supported RC beams targeting the simply supported beam-type or slab-type RC bridges. The effects of steel-concrete bond are not considered because the investigation is focused on the initial stages of damage and crack formation is under consideration. The modal analysis will be carried out only for the sake of comparison purposes with the nonlinear method proposed. Prestressing effects, time-dependent damage (fatigue) phenomenon have not been taken into account in this research. The major focus is on using convenient constitutive laws for damage assessment while eliminating the baseline data using this research. The practical aspects have also been taken into account by considering only a few input parameters for constitutive modeling.

## 1.5 Significance of the study

Structural health monitoring in civil infrastructure, especially reinforced concrete structures, has not successfully gained its grounds even after half a century. This research is aimed at modeling the mechanical behavior of concrete in a way that the vibration behavior of damaged (cracked) concrete is more accurately represented. Phenomenological model of concrete will be developed that would represent the multiaxial and cyclic behavior quite accurately. This phenomenological model will be further used in FE model of RC beam, which will be later simulated with damage. The dynamic system will be investigated with possible response of nonlinearities with increasing damage. Resultantly, it will be possible to model reinforced concrete structures using material strength indices from routine laboratory tests, and then simulating the dynamic behavior of the structure to identify the presence of non-linearities from undamaged state to complete failure.

The sensitivity of nonlinear procedures is more as compared to linear procedures. The nonlinear procedures may need optimization to be computationally efficient but their sensitivity is more to damage and less influenced by the environmental factors. Therefore, a comparison of linear and nonlinear methods will be made in terms of sensitivity, which will give the reason for the importance of nonlinear procedures.

The SHM paradigm faces the biggest challenge of using 'grey system' to estimate baseline data of the structure, which is not reliable and sensitive enough to be deployed in damage detection of concrete structures. This will be addressed by characterizing the nonlinear behavior to assess damage. Simulating progressive damage gives a better understanding of the anticipated failure. This will help in eliminating the identification of system based on the baseline data. The damage detection algorithms proposed will be used for optimizing the method for generalized application in beam-type structures. This study can be one of the baseline studies for a generally applicable, convenient and global damage detection method in reinforced concrete structures.

## 1.6 Thesis structure

Chapter 1 gives introduction to the existing civil infrastructure and the problems faced in detecting damage to the immense inventory of structures. The problem has been identified and scope of the research has been explained. Chapter 2 gives a comprehensive review of literature to date about the existing techniques for damage detection in civil engineering structures. Linear and non-linear damage detection techniques are discussed and the importance of non-linear damage detection techniques is discussed in the conclusion. Chapter 3 presents the preliminary study carried out to detect non-linear behavior with increase in damage of reinforced concrete beams. The test data are used from previous research for comparison. Chapter 4 gives a detailed account on the material modeling using plastic damage model with the calibration of the parameters used in model. Chapter 5 gives the implementation of the model on a reinforced concrete beam to reproduce the nonlinear behavior computationally, which is also validated experimentally. Chapter 6 gives the discussion on the simulation and the experiment performed on RC beams. Finally, conclusions of this study and the future direction of this research have been presented in Chapter 7.

# CHAPTER 2: LITERATURE REVIEW

## 2.1 Introduction

Structural health monitoring is gaining more and more importance with innovations in design procedures in civil engineering structures. Reinforced concrete construction is getting more popular day by day and the civil infrastructure is expanding rapidly. However, a reliable health monitoring technique for RC structures has still not surfaced yet. A review on the current condition of existing infrastructure, the currently employed damage detection approaches, their implications and the possible solution to them, has been presented in this chapter. The modeling framework of concretes, especially the crack modeling plays an important role in modeling the dynamic behavior of the concrete structures. Based on the current literature, a specific modeling framework of reinforced concrete was necessitated as a result of the constraints in application of SHM applications of RC structures.

## 2.2 Background and importance of study

Among the construction materials, reinforced concrete is the most popular construction material. It is the mostly used man-made construction material in the world and the its use in construction goes back to centuries (Lomborg, 2003). Reinforced concrete (RC) structures are comparatively more economical, stable, serviceable and durable. However, these structures are constantly exposed to environmental loads such as weather fluctuations, wind loads, temperature gradients, seismic activity, increase in traffic frequency as well as man-made hazards and are deteriorating before their intended design life (Yun et al., 2003) . The main reasons for the deterioration of structures are due to the existence of outdated design codes, environmental changes, increasing service loads, and the unpredictable nature of natural hazards. For instance, a bridge that was serviceable decades ago may not be serviceable due to the increase in the frequency of traffic, or an earthquake of significantly higher magnitude than the historical data may necessitate a review of the seismic design procedures for the structural design. The service life of the reinforced concrete structures during design phase is specified to be from 50 to 100 years (Table 2.1). The serviceability of a structure in any condition relies on its structural health which is obtained by structural health monitoring (SHM) practices**.** The SHM of a system requires an understanding of the failure mechanisms and system identification. The major goal of the SHM research is to assess the condition of the structure with least human effort and trigger a timely warning when the structural condition goes beyond serviceability limits. Recently researched SHM advancements include automation, real-time and online monitoring practices (Chae et al., 2012).

**Table 2.1:** Design service life specified by different design codes

| Code | Reference | Service Life |
|---|---|---|
| **EN 1992-1-1 (2004)** | EN 1990: Basics of structural design | 50 years for common structures<br><br>100 years for monumental structures |
| **AASHTO (2010)** | AASHTO LRFD Bridge design specifications | 75 years |
| **ACI 318-14** | ACI 318-14, Building code requirements for structural concrete | Not specified |

Structural health monitoring has achieved vital success in structural steel bridges in terms of automation and online monitoring (Chae et al., 2012; Follen et al., 2014). In reinforced concrete (RC) bridges, the SHM paradigm is still in developing stages. Currently, structural condition assessment involves most commonly of biennial to quinquennial inspection by technical staff who use visual aids and crack recordings, which requires lot of financial and human resources. Usually, a consultancy firm is hired to do the inspection, detailed analysis and then produce a report, based on which rehabilitation measures are suggested if the structure is damaged (Hartle et al., 1995; Hearn, 2007). This consumes a lot of resources in terms of time and finances, and is not adequate for the extent of unmonitored infrastructure present.

The demographics of Europe, US, Asia regions have been collected from different resources and tabulated in Table 2.2 (Daly, 2000; FHWA, 2013; Fujino & Siringoringo, 2008; Geiger et al., 2005; Global Times, 2017; King, 1999; Neild, 2001). From the demographics, on average, 76% of the bridges are RC bridges which mostly include small scale beam or slab-type bridges. 34% of the bridges are structurally deficient, which constitutes a major figure in the total infrastructure. Countries like Finland, Germany, Japan and Malaysia, had bridge construction boom in 1970's, and this immensely constructed infrastructure will soon be reaching the designated serviceability life in the next few years. Either reaching design life or becoming structurally deficient, this immense infrastructure needs to be assessed for possible damage, which requires general applicability, efficiency, economy and reliability. The conventional inspection methods are not efficient enough to cater this immense inventory of structures to monitor, although a rigorous work has been carried out for last half century in developing SHM procedures for RC structures.

For an accurate modeling of concrete structures, the mechanical behavior of concrete needs to be accurate representation of the structure. The mechanical properties of concrete have not been completely understood yet. Different phenomenological models have been developed which replicate the behavior of concrete for different loading conditions, and are based on calibrating the analytical expressions with the experimental data. Although these models do not explain the mechanisms involved at microscopic level, but they are popular in engineering applications because of their simplicity. The phenomenological models of plasticity theory (Lubliner, 2008), continuum damage mechanics model

(Kachanov, 1958) and fracture mechanics (Hillerborg et al., 1976) provide an adequate understanding of the macroscopic behavior of concrete. In contrast to that, the models which attempt to explore the mechanisms involved microscopically are sophisticated and computationally intensive, and cannot be generally applicable to complex structures.

**Table 2.2:** Demographics of existing bridge inventory

| Country | Inventory Bridges | Deficient (%) | Type (%) | | |
|---|---|---|---|---|---|
| | | | RC | Steel | Other |
| Canada (Alberta) | 3,870 | - | - | - | - |
| China | 805,300 | - | - | - | - |
| Denmark | 1,315 | - | 73 | 25 | 2 |
| Finland | 20,000 | - | 78 | 19 | 3 |
| France | 236,000 | 47 | - | - | - |
| Germany | 71,926 | 42 | - | - | - |
| Japan | 155,159 | 15 | - | - | - |
| Malaysia | 6,647 | 15 | 88 | 9 | 3 |
| New Zealand | 26,000 | - | - | - | - |
| Norway | 21,500 | 42 | 70 | 29 | 1 |
| Slovenia | - | 15 | - | - | - |
| South Africa | 21,000 | - | - | - | - |
| Sweden | 24,000 | - | 72 | 22 | 6 |
| Switzerland | 3,380 | - | - | - | - |
| United Kingdom | 155,000 | 30 | 80 | 15 | 5 |
| United States | 591,707 | 28 | 61 | 33 | 6 |

For structural health monitoring there are various methods for damage identification. Vibration methods are the most attractive due to convenience in field applications. Complete global response of a structure from a few measurement and capability to analyze the ambient excitation are the major factors for them being the ideal case scenario for field data retrieval. While a lot of effort has been put into developing these methods, the modeling of cracked vibration has not been successfully deployed in damage detection of RC structures because the vibrations are assumed to be linear. In contrast to this assumption, a realistic cracked beam model can lead to modeling the nonlinear behavior of cracked concrete.

The damage detection by natural frequency degradation is a popular method for damage detection. The natural frequencies for a structure are obtained through free vibrations. To obtain the baseline data, computational models are used, stiffness degradation is incorporated or a discrete spring is modeled as a crack. The model is then calibrated by comparing the stiffness to identify the condition of the structure. The information about the structure in its undamaged state is called the baseline data of the structure. The systems which use the baseline data obtained from the natural frequencies are called grey systems, which are reliant on the baseline data obtained from model updating (Dharmaraju et al., 2004). This is the major constraint in the deploying of these methods in SHM procedures in RC infrastructure.

In ideal case scenario, the stiffness of the structures drops with the increase in damage, resulting in the drop of natural frequencies. But while applying this on full scale specimens, the natural frequencies are influenced by the environmental factors and support conditions, and the drop in natural frequency may not be necessary. Therefore, these methods may not be accurately applicable when deployed in field measurements. Based on the above discussion, following are the key constraints in successful implementation of the linear vibration methods in RC structures.

1. Efficiency (model updating is an iterative process)
2. Economy (every investigation is a unique case study, and not economical)
3. Uniqueness (Every structure is designed unique)
4. Sensitivity (environmental influences may influence the sensitivity)
5. Inverse engineering problem (baseline data are based on the model updating)

If not all, the constraints of sensitivity, proper material modeling and baseline data need to be addressed first. For material modeling to be applicable, the term damage needs to be defined based on the literature.

## 2.3 Damage assessment of RC structures

RC structures are more durable and they have better service life; but once damaged, the repairing procedures are more complex as compared to the other construction materials. A damage once done, is not easily repairable by replacing a structural member. Damage in RC structures is caused by many factors such as extreme weather fluctuations, chemical reactions, crack formations, cold joint crack propagations, overloads, human-induced accidents and poor construction practices. Damage in concrete is indicated by the appearance of cracks and excessive deflections. The crack formation due to many reasons can be seen in Figure 2.1.

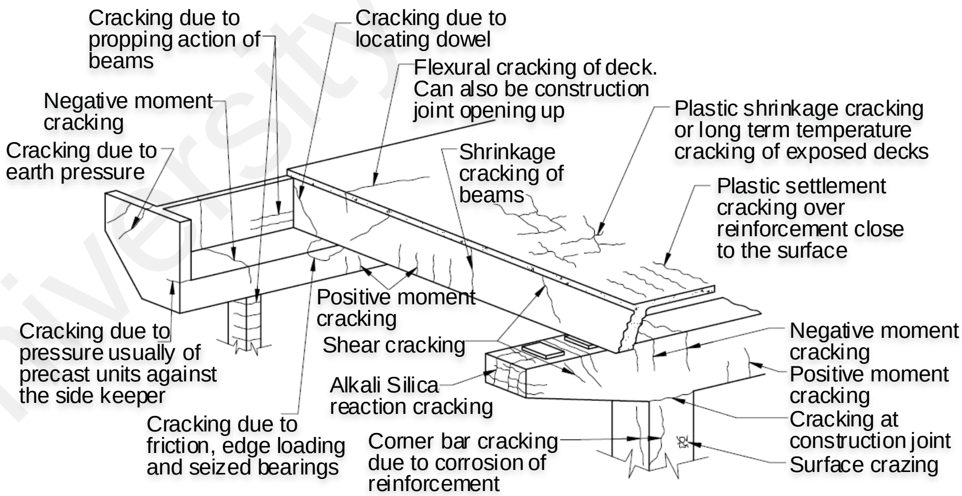


**Figure 2.1:** Types of cracking in RC bridges (Transport and Main Roads, 2016)

In most of the cases, the damage starts by initiation of cracks, which propagate further by the action of repetitive loading until the collapse. Damage, in general, is defined as the condition of the structure when it is not operating in its ideal condition but still is serviceable. A fault on the other hand is the state when it is no longer serviceable, and a defect is inconsistency in the material. A damaged stage is the stage where the problem in the structure is intended to be detected so that it could be taken care of before the occurrence of fault (Worden & Dulieu-Barton, 2004).

The damage in reinforced concrete structures is usually the measure of stiffness, which reduces when the structure gets deteriorated. It is used as a relative term for measuring the degradation in the stiffness. It has been used by various researchers as a measure of reduction in modal frequency (Cawley & Adams, 1979; Doebling et al., 1998; Farrar & Doebling, 1997; Lee & Shin, 2002). Crack formation is a good visual indication of initiation of damage. The cracks can be hairline (<0.1mm), minor (0.1-0.3mm), moderate (0.3-0.6mm) or severe (>0.6mm), with only crack size greater than 0.2mm visible to naked eye. The incremental damage or progressive damage, has also been used to investigate the RC beams (Hamad et al., 2015; Neild, 2001; Shah & Ribakov, 2009; Benedetti et al., 2018). Using the incremental damage in investigating RC beams can be used to validate the constitutive law of the modeling method. Furthermore, the crack growth and different damage indicators can be studied in relation with the damage.

Structural health monitoring of civil engineering structures comprises of various methods for damage detection like, visual inspection, eddy current, acoustic emission, ultrasonic, magnetic particle, radiography, magnetic particle and vibration methods (Farrar & Worden, 2007; Kim et al., 2007; Li et al., 2014; Moreu et al., 2012; Rytter, 1993; Sohn et al., 2001; Worden et al., 2007). Visual inspections are the biennial inspections adopted in currently applied conventional monitoring methods. The damage detection algorithms used currently have their own advantages for different situations. The eddy current technique uses the generation of magnetic field from alternating current, which in case of damage, causes change in eddy current. The technique is simple but utilizes large power and complicated data. Ultrasonic techniques use high frequency sound waves for damage detection. Nonlinear ultrasonic techniques are said to be more effective than the linear ones (Kim et al., 2017; Zaitsev et al., 2006). The acoustic emission damage detection technique has good prospects in online damage detection (Carpinteri et al., 2007), but the signals being weak, can easily be influenced by noise. Further details of these techniques can be found elsewhere (Farrar & Doebling, 1997; Yun et al., 2003).

The above-mentioned techniques are localized damage detection techniques and the knowledge of the damaged area needs to be known and accessible prior to the application of the technique. Vibration-based damage detection techniques, on the other hand, do not require complex equipment, are global techniques and have been the mostly used and researched to date (Doebling et al., 1998; Rytter, 1993). Vibration methods are used in estimating modal parameters in undamaged stage (model), which are calibrated with the modal parameters obtained from the structure by obtaining frequency response functions (FRF). The modal parameters of the model are varied based on varying stiffness to match with those of experiment (Lee & Shin, 2002).

## 2.4 Vibration methods

The foremost step in developing an efficient method for the SHM of RC structures is examining the achievements and practical applicability of the identified damage assessment methods. The various methods for damage detection include visual inspection, eddy current, acoustic emission, ultrasonic, magnetic particle, radiography, magnetic particle and vibration methods (Farrar & Worden, 2007; Kim et al., 2007; Li et al., 2014; Moreu et al., 2012; Rytter, 1993; Sohn et al., 2001; Worden et al., 2007). Each of the above-mentioned methods has its own advantages for specific situations. The eddy current technique uses the generation of magnetic field from alternating current, which, in case of damage, causes change in the eddy current. The technique is simple but utilizes considerable power and complicated data. The ultrasonic techniques use high frequency sound waves for damage detection. Nonlinear ultrasonic techniques are usually considered to be more effective than the linear ones (Kim et al., 2017; Zaitsev et al., 2006). The acoustic emission damage detection technique has shown good prospects in online damage detection (Carpinteri et al., 2007), but the weak signals can easily be influenced by noise. Further details of these techniques can be found elsewhere (Farrar & Doebling, 1997; Yun et al., 2003).

Vibration methods have proved more effective in damage detection as compared to other methods given in the literature (Carden, 2004; Magalhães et al., 2012). Among the above-mentioned methods, vibration methods are the most popular due to their convenience for field applications (Kong et al., 2017). The damage assessment is done by monitoring the changes in the vibration characteristics or signatures. The vibration response for a structure is registered through ambient or forced vibration tests. Either of the two approaches – model-based (inverse strategy) or data-driven (pattern recognition) – is used to analyze the vibration data (Cavadas et al., 2013). Data-driven approaches that look for changes in the signatures of a structure relating to its response to excitation, are successful in online monitoring techniques where the present-day-baseline is known, i.e. embedment of sensors in a recently constructed structural system for online health monitoring. However, the best that can be achieved for a constructed system is to compare the future results with the present-day baseline. The model-based approaches better address the systems that largely rely on the baseline (data from the structure in its intact state). In any of the above-mentioned approaches, the damage assessment requires the comparison between two system states (Carpinteri et al., 2007). The baseline is estimated by the aid of FE modeling.

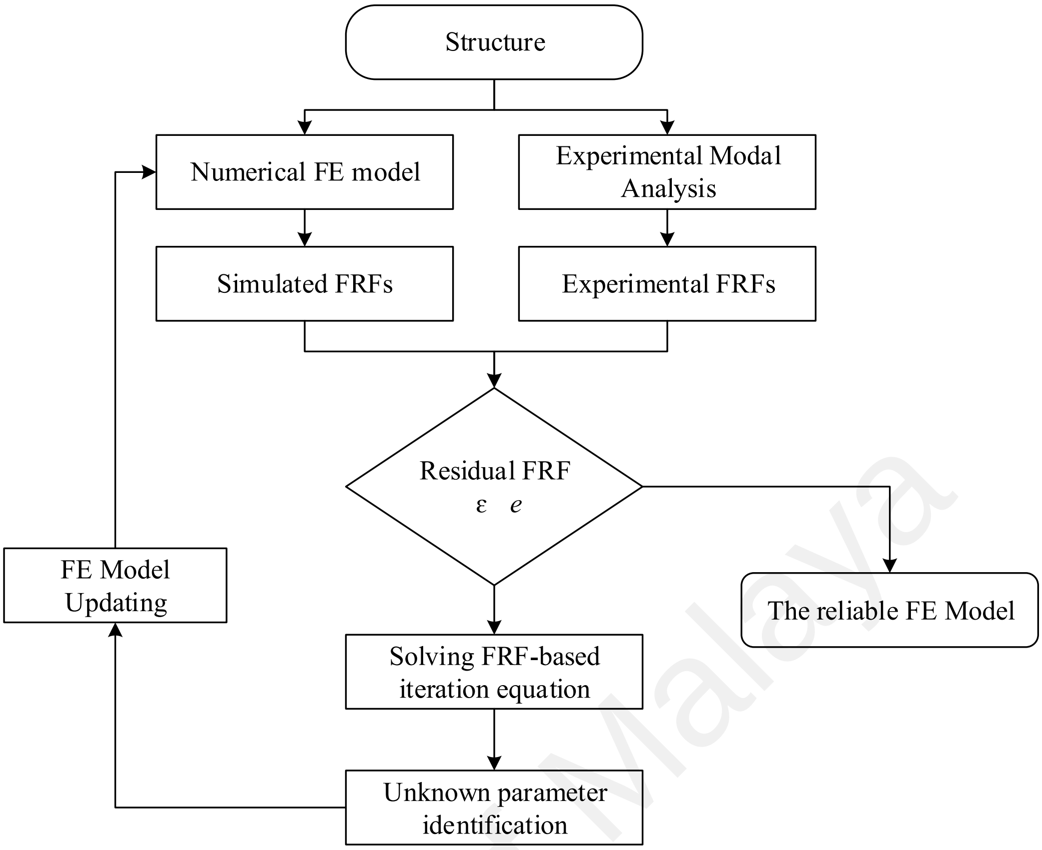


**Figure 2.2**: General model updating scheme (Cao et al., 2013)

Generally, model-based methods are based on changes in natural frequencies $f_r$ or eigenvalues $\lambda_r=(2\pi f_r)^2$, which are known to be affected by structural stiffness. Frequency domain data can also be used for model updating; like frequency response functions (FRFs), which also requires the knowledge of the excitation force. These methods face various constraints when employed on constructed systems (Simoen et al., 2015). This is due to uncertainties that influence their mechanical characteristics and performance (Çatbaş et al., 2013). These constraints are stated below.

6. Efficiency (model updating is an iterative process)
7. Economy (every investigation is a unique case study, and not economical)
8. Uniqueness (Every structure is designed unique)
9. Sensitivity (environmental influences may influence the sensitivity)
10. Inverse engineering problem (baseline data are based on the model updating)

The gap between the model and the real structure needs to be bridged while addressing the above-mentioned uncertainties. A brief overview of the existing studies on constructed systems is useful in this regard to identify these uncertainties, as mentioned in Section 2.4.1. The attempt to address these uncertainties is detailed in Section 2.4.2.

### 2.4.1 Linear vibrations

Most of the dynamic systems have been represented by linear vibration models. The linear model concept assumes that the dynamic response of the structure does not change with the increasing magnitude of the applied force. However, although this can be incorporated into systems where nonlinearities are not significant, in RC structures, the nonlinear behavior plays a significant role when concrete cracks. Nevertheless, the linear systems have been adopted for damage detection in various full-scale testing studies, as shown in Table 2.3. Furthermore, the capabilities of these studies are interpreted in terms of Rytter's four levels of damage detection (Rytter, 1993).

From the Table 2.3, it can be seen that the changes in natural frequencies are discernible, but not significant. It has also been argued that the models incorporating linear systems in damage assessment of constructed systems are not as accurate as those in manufactured systems (Neild et al., 2003b). The major constraints are that the massiveness of structures, complexity of constituent materials and environmental influences make the minor changes in the natural frequencies due to damage almost indiscernible. Liu et al. pointed out that the variation in natural frequencies can be as much as 5% for a 24-hour cycle (Liu et al., 2009). Other studies suggested that the total natural frequency reduction at failure is only 10-14 percent (Hamad et al., 2015), and 7% for a full-scale damaged bridge (Farrar & Jauregui, 1998). However, the linear methods are successful in newly constructed systems where data-driven approaches are more easily applicable (Song et al., 2008; Ubertini et al., 2014).

The survey on studies in Table 2.3 also highlights the uncertainties like inverse engineering problem, general applicability and environmental influences that have not been addressed by these studies. These uncertainties are considered while discussing the nonlinear damage assessment methods in the Section 2.4.2.

**Table 2.3:** Summary of damage assessment for constructed systems for last 3 decades

| No. | Study | Structure | Current condition | Type | Damage Detection levels* | | | | Analysis Type | | | | | | Applications/Capabilities |
|---|---|---|---|---|---|---|---|---|---|---|---|---|---|---|---|
| | | | | | 1 | 2 | 3 | 4 | SL | AV | IH | FR | FC | MU | |
| 1 | (Lee et al., 1987) | RC Bridge in Hong Kong | For Demolition | Double T arch bridge | • | • | | | ✓ | | ✓ | ✓ | | ✓ | (i) Static and dynamic tests can be used to calibrate the mathematical model.<br>(ii) The importance of making appropriate assumptions about the boundary conditions is demonstrated. |
| 2 | (Maguire & Severn, 1987) | Chimney, elevated piled tank, RC bridge beams | Prototype structure | Post tensioned I girder, chimney, elevated piled tank | • | | | | | | ✓ | | | | (i) IH is suitable for quick and accurate determining of dynamic properties |
| 3 | (Saiidi et al., 1994) | Golden Valley Bridge | | Post tensioned box girder bridge, post tensioned beam. | • | | | | | ✓ | | | | ✓ | (i) With initial value of prestressing force known, the damage detection can be carried out.<br>(ii) The relative change in dynamic signatures can be used to assess damage, aided by visual inspections. |
| 4 | (Salawu & Williams, 1995) | RCC Bridge | | Hollow core slab bridge | • | • | | | | | | | ✓ | ✓ | (i) The natural frequencies do not significantly change as a result of structural repairs (3% decrease).<br>(ii) Modal assurance criteria and co-ordinate modal assurance criteria are sensitive to damage can be used for locating damage if the mode shapes adequately reflect damage.<br>(iii) Procedure suitable for periodic bridge assessment |

**Table 2.3:** Summary of damage assessment for constructed systems for last 3 decades (Continued...)

| No. | Study | Structure | Current condition | Type | Damage Detection levels* | | | | Analysis Type | | | | | | Applications/Capabilities |
|---|---|---|---|---|---|---|---|---|---|---|---|---|---|---|---|
| | | | | | 1 | 2 | 3 | 4 | SL | AV | IH | FR | FC | MU | |
| 5 | (Salawu, 1997) | Holway Road Bridge, UK | Testing after repair | Hollow core slab bridge | • | | | | | | | | ✓ | ✓ | (i) Repair of bearings doesn't affect the natural frequencies (1.7% increase) |
| 6 | (Wahab & De Roeck, 1999) | Z24 Bridge, Switzerland | | Post tensioned box girder | • | • | | | | ✓ | | | | | (i) Modal curvatures from different modes can be used to detect damage.<br>(ii) Higher modes require more accelerometers.<br>(iii) Central difference approximation is used for compute modal curvatures. |
| 7 | (Jáuregui & Barr, 2004) | I-40 Bridge over Rio Grande River, USA | In service | Prestressed | • | • | | | ✓ | | | | | ✓ | (i) Load rate analysis carried out and showed that inventory and operating ratings were 1.70 and 2.85.<br>(ii) The procedure can be used accurately for examining the load rating factors of design codes. |
| 8 | (Ren et al., 2004a) | John A. Roebling suspension Bridge, USA | In service | Cable stayed | • | | | | ✓ | | | ✓ | | ✓ | (i) Modal analysis carried out in FE model shows that dead load increase can increase natural frequencies 20% transversely and 5% vertically.<br>(ii) Decreasing the cable stiffness significantly (50%) does not affect the natural frequency. |
| 9 | (Ren et al., 2004b) | John A. Roebling suspension Bridge, USA | In service | Cable stayed | • | | | | | ✓ | | | | ✓ | (i) Full-scale testing of the bridge shows that the cable stiffness reduction does not affect natural frequency.<br>(ii) Analysis performed showed that the stiffness of the cables can be reduced to 40% without affecting factor of safety. |

**Table 2.3:** Summary of damage assessment for constructed systems for last 3 decades (Continued...)

| No. | Study | Structure | Current condition | Type | Damage Detection levels* | | | | Analysis Type | | | | | | Applications/Capabilities |
|---|---|---|---|---|---|---|---|---|---|---|---|---|---|---|---|
| | | | | | 1 | 2 | 3 | 4 | SL | AV | IH | FR | FC | MU | |
| 10 | (Zanardo et al., 2006) | MRWA Bridge No. 3014, Australia | Repaired with CFRP | Continuous RC slab beam | • | | | | | | | | ✓ | ✓ | (i) Comparison of damaged bridge before and after repair by model updating is effective in examining the improvement<br>(ii) After repair, the improvement in fundamental frequencies was 4.7% to 10.6% |
| 11 | (Liu et al., 2009) | Bridge in Connecticut, USA | Repaired | Box girder | • | | | | | ✓ | | | | ✓ | (i) Attempt has been made to develop baseline with data available from undamaged structure.<br>(ii) Method is proposed for real-time health monitoring |
| 12 | (Dilena & Morassi, 2011) | Dogna Bridge, Italy | Ready to raze | Simply supported beam-slab | • | • | | | | | | ✓ | | | (i) The damage has been introduced and fundamental frequency degradation is investigated<br>(ii) A damage identification method is proposed based on changes in modal curvatures<br>(iii) The model is capable of giving rough localization of the damage. |
| 13 | (Dilena et al., 2011) | Dogna Bridge, Italy | Ready to raze | Simply supported beam-slab | • | • | | | | | | ✓ | | ✓ | (i) The natural frequency does not decrease monotonically, the paper provides justification of this behavior observed in (Dilena & Morassi, 2011). |

**Table 2.3:** Summary of damage assessment for constructed systems for last 3 decades (Continued...)

| No. | Study | Structure | Current condition | Type | Damage Detection levels* | | | | Analysis Type | | | | | | Applications/Capabilities |
|---|---|---|---|---|---|---|---|---|---|---|---|---|---|---|---|
| | | | | | 1 | 2 | 3 | 4 | SL | AV | IH | FR | FC | MU | |
| 14 | (Gomez et al., 2011) | West Street On-Ramp (WSOR) bridge, USA | New construction | Curved box girder | • | | | | | ✓ | | | | ✓ | (i) The natural frequency reduction is consistent for long term monitoring because of aging (5% to 8%).<br>(ii) The sensors used in vehicle is potentially proposed method for frequency measurement using instrumented vehicle. |
| 15 | (Çalık et al., 2014) | Masonry Vault | Closed | Heritage structure | • | • | | | | ✓ | ✓ | ✓ | | ✓ | (i) Structural dynamic identification using ambient vibrations<br>(ii) Vibration test was performed before and after testing. The natural frequencies improved after repair.<br>(iii) The method is indicated to be effective to observe restoration effects on the response of structures. |
| 16 | (Xu & Xia, 2018) | Ahai Hydropower Station | In service | semi-cushion spiral case structure | • | • | | | | | | | | ✓ | (i) The importance of this study is in situations where the laboratory testing is not possible and the FE model is the way to predict structural behavior<br>(ii) The natural frequency decreases with damage, it can be used in safety evaluation and damage identification by performing periodic tests. |

*SL: static loading, AV: ambient vibrations, IH: impact hammer, FR: free vibrations, FC: forced vibrations, MU: model updating*

**The damage detection levels are based on Rytter's four levels of detection, localization, assessment and consequence* (Rytter, 1993).

### 2.4.2 Nonlinear vibrations

Nonlinearity is a phenomenon that is significant in RC structures due to the presence of micro-cracks. These micro-cracks are present in the interfacial transition zone which is the weak link between the aggregates and the cement paste. After the onset of loading, these micro-cracks join together to form larger cracks. The factors responsible for these micro-cracks include the size of the aggregate, water to cement ratio (w/c ratio), concrete mix design, casting method, ambient environment, and the curing procedures. Vibration measurements are sufficiently sensitive to detect these micro-cracks (Van Den Abeele & De Visscher, 2000). Most of the vibration-based studies assume the vibrations to be linear. Although considerable effort has been put into developing model-based methods, but the recent studies debate the applicability of these methods. The inclusion of nonlinear behavior in FE modeling has been quantitatively studied in to support the debate that nonlinear behavior incorporation is necessary to have effective damage assessment mechanism (Hamad et al., 2015). While investigating the cracked concrete behavior in RC beams, Neild (2001) and Tan (2003), reported that the cracked concrete modeling using open and breathing crack models was not suitable for characterizing nonlinear behavior. This is further supported by the recent studies Hamad et al. (2013). Adams & Allemang (1998) surveyed the nonlinear damage assessment techniques. According to them, the frequencies and mode shapes for a nonlinear system generally change with the amplitude of the input force and a larger data set with more variables is produced. According to their study, non-linearities are characterized in three steps, which are necessary for system identification.

- Detection – identifies the presence of non-linearity
- Classification – categorizes into the type of non-linearity
- Location – the source of the non-linearity

Hamed & Frostig (2004), presented an analytical method for examining the effect of incremental static damage on the natural in pre-stressed concrete beams, while incorporating material nonlinearities. An implicit nonlinear equation was formulated and solved using multiple shooting method. They contended that the natural frequencies identified from the nonlinear formulation drop drastically with the crack formation. However, this is not the case with linear conventional methods, which shows that the linear methods may overestimate the natural frequencies.

According to Waltering et al. (2007), the damage in the form of cracks results in the inducing of non-linear damping and stiffness for a nonlinear system. The coefficients in the equation of motion are dependent on the amplitude of vibration, its velocity and the excitation force. To create the descriptions and characteristics of nonlinear behavior like the intensity and type of nonlinearity, several approaches have been introduced. Various other studies have investigated the nonlinear behavior. A brief summary of these studies used in the characterizing of nonlinear behavior is presented in Table 2.4.

**Table 2.4:** Investigations on modeling techniques with nonlinear behavior

| **Nonlinearity** | **Excitation method** | **Studies** |
|---|---|---|
| Super-harmonics | Harmonic | Hamad et al. (2015) |
| | | Nandi & Neogy (2002) |
| Restoring force surface, restoring force vs displacement method | Swept-sine, harmonic | Masri & Caughey (1979) |
| | | Worden & Tomlinson (2000) |
| | | Hamad et al. (2011a) |
| Geometric nonlinearity | Impact load | Huszár (2001) |
| | | Huszár (2006) |
| Material nonlinearity | Free vibrations | Hamed & Frostig (2004) |

| | | |
|---|---|---|
| Amplitude | Swept-sine | Waltering et al. (2008) |
| Ultrasonic | Nonlinear resonant ultrasonic spectroscopy (NRUS) | Kim et al. (2017) |

Van Den Abeele & De Visscher (2000) incorporated nonlinear behavior while investigating experimental modal analysis. They made a comparison of linear and nonlinear models to investigate RC beams undergoing progressive damage. Experimental modal analysis showed a gradual decrease in modal frequencies. The nondestructive acoustic measurement for low excitation (linear) and increasing dynamic amplitude (nonlinear) were carried out using frequency domain and time domain techniques. It was found that these techniques were more sensitive to damage compared to the linear methods, especially in the initial damage regime when the micro-cracks were formed.

Tsyfansky & Beresnevich (2000), showed that damage detection using non-linear methods is 10 times more sensitive to damage than the linear methods. Figure 2.3 shows the frequency domain response of an un-cracked (linear) and cracked steel bar (nonlinear). It can be observed from the figure that, the presence of distortion, higher harmonics and frequency shifts occur due to the presence of a crack. Although, modeling homogeneous materials, like metals, is simpler, in the case of concrete, the nonlinear behavior is even more significant. Hamad et al. (2015), showed that the modal stiffness (nonlinear) decreases by 45% as compared to the natural frequency (linear), which decreases by 10%; this indicates that the nonlinear behavior shows more sensitivity to the damage. The modal stiffness degradation was observed through the formation of restoring force surfaces, which, in terms of a linear system, are not influenced by damage.

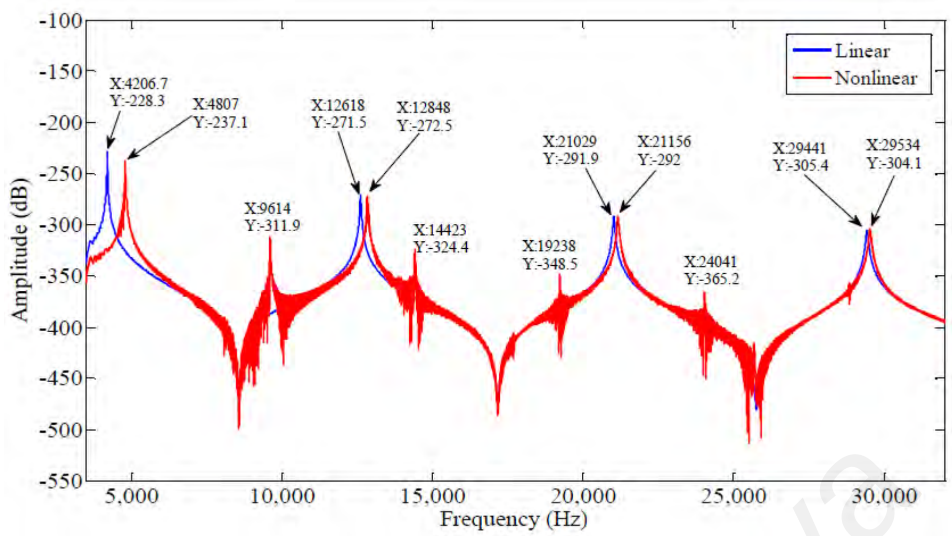


**Figure 2.3:** Frequency response of cracked and un-cracked bar (Hiwarkar, 2010)

Kim et al. (2017) also made the comparison of linear and nonlinear ultrasonic methods for damage in prestressed concrete beams. They showed that the non-linear method employed for damage detection was 25-93 % more sensitive compared to the linear method, which was only 1%. This means that the nonlinear methods are significantly more sensitive to damage in the case of RC structures even when the effects of prestressing are incorporated, which, in terms of linear methods, is not effective (Saiidi et al., 1994). The details of the nonlinear characterization procedures involved can be studied in the next subsection.

#### 2.4.2.1 Nonlinearity characterization procedures

There are various characterization methods of nonlinear behavior; namely, first order and higher order FRF methods, least square coherence functions, first order dynamic stiffness, Hilbert transform, formation of higher harmonics and restoring force surfaces (RFS). This study attempts to present the nonlinear characterization in damage detection focusing on the last two of the above-mentioned methods.

(a) ***Presence of super-harmonics***

With the presence of imperfections or micro-cracks, the response of a structure to a harmonic excitation is not a total sine wave and the imperfections can be seen as super-harmonics in the response (Pugno et al., 2000). Nandi & Neogy (2002) induced damage in a cantilever beam by edge cracks. Harmonic excitation with a frequency less than the fundamental frequency was applied on the beam and the formation of super-harmonics was observed. They found that the harmonics are the most noticeable at the frequency of approximately half the fundamental frequency. It can be seen in Figure 2.4 that the super-harmonics are most prominent at the excitation frequency of 50 Hz, which is half of the first natural frequency. They also pointed out that the imperfection in support conditions may falsely lead to the formation of super-harmonics.

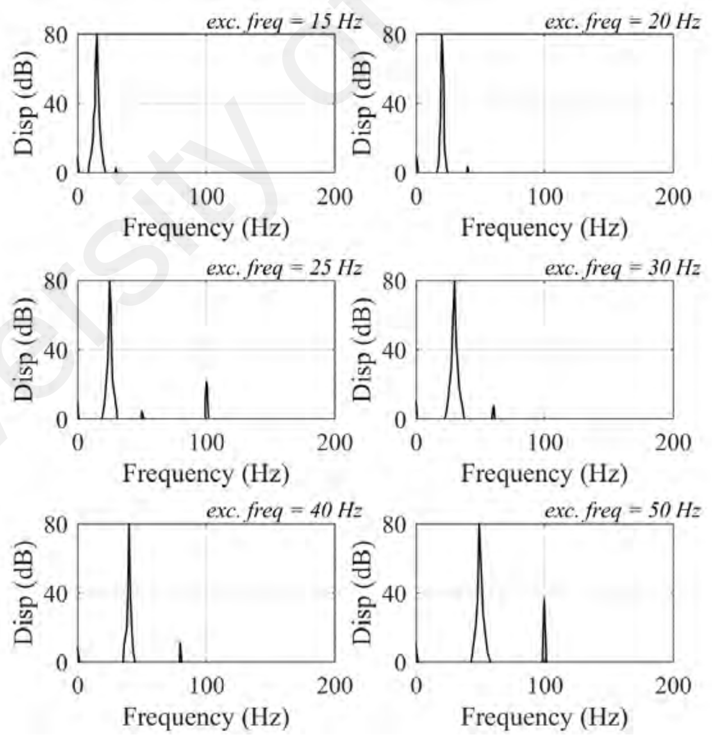


**Figure 2.4: S**uperharmonics at different exciting frequencies (Nandi & Neogy, 2002)

The relation between the nonlinear behavior and damage was investigated by Neild (2001). It was pointed out that the nonlinear behavior does not follow a monotonic pattern with increasing damage and that the nonlinearities are highest at 27% of the damage load of the maximum failure load. Neild also established that the crack closure behavior does not happen in cracked concrete under vibration, and that the breathing or open crack models are not suitable for modeling the vibration behavior of a cracked beam.

Hamad et al. (2015) supported Neild's study by determining that the nonlinear behavior does not change monotonically with damage and that the open and breathing crack models do not represent the nonlinear vibration behavior. They used the fictitious crack model (FCM) and proposed a flexural damage model for detecting damage through non-linearities. The damage evolution was compared with the nonlinear behavior of a harmonically excited system. The non-linear behavior was investigated by the appearance of super-harmonics and the response of restoring force surfaces with displacement. The nonlinearities were found to be more sensitive to damage at lower levels. The model was considered to be a more sensitive approach to damage detection compared to natural frequency degradation, especially in terms of the ability to detect damage without the need of baseline data (Hamad et al., 2011a; Hamad et al., 2015).

(b) ***Restoring force surface (RFS) method***

It has been proven that, the RFS method is very efficient in identifying the nonlinear behavior of a system (Masri & Caughey, 1979). In this method, the harmonic signal for the desired frequency range is applied on a specimen and the displacements and accelerations are recorded through accelerometers. The advantage of using restoring surface method is its applicability in single degree of freedom and multi degree of freedom (SDOF and MDOF) systems, and the direct visual representation of non-linear behavior – which can be further studied at different damage levels (Silva & Maia, 1999). The restoring force of the system, depending on the displacement and velocity, is represented by a surface over phase plane (Hamad et al., 2011a; Krauss et al., 1999; Tan, 2003; Worden & Tomlinson, 2000). The equation for the restoring force is given by

$$m\ddot{u}(t) + f(u, \dot{u}) = F(t) \tag{2-1}$$

Where *F(t)* is the excitation force, f*(u,u̇)* is the internal restoring force as a function of velocity and displacement, and *mü* is the inertial force. For equivalent linear cases, the restoring force can also be given as

$$f(u, \dot{u}) = c\dot{u} + ku \tag{2-2}$$

Where c represents damping and k represents the stiffness. The restoring force is represented as the phase plane (displacement-velocity plane). Therefore, Equation 2-1 can be rearranged to

$$f(u, \dot{u}) = F(t) - m\ddot{u} \tag{2-3}$$

Tan (2003) recorded the velocity and the excitation data at regular intervals when the velocity data were integrated and differentiated the velocity data to obtain displacement and acceleration, respectively. Using the obtained data, the restoring force can be achieved as a function of the phase plane.

Hamad et al. (2011a) presented a model that replicated this behavior for flexural damage in RC beams. The comparison of bilinear and non-linear crack models was made to show the restoring force surfaces for the bilinear model overlap. The presence of nonlinearities can be visualized when the restoring force surfaces show change in slope, which is known as modal stiffness, as shown in Figure 2.6.

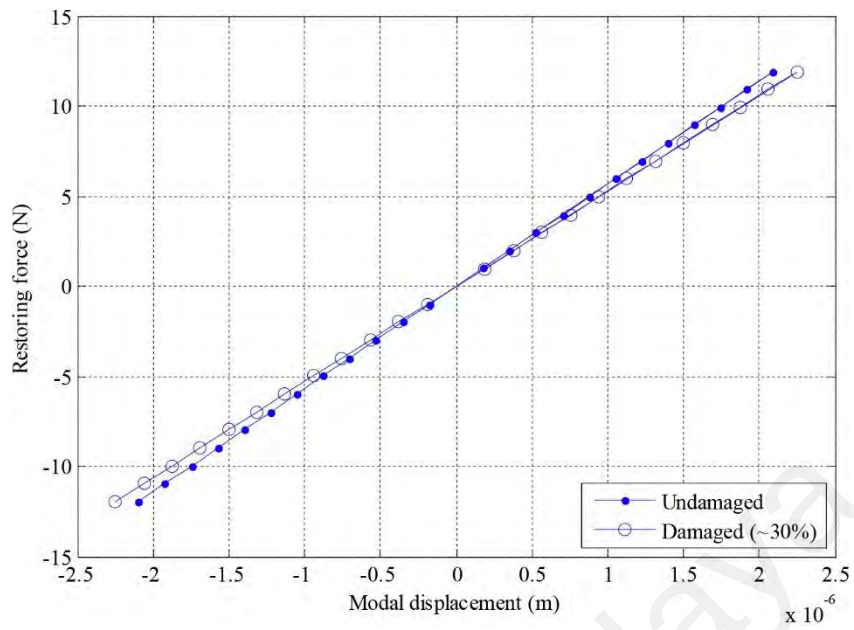


**Figure 2.5:** Restoring force-modal displacement curves (Hamad et al., 2011a)

Therefore, the RFS method is a very efficient method for identifying and visualizing nonlinear behavior. In terms of RC beams, the nonlinear crack vibration behavior must be incorporated to obtain the nonlinear response of the structures.

## 2.5 Concrete constitutive modeling

Concrete constitutive modeling is done using microscopic models (Cusatis et al., 2011a; Cusatis et al., 2011b) or macroscopic models (plasticity). The microscopic models are complex and are applicable to study certain mechanisms in concrete but are computationally expensive when incorporated in complex structures. Microplane models (Sadrnejad, 2010) are accurate and lie between the microscopic and macroscopic models, but they still are complex and may compromise the computational costs. However, the macroscopic models are phenomenological models that reproduce the concrete behavior in uniaxial, multiaxial situations to match with the experimental values. The macroscopic models are simple to apply and serve the purpose of modeling the concrete behavior with accuracy and efficiency. Plasticity approach, being a popular phenomenological model, is very efficient in modeling concrete. The developments of plasticity approach are given below.

### 2.5.1 Plasticity approach

For concrete modeling and damage mechanisms, plasticity approach has found success in the past. Out of all the plasticity-based models, the elastic strain-hardening plastic model is the most general and accurate. For modeling of concrete structures, one way is to apply stiffness method concrete structures like beams or 2-D frames. Hamad et al. (2013) presented a non-linear tensile constitutive relation with uniaxial constitutive relations to introduce damage in Euler Bernoulli's concrete beams. These relations have successfully achieved the desired capabilities in simpler models for specific loading situations. But structures are affected by multiaxial stress-strain conditions, which differ from the uniaxial states. For detailed analysis, finite element procedures are employed. For instance, Sima et al. (2008) proposed constitutive model of concrete which incorporated the combined tensile and compressive behavior. Plasticity approach is very effective in observing the behavior of RC structures in multiaxial stress states.

Plasticity approach is generally used in modeling various materials like soils, metals and ceramics. Plasticity involves a yield criterion which specifies the onset of plastic deformations for different loading combinations, a hardening rule which prescribes the work hardening of the material and effect on yield condition with increasing plastic deformations, and, flow rule that connects the plastic deformation with the stress components (Hu & Schnobrich, 1989).

In concrete structures, using plasticity may represent the permanent strains of concrete, but there is no stiffness degradation due to damage, as concrete exhibits the plastic as well as the irrecoverable damage behavior (Feenstra & De Borst, 1996). Lubliner et al., (1989) coupled the classical plasticity theory with continuum mechanics damage (CMD) model. The model represented the permanent strains as well as stiffness reduction. The model is usually referred to as concrete damaged plasticity model (CDPM) or concrete plastic damage model. The model was further enhanced by Lee & Fenves (1998) and many other researchers to date.

Krätzig & Pölling (2004) used plastic damage model dependent on the fewest possible parameters to present model of concrete and reasonably represented multiaxial stress states i.e. beams and slabs. Tao & Phillips (2005) investigated the key issue of separating tension and compression constitutive laws in reverse cyclic loadings. They presented a damage model, which is very effective in situations permanent strains (plastic damage) are not significant. The model is computationally efficient, validates the multiaxial behavior of concrete and is easily applicable in commercial finite element software codes.

The limitation (lack of permanent strains) of Tao & Phillips (2005) model was later improved by coupling their model with plasticity to cater for the permanent deformations (Taqieddin & Voyiadjis, 2009; Voyiadjis & Taqieddin, 2009). Plastic yield function with multiple isotropic hardening, non-associative plasticity flow rule was adopted to represent the permanent deformations.

Yuchuan et al. (2011) presented a more complex model for cyclic loading of concrete, which incorporates anisotropic damage model for cyclic loading. The model is capable of non-linear unloading and linear reloading phenomena for cyclic loading. The model shows the hysteretic behavior which is suitable for fatigue applications.

Aslani & Jowkarmeimandi (2012) used coupled plasticity and damage model (CDPM) successfully in the modeling of reinforced concrete shear wall against cyclic loading. The model presented efficiency, and relied only on convenient laboratory material testing data for building up the complete constitutive relation for the materials.

A plasticity model was utilized with scalar damage model with a non-linear unloading regime following the Bouc-Wen modeling of classical plasticity (Andriotis et al., 2016).

The model was calibrated in a heuristic way using eight parameters namely yield stress, yield strain, hardening parameter, damage threshold, damage evolution parameter, damage evolution power, unloading parameter 1 and unloading parameter 2. The calibration was done using the uniaxial stress-strain curves for different experiments. The model was implemented successfully in cantilever column element and RC frame analysis. The model gives more accurate behavior of non-linear unloading regime, as shown in Figure 2.6.

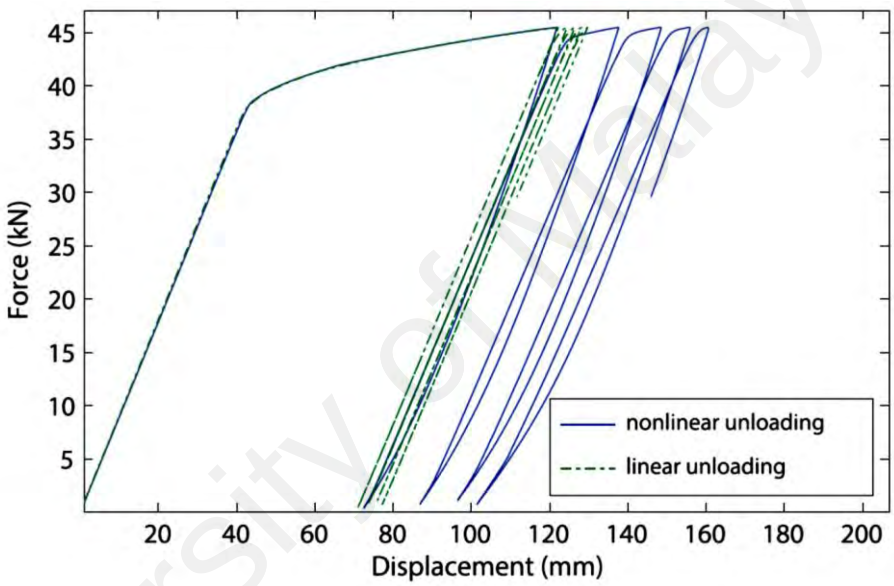


**Figure 2.6:** Comparison of linear and non-linear unloading (Andriotis et al., 2016)

Du et al, (2010) investigated the mechanical behavior of concrete using nonlinear Unified Strength Criterion for concrete. It was observed that the mechanical behavior of concrete can be explained by using nonlinear unified strength criterion. Concrete behavior in multiaxial stress states was investigated and compared with the experimental results. This was further incorporated in constitutive modeling of concrete using plasticity approach (Lu et al., 2016). It was also found that the associated plastic flow rule overestimates the dilatancy of concrete, which is more accurately represented by using non-associated plastic flow. Furthermore, the cohesiveness and the hardening and softening behavior of concrete were also calibrated. The model was further incorporated in modeling reinforced concrete column under eccentric axial compression loading. The calibrated model gave satisfactory agreement with the laboratory experiments.

Recently Alfarah et al., (2017), presented plasticity model with scalar damage model. Other than achieving the multiaxial accuracy of the materials, the main achievement of developing this plastic damage model was the insensitivity of the model to the mesh size. As plasticity models are usually computationally expensive, so this development of non-dependence on mesh size can be a good development in terms of efficiency of plasticity models.

Out of extensive developments in plasticity approaches for concrete the most recent ones are coupling of microplane-based damage and continuum plasticity models for analysis of damage-induced anisotropy in plain concrete (Daneshyar & Ghaemian, 2017) and crack band approaches (Xenos & Grassl, 2016). With the passage of time, the explanation of concrete modeling in CDPM framework is getting more complex and advanced. But these models have not yet been evaluated in terms of simulating the nonlinear behavior. Although the plastic damage approaches have not been used in modeling the vibration characteristics of cracked beams. The plastic damage model when incorporated in FE modeling of concrete beams can simplify the modeling algorithms to mere tools of modeling the RC structures.

### 2.5.2 Multiaxial compressive stress-strain behavior

Concrete behaves differently in biaxial stress states as compared to uniaxial stress state, in terms of compression. Kupfer et al. (1969) carried out laboratory tests of concrete specimens to evaluate the behavior of concrete under different multiaxial states. Concrete in biaxial compression is 16 % more strong than in uniaxial compression, while the tensile behavior remains the same in uniaxial and biaxial tension. The capabilities of different constitutive models in multiaxial states are compared with the experimental stress-strain behavior of the data from Kupfer et al. (1969).

Among those who investigated the multiaxial response of plasticity models, Hu & Schnobrich (1989) pointed out that non-associated plasticity is more practical as compared to associated plasticity, when used as a flow rule. They further validated the response of the model with the experimental results of Hu & Schnobrich (1989).

Grassl & Jirásek (2006) model was based on plasticity and effective stress, combined with the isotropic damage from plastic strains. The model agreed with wide variety of uniaxial, biaxial and triaxial loading cases. The model was further improved later and was called CDPM2 (Grassl et al., 2013).

The model by Voyiadjis & Taqieddin (2009) used a plastic yield function with isotropic hardening and non-associated plastic flow. This model showed good agreement with experimental multiaxial loading scenarios.

Therefore, the plasticity approach has found more accurate behavior in uniaxial and multiaxial stress states using non-associated plastic flow rule. Isotropic hardening is adopted for convenience in calculation procedures without compromising the accuracy of the model. The validation of the above-mentioned iterations of the plasticity and damage models with the experimental biaxial test data by Kupfer et al. (1969) shows the strength of plasticity approaches in concrete applications.

### 2.5.3 Fictitious crack model

The tensile behavior of concrete is important in determining behavior of cracked concrete and has been interpreted by various models. Figure 9 shows the hierarchy of various models of concrete in tension. The cracking behavior of concrete is important when it comes to the dynamic response of the structure. The dynamic behavior of cracked concrete has been explained by various crack models which become more complex on reaching higher levels. The cohesive crack model offers a reasonable description of the mechanisms involved in damage (Figure 2.7).

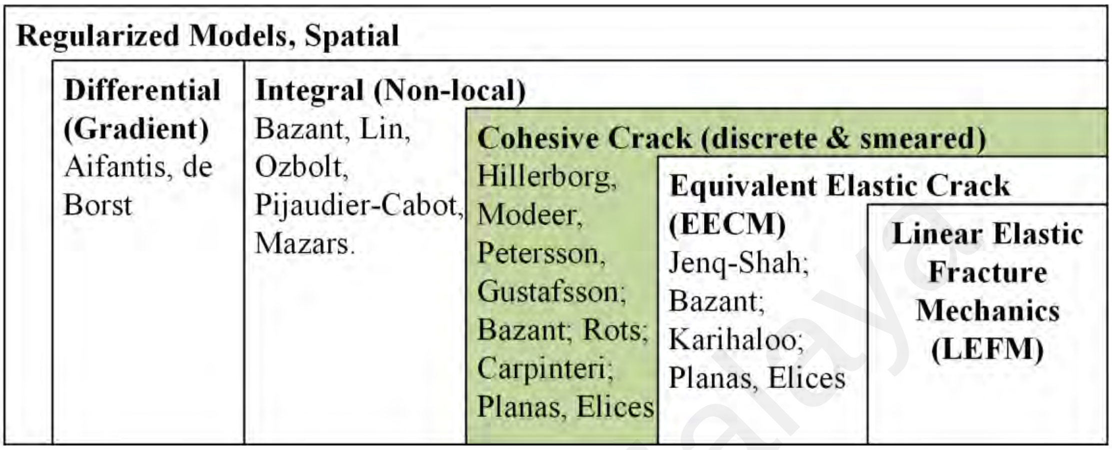


**Figure 2.7:** Hierarchy of various fracture models of concrete (Elices & Planas, 1996)

In concrete, cracking was first investigated using the smeared crack approach (Rashid, 1968). In this approach, there was a vertical drop of stress (stress-strain curve) to zero after reaching the tensile strength. No softening behavior was considered after cracking. Hu & Schnobrich (1990) worked on the post-cracking behavior of concrete (tension stiffening) and proposed a smeared crack approach in the analysis of concrete structural members like beams, panels and columns. Later, the crack model was used several times in modeling structural concrete members using the smeared or discrete crack approaches (Arafa & Mehlhorn, 1998; Hamad et al., 2015; Hillerborg, 1983; Tudjono et al., 2016).

The fictitious crack model is the extension of the crack model proposed by Dugdale (1960) and Barenblatt (1962). Hillerborg et al. (1976) proposed a major development in applying the fictitious crack model to the fracture of concrete. A fictitious crack was assumed to form as the concrete stress reaches tensile strength. After tensile strength, the stress does not fall immediately to zero, but decreases with an increase in the crack width.

The fictitious crack model, was later incorporated in modeling concrete by Hamad et al. (2013). The model was implemented on a plain concrete prism for investigating the crack mechanism in concrete. The model was experimentally verified using the Digital Image Correlation (DIC) system to investigate the crack growth. The crack growth detection at the micro-level was experimentally investigated by Alam et al. (2014). Later, the model was used in the computational modeling of a cracked RC beam. The modeled beam successfully reproduced the vibration characteristics for harmonic excitation (Hamad et al., 2015).

In summing up, the fictitious crack model (FCM) concept is based on the fact that after the tensile strength of the concrete is reached, the stresses drop and a fictitious crack is formed with cohesive stresses present. This fictitious crack width increases until the cohesive stresses drop to zero, where a real crack is formed. FCM represents a realistic crack formation mechanism, as the cracked region acts in a nonlinear way and the surrounding region acts in a linear way. FCM has been used in the modeling of concrete (Hamad et al., 2013) and various plastic damage approaches (Alfarah et al., 2017). A recent research incorporated the nonlinear crack behavior in the modeling of concrete beams and the vibration analysis of the cracked beam showed that the FCM approach is a more realistic approach to modeling the vibration behavior of the cracked concrete (Hamad et al., 2015).

## 2.6 Modeling of cracked beam vibration

The vibration behavior of the cracked beams is modeled using open, breathing and nonlinear crack models. The definition and use of these models are given below.

#### 2.6.1.1 Open crack models

Open cracks are modeled where the crack doesn't close and the reduced stiffness (after damage) doesn't change for any magnitude of vibration excitation (Dharmaraju et al., 2004). The open crack models are not the realistic representation of the damage mechanism in concrete, as the crack opens and closes during the vibration cycle. The vibration response interpretation of open-cracks results in more drop in natural frequencies as compared to breathing cracks which may give higher values of modal parameters than actual (Chondros et al., 2001; Gounaris & Dimarogonas, 1988).

The open crack modeling was done to model the steel bridge by introducing damage using torch cuts. The non-linear effects could not be identified because the torch cuts prevent crack opening and closing during the vibration testing (Farrar & Jauregui, 1998). This is not a realistic representation for crack modeling in concrete beams because the cracks do not keep open during the vibration cycle.

#### 2.6.1.2 Breathing crack models

The opening and closing of a vibrating crack may be represented by breathing crack model (Figure 2.8), but the stress state around vibration changes between compression and tension because of opening and closing of the cracks. Therefore, the compressive action was chosen when the crack closed. And the frequency didn't dependent on the amplitude of vibration and the system was assumed linear (Chondros et al., 2001). Therefore, the transition between open and closed crack was still not incorporated, which is required in nonlinear situations.

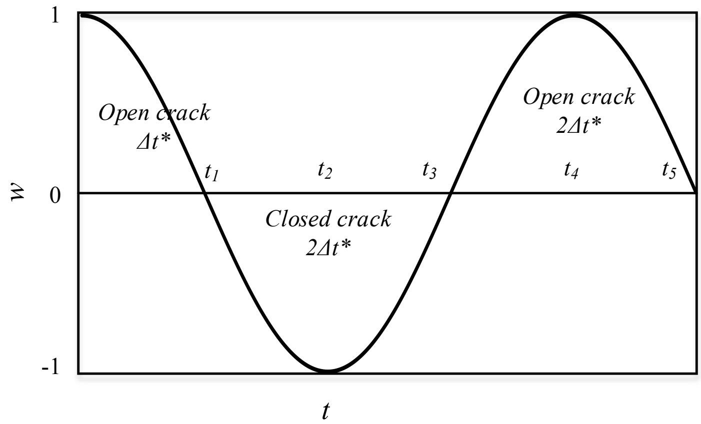


**Figure 2.8:** Bilinear breathing crack model (Chondros et al., 2001)

Breathing cracks give better representation of mechanics as compared to the open cracks. Law & Zhu (2004) studied the response of the reinforced concrete girder with statically induced damage on a beam, identified as 'small damage' and 'large damage' using breathing crack models. They made the comparison of breathing crack model with open crack model and found it suitable for dynamic response of damaged and undamaged states.

Bouboulas & Anifantis (2011) modelled a carbon steel beam using breathing crack approach. The problem was considered a non-linear problem. Discrete Wavelet Transform (DWT) was used to locate the crack and Fast Fourier Transform (FFT) and Continuous Wavelet Transform (CWT) were used as supplementary tools for crack detection.

Nandi & Neogy (2002) also used breathing crack models in identifying the nonlinear through the formation of super-harmonics in cantilever beam. Another investigation was attempted at identifying the load carrying capacity of a cracked reinforced concrete slab bridge using breathing crack model (Law et al., 1995a, 1995b).

Breathing crack models were also used in modeling the nonlinear behavior in a steel cantilever beam (Pugno et al., 2000) and showed good prospects in damage detection. The breathing crack models have been discussed in modeling of RC structures, and are said to lack the ability to reproduce the vibration behavior of cracked concrete (Neild, 2001; Tan, 2003).

#### 2.6.1.3 Nonlinear crack models (Cohesive crack models)

Nonlinear crack behavior gives the transition from tension to compression when a crack opens and closes. The nonlinear modeling has been used by Hamad et al. (2015) in modeling multiple cracks for modeling the harmonic response of a beam. It was found that the nonlinear vibration characteristics were reproduced in the model by introducing the crack by FCM.

### 2.7 Uncertainties in damage assessment of constructed systems

A comprehensive review of damage detection mechanisms and constitutive and FE modeling of concrete, has been presented so far. There have been numerous investigations on these models concerning their strengths and weaknesses. This section highlights the major challenges that constrain the implementation of the vibration methods in constructed systems.

#### 2.7.1 Environmental influences

The major issues that constrain the successful damage detection method to real life structures are the environmental factors like ambient temperature, weather fluctuations, relative humidity, wind speed (affects accelerometers) and the surrounding disturbances. All these environmental influences affect the structural response (Limongelli et al., 2016) and cannot be incorporated in the computational model. Different attempts have been made with different interpretations of environmental influences. Wahab & De Roeck (1997) found that for every 15°C-temperature change, there is 4 to 5% change in the natural frequency. It was also demonstrated that the temperature differentials caused the torsional damage on superstructure (Fu & DeWolf, 2004). An attempt was made to incorporate the temperature as a factor affecting the elastic modulus in the modeling of RC structures (Meruane Naranjo & Heylen, 2010; Xia et al., 2011). But again, the temperature gradient between the top and the bottom surfaces of a bridge can be a reason for the crack formation and may affect the natural frequencies by as much as 5% in a period of 24 hours (Liu et al., 2009).

However, a non-physics-based approach was made for damage detection without the influence of temperature (Serker et al., 2009). A recent study along these lines also suggested that the temperature change from 22℃ to 37℃ can cause 4% to 12% change in natural frequencies. Principal component analysis, as a statistical method, was used to eliminate the influence on the structural response (Shan et al., 2018).

Fröjd & Ulriksen (2018) pointed out that the variation in environmental conditions can conceal the damage on concrete while using the vibration approach. They used the Mahalanobis distance (De Maesschalck et al., 2000) from a moving window baseline data set to suppress these environmental influences. The method is more effective in investigations with baseline data available for long-term measurements.

Hence, the temperature effects that influence the vibrational behavior are the differential temperature that causes damage (torsional cracks), and the temperature that changes over time. The natural frequency as a damage indicator is influenced by the temperature and is not effective if solely considered a damage indicator. The temperature influences need to be incorporated in such a way that the algorithm is insensitive to temperature fluctuations.

### 2.7.2 Progressive damage

The reduction in natural frequency as an indicator of the damage has been studied by various researchers (Cawley & Adams, 1979; Doebling et al., 1998; Farrar & Doebling, 1997; Lee & Shin, 2002) by estimating the baseline condition. The progressive damage can be simulated or tested at the laboratory level, but in field conditions, it is still necessary to rely on the simulated model. Progressive damage has been studied for investigating reduction in natural frequency (Hamad et al., 2015; Neild, 2001), interpreting the higher harmonics based on nonlinear ultrasonic testing (Shah & Ribakov, 2009), and for predicting crack paths in plain concrete structures (Sadrnejad, 2010). There are only handful studies that investigate the damage assessment methods while considering progressive damage. However, these studies identify the importance of using the progressive damage in damage assessment methods.

Owen (2003) presented the idea of obtaining the data for the complete service life of the structure. Cyclic loading of 10 million cycles at different amplitudes was applied on a set of RC beams for 25% to 50% of the ultimate load capacity of the beams. It was found that the reduction in natural frequency was more significantly related to the crack height rather than the loading cycles. This suggested that the incremental loading within the failure load is not significantly affected by the number of cycles and can be used to simulate damage in the structure. This process of achieving damage in steps to the ultimate loading capacity is termed incremental or progressive damage. The possibility of progressive damage in simulation gives an idea about the complete life cycle of the structure and the failure mechanisms through the FE modeling (Sadrnejad, 2010).

Pešić et al. (2015) simulated progressive damage to investigate the dynamic characteristics of the FE model and experimental studies. It was found that model updating, can be minimized by simply relying on the static modulus of elasticity, which can be obtained from routine laboratory tests. It was also pointed out that the crack formation in concrete could be accurately visualized and predicted from the tensile damage parameter of the constitutive relations. The simulation of progressive damage can give an idea of the type of a failure a structure may go through.

Another approach to progressive damage, based on the material properties was applied on a 10 story RC frame structure (Yousefianmoghadam et al., 2018). The incremental static damage was applied by in-fill walls in steps, and then the seismic loading was applied to study the modal parameters. The modal parameters, throughout the damage were replicated in the model quite accurately.

The advantage of investigating structures in conjunction with the complete design life is that it gives more information about the anticipated structural failure type. This is more effective in situations where the collapse cannot be validated on constructed systems. The FE modeling of an arch dam is such an example, investigated by Sadrnejad (2010). Moreover, the natural frequency degradation and the behavior of modal parameters can be estimated with more confidence. In addition, it gives more ways to identify the parameters that are a general representation of the structural behavior; this is a promising aid in inverse problem solving, as pointed out by Hamad et al. (2015).

The importance of the structural response to the external loading relies on the concrete constitutive modeling. An accurate constitutive modeling framework can lead to a better replication of damage models and provide a better representation of static and dynamic response of the structure.

### 2.7.3 Sensitivity to damage

As mentioned in the previous section, simulating the progressive damage gives information about the sensitivity of the model to damage. Various studies have demonstrated and debated the sensitivity of the damage parameter to the extent of damage (Capozucca & Magagnini, 2017; Hamad et al., 2015; Neild et al., 2003b; Pešić et al., 2015). The authors have consolidated these studies to visualize the sensitivity of the natural frequency to damage; as shown in Figure 2.9. At complete failure, the maximum frequency deterioration is around 15%. Adding environmental influences to that, the sensitivity reduces further; this is acknowledged by (Hamad et al., 2015).

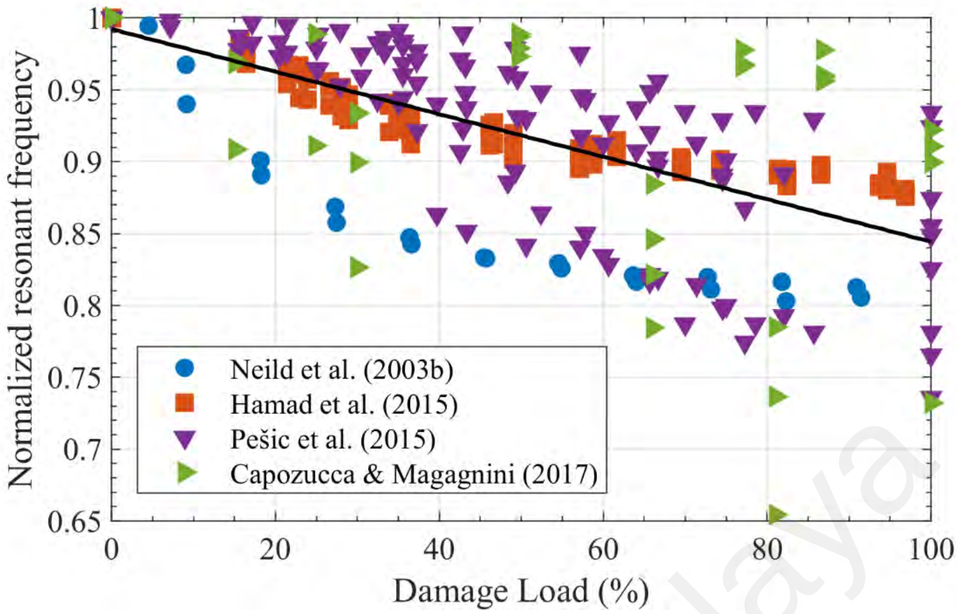


**Figure 2.9:** Natural frequency degradation with damage for past research

However, when nonlinear behavior is incorporated, the sensitivity becomes 45% (Hamad et al., 2015) for nonlinear vibrations and 25% to 90% using nonlinear resonant ultrasonic spectroscopy (Kim et al., 2017). The improved sensitivity of nonlinear methods, supported by the laboratory validation provides a more accurate representation of concrete behavior.

### 2.7.4 Inverse engineering problem

The last and the most important problem in implementing damage detection in the field is the lack of baseline data. The baseline data for existing structures are subject to the availability of the structural design, or the accuracy of the FE model from model updating (Hearn, 2007; Mottershead & Friswell, 1993). The baseline data are also referred to as the pre-damage and undamaged state or virgin state data. Stubbs & Kim (1996) attempted to assess the damage based on the post-damage modal parameters available, and iterating the relative eigenvalues between the damaged structure and the FE model. The attempt to eliminate the dependence on the baseline was successful, but the modal parameters were estimated based on the 'grey system' or the parameters obtained from model updating (see Figure 2.2) (Dharmaraju et al., 2004). The field-testing application based on modal parameters showed that the modal parameters are sensitive at higher damage severity, as the modal parameters did not necessarily degrade with increasing damage. From the practical point of view, that damage level is considered to be too late to avoid catastrophe (Farrar & Cone et al., 1994). Accordingly, the inconsistencies between the model updating and the post-damage modal data would magnify in application in concrete structures because of the more complex material behavior compared to steel structures.

According to Gomez et al. (2011), the natural frequencies drop continuously during the service, when there is no damage. They found an average of 5% drop in the natural frequency for an undamaged bridge for the time of 8 years. The model updating was also investigated in other studies (Guan, 2006; Teughels & De Roeck, 2005). Notwithstanding the focus on model updating, so far, the uncertainties in robustness and reliability have not been addressed and the inverse engineering problem has not been resolved using model-based methods (Simoen et al., 2015).

Neild et al. (2003b) emphasized the need to eliminate baseline data for the successful implementation of SHM in RC structures. For an existing structure, the information that can be achieved is the data based on that instant. Hamad et al. (2015), in characterizing the nonlinear behavior for RC beams found that the nonlinear behavior is not monotonic in nature and may not be suitable for damage detection. Nevertheless, this study showed promising prospects in eliminating the reliance on baseline data for concrete beams.

Rucevskis et al. (2016) made an effort to detect damage without the use of baseline data using the mode shape curvature-based method. The damage was indexed as the absolute difference between the measured curvature of the damaged structure and the smoothed polynomial representing the curvature of the intact structure. It was suggested that this method is effective in cases when the damage severity is relatively high.

Therefore, the baseline data cannot be obtained accurately based on the current measurements. A precise concrete constitutive law can be used to model the mechanical behavior of the model and then related to the dynamic parameters. This is different from usual model updating because, in this case, the model updating or system identification is the basis for further proceeding in identifying the damage sensitive parameters like cracks, nonlinear parameters, and modal parameters.

## 2.8 Summary

From the above comprehensive review, it can be seen that there have been many developments in the modeling of concrete damage behavior and the vibration-based damage detection. Only a handful of researches have combined these major procedures in use of health monitoring of structures. Based on the above review, the uniaxial constitutive relations will be used in compression and tension and incorporated in the plastic modeling of concrete and the continuum damage model (Figure 2.10). The details in developing this model are given in Chapter 4.

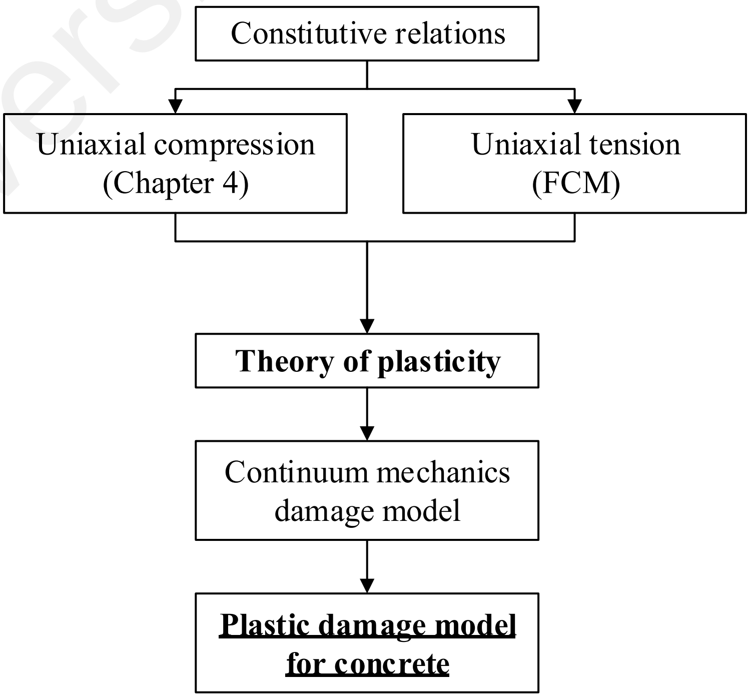


**Figure 2.10:** Components of plastic damage model (CDPM)

Based on the above review, following conclusions can be drawn

- Nonlinear modeling methods for vibrations are more sensitive to damage as compared to the linear vibration methods.
- A bilinear crack model is not suitable for modeling nonlinear vibration characteristics of the beam, a nonlinear crack model on the other hand, replicates the vibration response of a structure.
- Super-harmonics, being the characteristics of non-linear behavior, are more pronounced when the excitation frequency is approximately half of the first natural frequency. This is very useful in tests performed on concrete because, the super-harmonics may be lost in the noise of vibration.
- Plasticity approach has been used successfully used in modeling concrete, but has not been used to characterize nonlinearities in reinforced concrete beams with evolution of damage. In simple words, plasticity approach has not been used in detecting nonlinear behavior through simulation.
- The damage detection through nonlinear characteristics is at its premature stage but the prospects of damage detection with eliminating the need of baseline data are high while proceeding with these methods.

Plasticity model when coupled with continuum mechanics damage model to model concrete represents the phenomena of permanent strains and the stiffness reduction. The monotonic, cyclic stress-strain states, crack closure behavior can be used to validate the efficacy of the model with the experimental investigations on concrete. This concrete model can then be used in modeling of a reinforced concrete beam, which when damaged, can be used to characterize nonlinear behavior with evolution of damage.

# CHAPTER 3: IDENTIFYING NONLINEAR BEHAVIOR

## 3.1 Introduction

A review on of literature in the previous chapter shows the importance of non-linear behavior modeling using more accurate concrete damage mechanisms and using them in health monitoring of structures. This short chapter presents the use of concrete damaged plasticity model in modeling the nonlinear behavior in a reinforced concrete beam. The material properties for reinforced concrete beam model were taken from a recent research (Hamad et al., 2015). The nonlinear characteristics such as formation of super-harmonics are studied based on the data from a previous study. Similar procedure is followed using modal dynamic analysis, which uses linear approach in analysis. On a comparison - It was found that the modal dynamic analysis was not capable of reproducing nonlinear behavior.

## 3.2 Identifying Nonlinear behavior

For identifying nonlinear behavior, a constitutive law was selected and implemented in finite element modeling of a reinforced concrete beam, which was loaded with four-point incremental static loading. After every loading cycle, the dynamic testing was performed to identify the nonlinear behavior. The results were compared with a similar recent research (Hamad et al., 2015). The complete procedure involved in this investigation is shown in Figure 3.1.

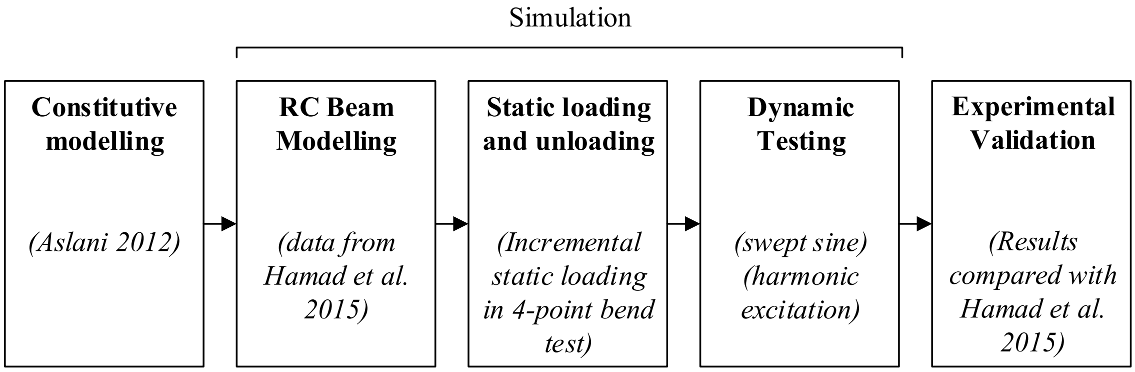


**Figure 3.1:** Summary of preliminary methodology for identifying nonlinear behavior

The main idea of the investigation by Hamad et al., (2015) was to propose an efficient methodology which could reproduce the vibration behavior of concrete. The model was implemented into the framework of Euler Bernoulli's Beam theory, where the model was capable of flexural crack formation. The model proposed was efficient, accurate and represented the vibration behavior of concrete. It was established that the damage could be detected at initial stages successfully using the aforementioned approach.

Concrete behaves different in compression, tension, combined compression and tension. And this behavior has to be considered while modeling concrete. Plasticity-based approaches have proven to be more accurate in that regard but are argued to be computationally expensive. However, the advancements in computation power of computers have allowed us to investigate computationally costly approaches. This chapter is aimed at using uniaxial constitutive relations to complete stress-strain behavior of concrete, and implement on an RC beam model to investigate whether nonlinear behavior can be reproduced with increasing damage or not.

The methodology involves material modeling, finite element modeling, simulating static damage, and simulating the harmonic excitation to detect nonlinear behavior. The details of the steps involved are summarized in Figure 3.1 and further detailed in the rest of the chapter.

### 3.3 Nonlinear behavior characterization (Preliminary Study)

A finite element modeling was carried out based on the existing specimen details. Commercial finite element software, ABAQUS was used for this purpose (Dassault Systèmes, 2013). Concrete damaged plasticity model (CDPM) was used to model concrete stress-strain behavior in compression and tension.

#### 3.3.1 Description of reference model and material properties

Recently, a simplified model for degradation in vibration characteristics of reinforced concrete beams was presented (Hamad et al., 2015). The model incorporated fictitious crack model (Hillerborg et al., 1976) for modeling cracking behavior in concrete was capable of reflect the crack formation while satisfying the assumptions of Euler Bernoulli's beam theory. To validate the model, experimental investigation was carried out on a set of three reinforced concrete beams.

Normal weight concrete with ultimate compressive strength of 36.5 MPa was used for casting of beams. The tensile strength of concrete was taken as 10% of the ultimate compressive strength. Clear cover of 20mm was provided to the reinforcement. The main bottom reinforcing bars were Type-2 bars (ribbed bars) and the remaining reinforcement was provided as plain bars. The material properties for concrete and steel reinforcement are shown in Table 3.1 and Table 3.2 respectively.



**Table 3.1:** Mechanical properties of concrete (Hamad et al., 2015)

| Density (Tonne/mm$^3$) | $f_{cu}$ (*MPa*) | $f_{ct}$ (*MPa*) | $E_{cm}$ (*GPa*) | $\nu_c$ |
|---|---|---|---|---|
| **2.400E-9** | 36.500 | 3.650 | 26957.850 | 0.150 |

**Table 3.2:** Mechanical properties of steel reinforcement (Hamad et al., 2015)

| Bar type | $D_o$ (mm) | $f_y$ (MPa) | $E_s$ (MPa) | $\varepsilon_s$ | $\nu_s$ | $\rho_s$ kg/m$^3$ |
|---|---|---|---|---|---|---|
| **Plain Bars** | 6 | 393.600 | 208000 | 0.250 | 0.300 | 7850 |
| **Main Bars** | 10 | 540.800 | 199200 | 0.320 | 0.300 | 7850 |

The beam was loaded in four-point bending and a vibration shaker was placed right below the loading point. The loading was applied in the increments of 10% of the ultimate beam capacity until the beam failed. After each static loading cycle, dynamic loading was applied using a vibration shaker and the response was recorded. The geometric properties, static loading setup and the dynamic testing regime are shown in Figure 3.2. The complete experimental procedure was reproduced numerically to detect the presence of nonlinearities.

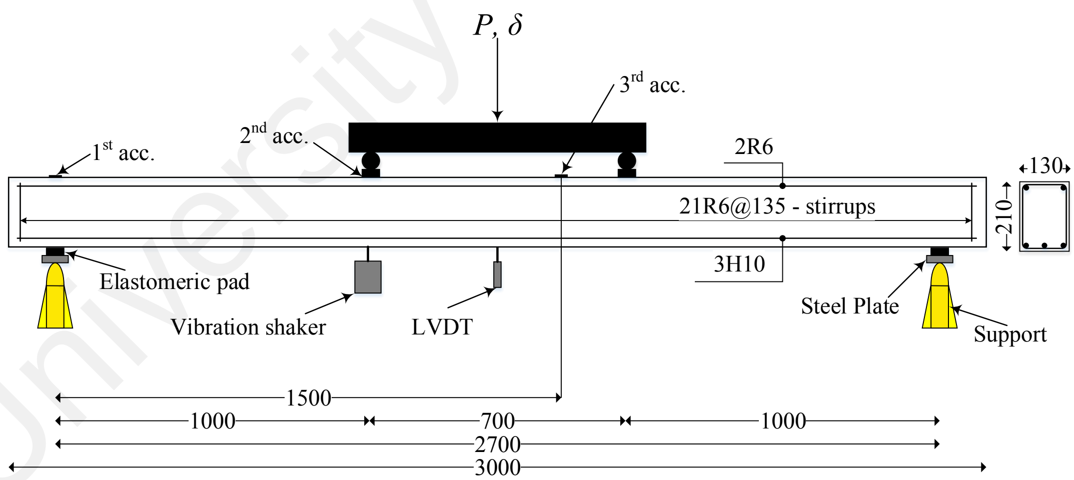


**Figure 3.2:** Reference test setup for detecting nonlinearities (Hamad et al., 2015)

### 3.3.2 Constitutive Law and FE modeling

The stress-strain relation proposed by Carreira and Chu (1985) was used for this investigation because of its simplicity and dependence only on one input parameter; the compressive strength of concrete. Concrete damaged plasticity model (CDPM) was used for concrete modeling in the finite element software, ABAQUS. CDPM couples the plasticity and a damage model in compression and tension to represent the cyclic behavior of concrete. The relation between inelastic stress and inelastic strain are shown in Figure 3.3. The compressive and tensile damage evolution can also be seen there. It can also be seen that there is no damage in compression until the ultimate compressive strength is reached.

The tensile stress strain can be seen in Figure 3.3. The post-crack non-linear strain was chosen based on model by Aslani & Jowkarmeimandi (2012). This model gives representation of stress-strain behavior from the fictitious crack model (Hillerborg et al., 1976). A rigorous research on investigating FCM can be found elsewhere (Hordijk, 1992).

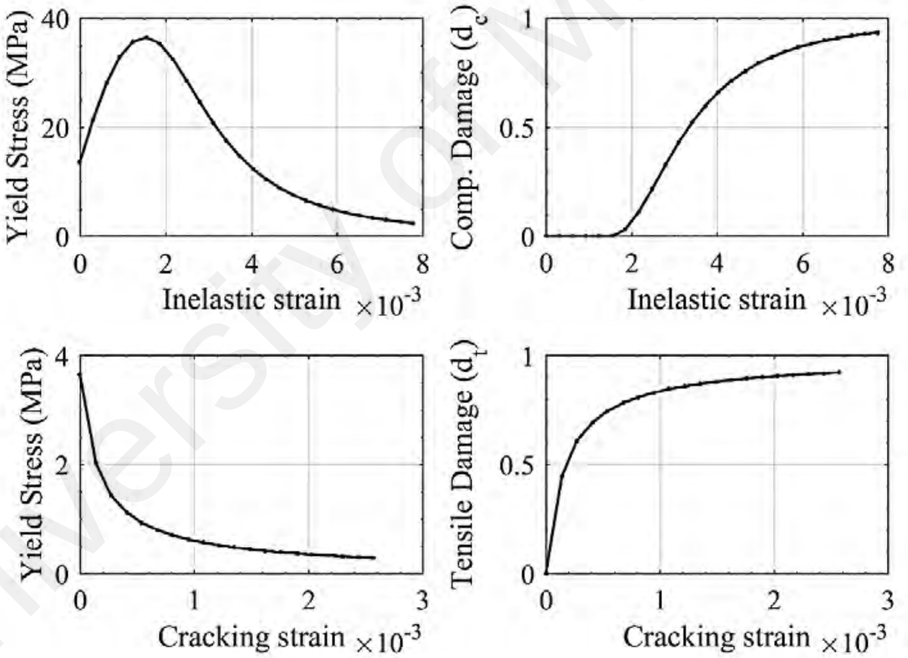


**Figure 3.3:** Constitutive relations using CDPM (Aslani & Jowkarmeimandi, 2012)

The modeling of beam was done using finite element software ABAQUS using constitutive relations shown in Figure 3.3. The boundary conditions were specified as a combination of a roller and a hinge, which was suitable for calibrating with the first natural frequency with the tested beam. The beam model was then subjected to static four-point bending. The loading was divided into ten equal incremental steps of the total percentage of the maximum failure load. After each loading increment, the beam was unloaded and the response of the beam was recorded in the form of displacement using a harmonic excitation. A complete procedure involved can be seen in the flowchart shown in Figure 3.4.

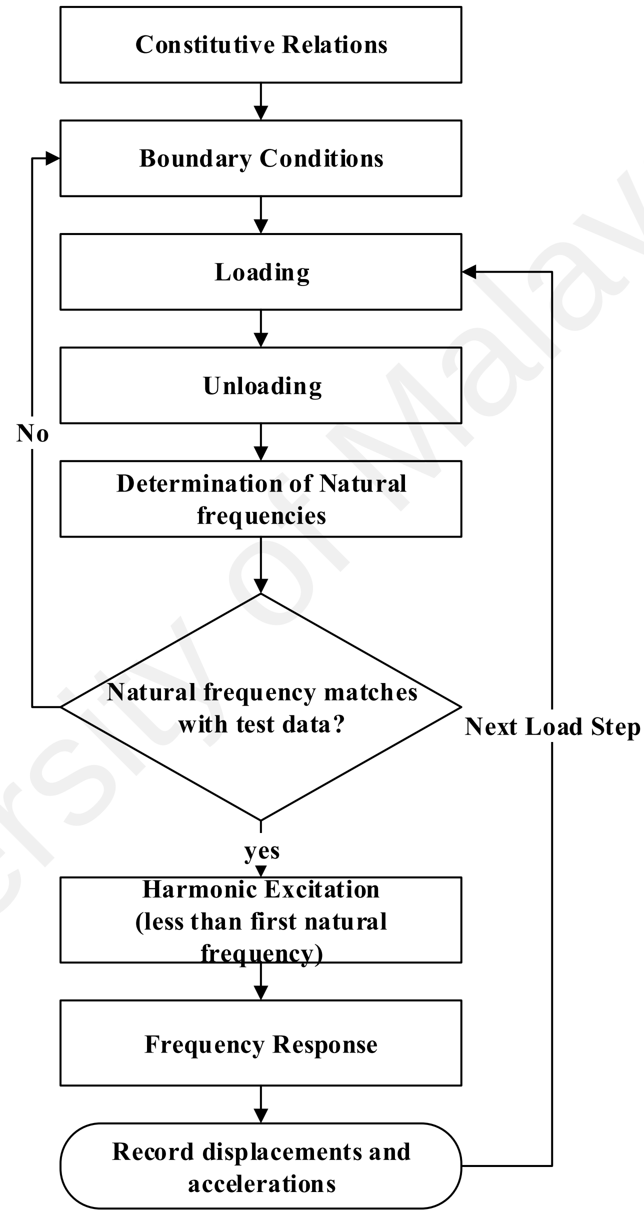


**Figure 3.4:** Flow chart for finite element simulation for detecting nonlinear behavior

### 3.3.3 Simulation results

#### 3.3.3.1 Load-Deflection results

For four-point loading, the deflections were recorded at the mid-span of the beam. The load-deflection response was recorded for comparison with the experimental data. The load deflection response was then compared with the model proposed by Hamad et al., (2011a) for a 50% damage load. The load-deflection response of the current model agrees well with the model reference model. The current model shows slightly less stiff behavior compared to the reference model, which can be attributed to the support conditions and effects of the multiaxial behavior, which have been ignored in the reference model. The comparison of the load-deflection plots is shown in Figure 3.5.

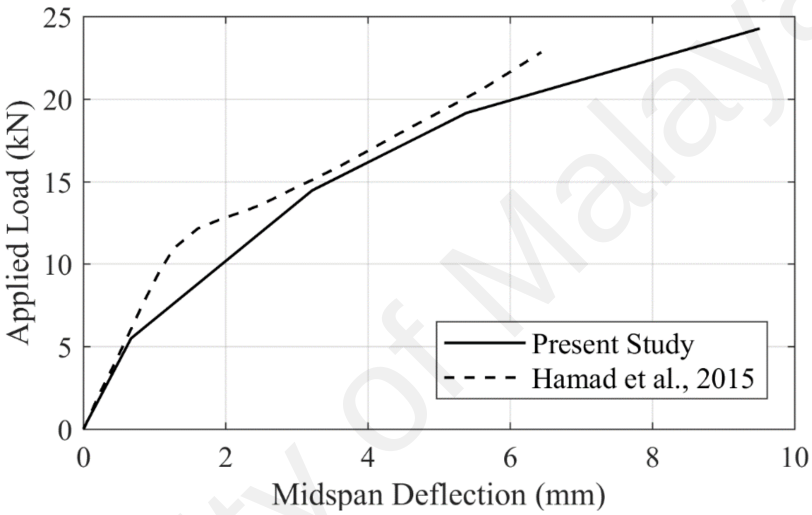


**Figure 3.5:** Static load-deflection plot comparison with Hamad et al., (2015)

#### 3.3.3.2 Crack propagation

The CDPM was capable of reproducing the inclined crack propagation, which shows the capabilities of this model in multiaxial stress-states. The cracking pattern was compared with the analytically developed flexural model (Hamad et al., 2015). The reason for crack investigating crack propagation was to validate the capability of the present study for mixed-mode crack formation. The major cracks seemed to be significantly vertical to match the cracking pattern predicted by similar research (Hamad et al., 2015), which assumed the initiation of the cracks along the stirrup lines. The slight differences in the crack formation were refined using a finer mesh. The present study validates the initiation of cracks by the flexural damage model at lower damage levels, as shown in Figure 3.6. The dotted lines are overlain along the initiation of the cracks in similar research, which gives an idea of the crack formation in the simulated model. The onset of the vertical cracks was inclined, which indicates the capability of the present study for mixed-mode cracking as well, which can be separately investigated by applying a three-point loading. The mixed-mode cracking in the cracking is a combination of flexural and shear (or torsion) cracking, which is the practical case scenario for damage being induced in structures.

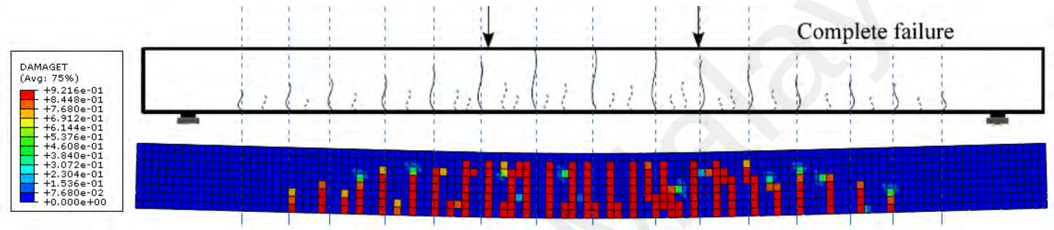


**Figure 3.6:** Comparison of cracking (below) with Hamad et al., (2015), (above)

#### 3.3.3.3 Modal frequency deterioration

The modal frequency response of the modal analysis is illustrated in Figure 3.7. In the figure, first, five normalized modal frequencies were plotted against the damage levels to see the trend of each mode. In the elastic range, there was no degradation in the natural frequency. The reason for discussing the modal frequency deterioration is to make a comparison with the intensively used past methods (Salawu 1997) with the current study in terms of sensitivity to damage. As the stiffness of the beam reduced with increasing damage, there was a reduction in the natural frequency but not significant enough even at complete failure. In field conditions, this small difference in response can be easily influenced by environmental conditions. Herein, the study attempted to analyze the deterioration of the system with the use of a fewer modes. The decline in the first modal frequency by non-linear analysis was performed by Hamad et al., (2011b), as illustrated in Figure 3.7, which also showed degradation in natural frequency but not enough to overcome the environmental effects in field application.

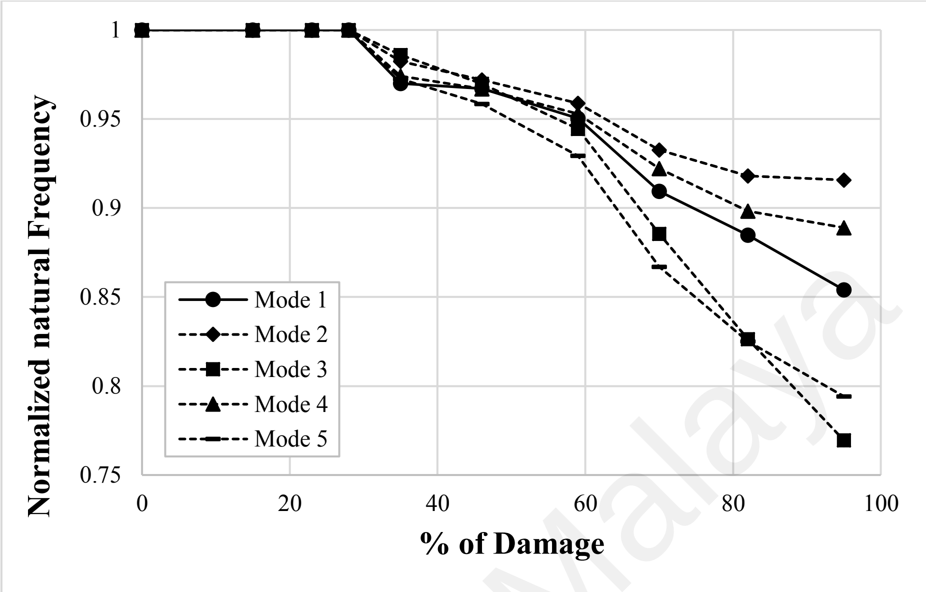


**Figure 3.7:** Reduction in normalized frequency against the percentage of damage

#### 3.3.3.4 Linear and Nonlinear dynamic analysis

The dynamic response of the structure for each damage level is shown in Figure 3.8 (a). The structure was loaded and unloaded monotonically incrementally to induce damage. Modal dynamic analysis was performed after each loading cycle (Ewins, 1984). A harmonic excitation was applied with a frequency of 30 Hz for 5 seconds. The response of the system was transformed to frequency domain using Fast Fourier Transform (FFT), and the formation of super-harmonics was. The procedure showed that there was no formation of super-harmonics at any damage level, as shown in Figure 3.8(a). Hence modal dynamic analysis, which assumes the system to be linear, is not suitable for replicating the nonlinear behavior computationally.

The dynamic implicit analysis was done through a significantly lower time step (0.0001 s). Again, a harmonic excitation was applied at a frequency of 30 Hz for 5 s. The response, transformed like previously, is illustrated in Figure 3.8 (b). The formation of super-harmonics with increasing damage is the indication of presence of nonlinear behavior.

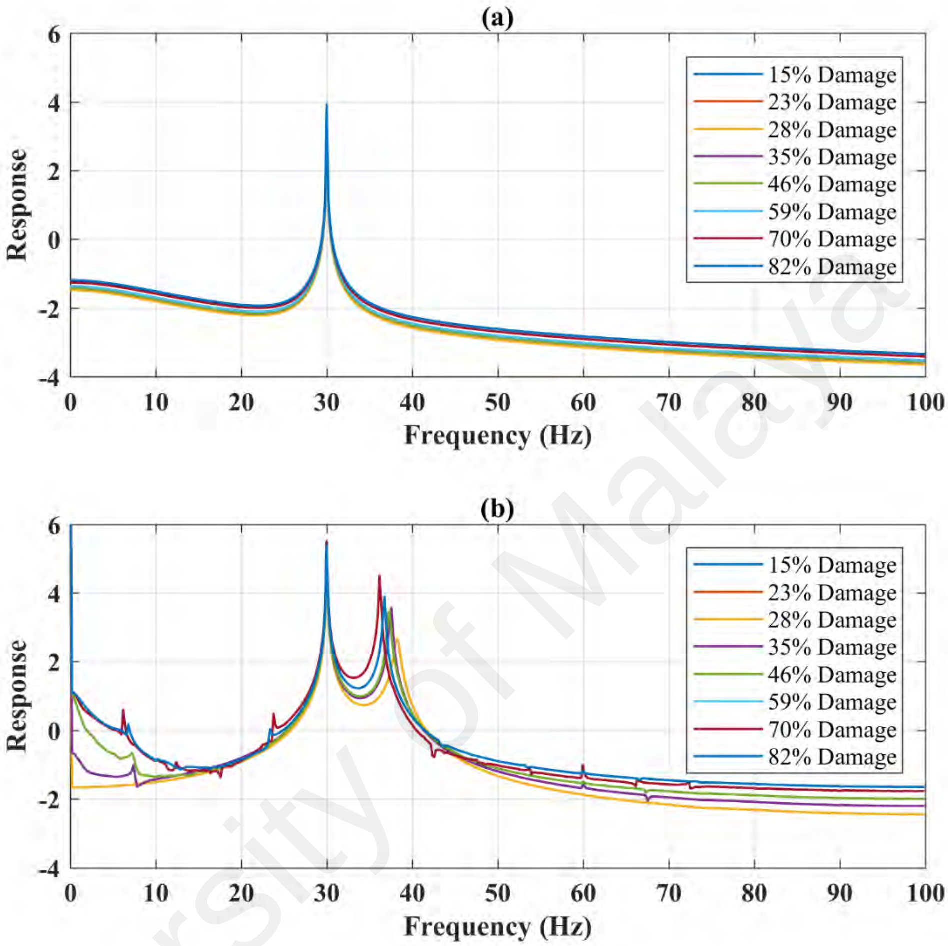


**Figure 3.8:** Comparison of response to harmonic analysis (a) linear (b) non-linear

The formation of super-harmonics indicated the presence of nonlinearity. The super-harmonics amplitude was compared with each damage level to investigate the trend of increase in damage to the nonlinearity. It can be seen that the non-linearity increased up to 35% of damage and then decreased, and after a damage level of 50% it showed a different behavior. The trend of amplitude of super-harmonics with increasing damage can be seen in Figure 3.9. According to the results, the nonlinearity increases up to the 35% damage level and then starts decreasing after the 46% damage level. This implies that the presence of nonlinearity is at its maximum at lower damage levels, and starts reducing when the damage is further increased. The non-monotonic behavior of the nonlinearity with increasing damage agrees well with the previous studies (Hamad et al., 2015; Neild et al., 2003a). Therefore, the nonlinear behavior can be a damage indicator at lower damage levels. A similar trend of non-linearity with damage has also been observed elsewhere (Hamad et al., 2015; Neild et al., 2003a).

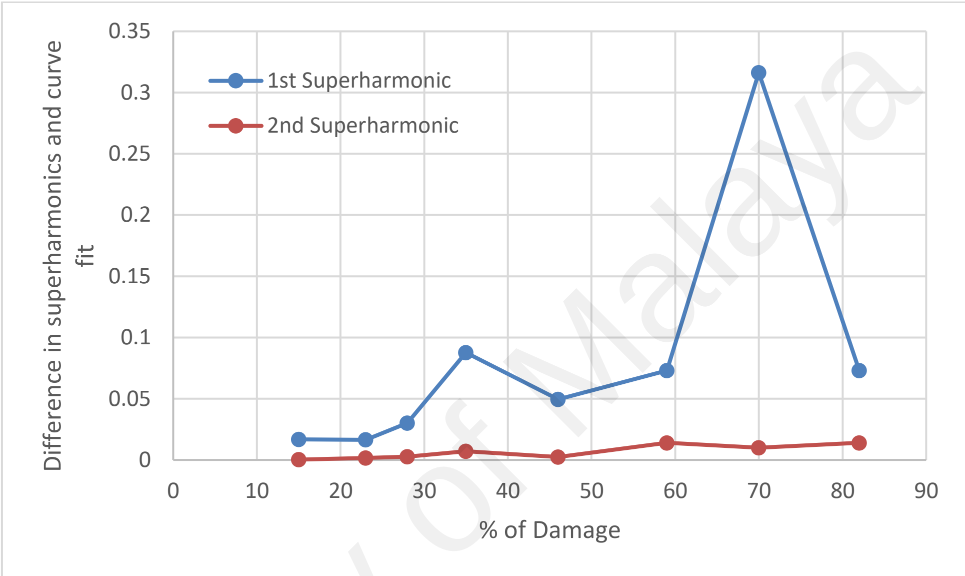


**Figure 3.9:** Nonlinear trend (super-harmonics) against damage

## 3.4 Initial findings and proceeding further

The procedure explained in this chapter was aimed at replicating the nonlinear behavior in RC structures through FE modeling. It was found that the coupling of plasticity and continuum damage model is capable of replicating the nonlinear behavior in RC beams. It was also found that the incremental damage used in model can give more insights into relating the model with the damage mechanisms involved in the actual structure. Furthermore, a comparison with the modal dynamic analysis shows that modal dynamic analysis is not capable of detecting the nonlinear behavior. It was also found that the nonlinear characteristics do not vary in a monotonic manner with increasing damage.

Based on the initial findings, the methodology proposed can be summarized in Figure 3.10. The main steps are constitutive modeling (Chapter 4), investigation on an RC beam (Chapter 5), detecting and characterizing nonlinear behavior (Chapter 6), and using the nonlinear behavior to propose a damage assessment method which does not rely on baseline data and resolves the inverse engineering problem (Chapter 6).

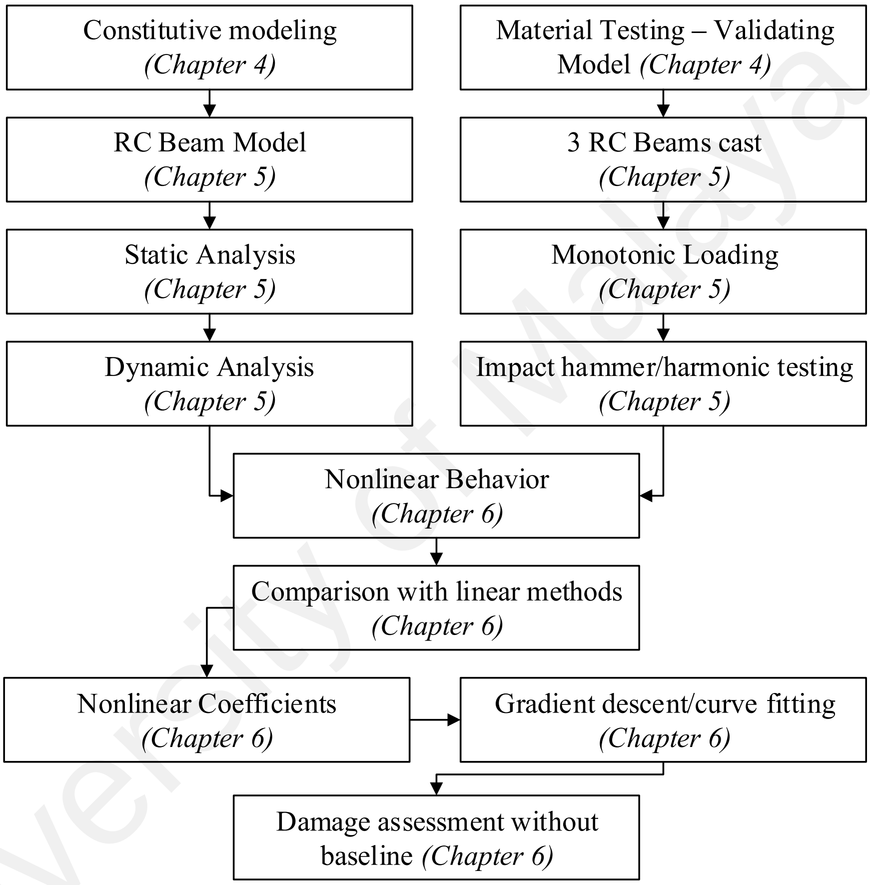


**Figure 3.10:** Summary of steps involved in proposing damage assessment method

# CHAPTER 4: MODELING OF REINFORCED CONCRETE

## 4.1 Introduction plasticity approach

Numerous concrete models have been proposed in last decades. These concrete models are either microscopic or macroscopic. The microscopic models are more sophisticated models and they describe only certain aspects of concrete behavior. The practicality of these models is limited to very few applications. The macroscopic models on the other hand, are based on theory of elasticity, theory of plasticity and fracture mechanics theory (Comité euro-international du béton, 1996). The plasticity and fracture mechanics models can simulate the mechanical behavior of concrete, but they are dependent on the parameters which are not easy to obtain from conventional laboratory tests (Sima et al., 2008). Aslani & Jowkarmeimandi (2012) presented a constitutive model that was capable of replicating concrete behavior in any case of uniaxial monotonic or cyclic loading. The input data for complete constitutive model could be obtained through conventional laboratory tests. This chapter is aimed at presenting a constitutive model that represents the concrete behavior at macroscopic level, can be dependent on conventional uniaxial laboratory tests, easy to implement in FE formulations and is capable to replicate the vibration behavior of cracked concrete.

The classical theory of plasticity has been used to model concrete degradation with permanent strains. However, these modeling approaches have not been able to capture the stiffness degradation due to damage. There is a limitation for using the plasticity approach in cyclic loading - which is the stiffness degradation due to progressive damage (Feenstra & De Borst, 1996). This may be suitable for monotonic loading arrangements, but for cyclic loading, the stiffness degradation is not possible. Furthermore, the experimental investigations show that this stiffness degradation is quite significant for tensile damage but not for compression damage.

Similarly, the continuum damage mechanics model (Kachanov, 1958) has been used to model concrete for linear elastic analysis of concrete where the degradation is governed by a set of internal variables. This model was quite a success in capturing concrete behavior for uniaxial conditions but didn't find any success in more complex loading arrangements where permanent strains were significant (Voyiadjis & Taqieddin, 2009).

Therefore, the capabilities of plasticity (plastic irreversible damage phenomenon) and the continuum damage mechanics models (elastic stiffness degradation due to damage) were coupled to present the model which catered these two mechanisms. The strengths and shortcomings of the plasticity and continuum damage mechanics behavior can be visualized in Figure 4.1.

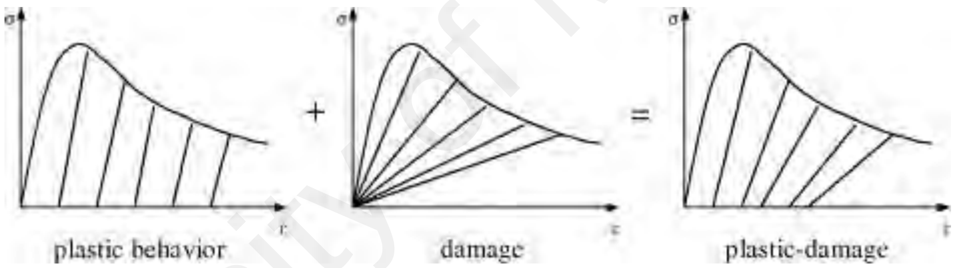


**Figure 4.1:** Plastic and damage behavior of concrete (Tao & Phillips, 2005)

It can be seen in Figure 4.1 that the coupling of plasticity and damage mechanics models, collectively called as concrete damaged plasticity model (CDPM), describes the mechanical behavior of concrete with permanent strains as well as stiffness degradation. Furthermore, the concrete models based on the laboratory tests for compression as well as tension can be incorporated this CDPM.

## 4.2 Uniaxial constitutive relations

Constitutive relations in uniaxial compression and tension are the input parameters for CDPM models. This section presents a review of these models and the selection of the simplest but the accurate model for incorporating in CDPM. The efficacy of the models under investigation was validated through comparison with laboratory tests from the previous researches.

### 4.2.1 Concrete in uniaxial compression

Concrete in uniaxial compression consists of three parts, the linear part, the hardening part and the softening part. Concrete in uniaxial compression is assumed to act linearly until 40% of the compressive strength. Then hardening occurs, followed by softening. A typical stress-strain shape of concrete in compression is shown in Figure 4.2.

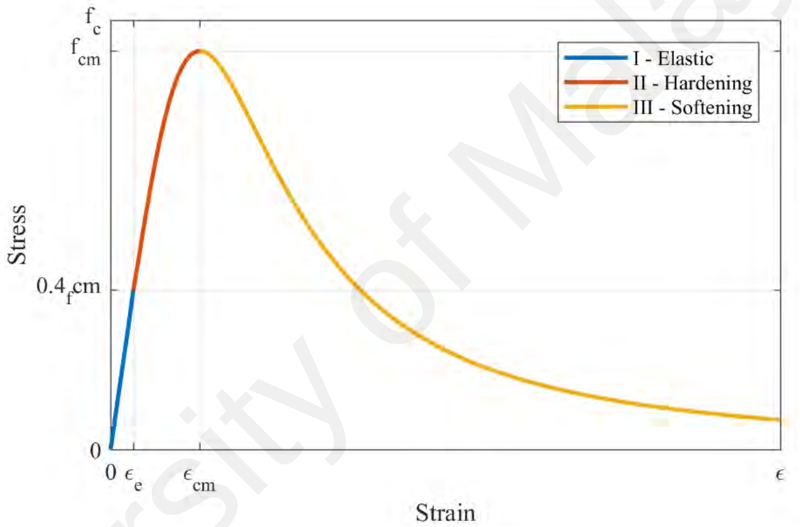


**Figure 4.2:** Parts of uniaxial compressive stress-strain curve

For different concrete strengths, the initial modulus of elasticity ($E_o$) varies with the strength. The slope of the hardening and softening branches also varies with the strength, as shown in Figure 4.3 (Papanikolaou & Kappos, 2007; Wischers, 1978). Concrete behaves differently for different compressive strengths. For high strength concrete, the softening branch acts in a brittle manner as compared to the lower strength concrete. This variation in softening behavior needs to be incorporated in the constitutive modeling to be applicable to most of the concrete strengths (Breccolotti et al., 2015).

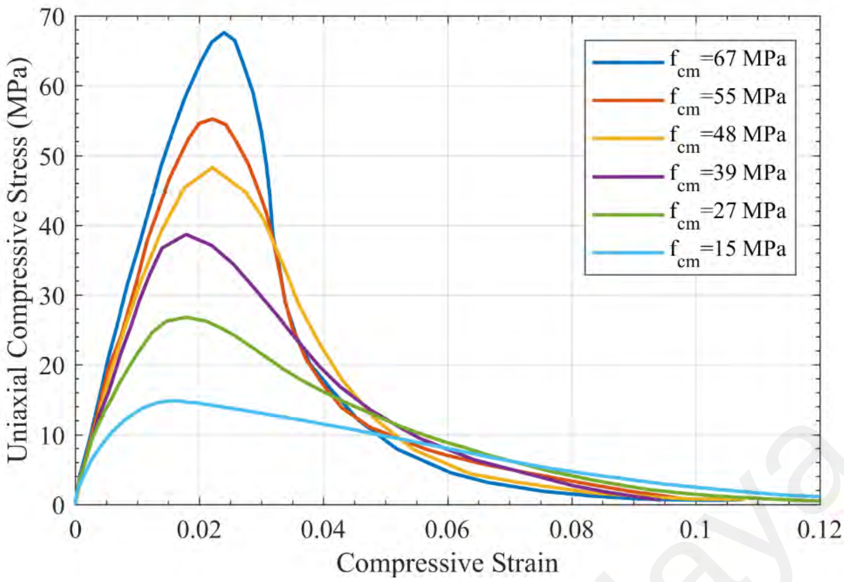


**Figure 4.3:** Complete stress strain curves, reproduced from (Wischers, 1978)

The behavior of the softening branch in cyclic stress-strain was further observed by comparing the compressive tests performed by different researchers for normal strength concrete. Figure 4.4 shows the normalized reduction in slope of softening branch with increase in strength (Karsan & Jirsa, 1969; Okamoto et al., 1976; Sinha et al., 1964; Tanigawa & Uchida, 1979). This entire range is classified as normal strength concrete. The normalized experimental plots show that higher the strength, brittle will be the softening branch and vice versa.

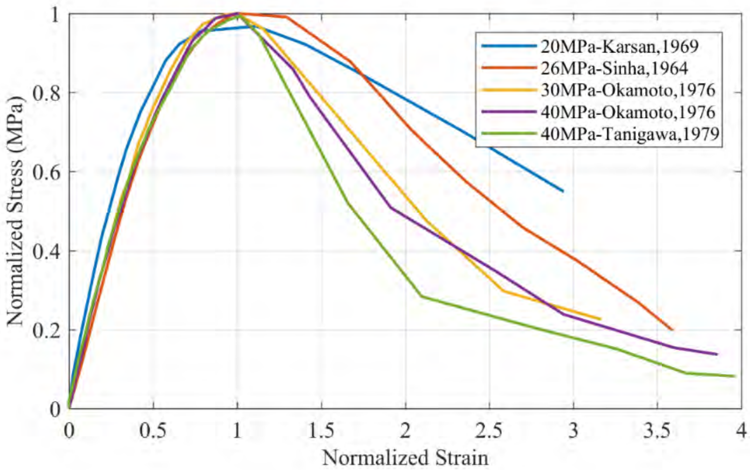


**Figure 4.4:** Experimental compressive stress-strain curves (peak picking method)

To debate on the hardening and softening branches, numerous concrete models have been investigated. The review of most of the models can be found in Babu et al., (2005). The softening behavior of these models was studied using the experimental data shown in Figure 4.4. The results of the studied models are summarized in Figure 4.5 (Ali et al., 1990; Carreira & Chu, 1985; Cervera et al., 1987; Desayi & Krishnan, 1964; EN1992-1-1, 2004; Majewski, 2003; Pavlović et al., 2013; Wang & Hsu, 2001). A comparative analysis of these models showed that Carreira and Chu (1985) model was most suitable for this investigation, as it showed more accurate softening behavior. Furthermore, the model depends only on compressive strength, which is easy to obtain from conventional laboratory tests. This model uses a parameter $\beta_c$ which governs the shape of the stress-strain diagram and the softening branch of the stress strain curve, and initial tangent modulus ($E_{it}$). The equation for stress-strain behavior is given below:

$$\frac{f_c}{f_{cm}} = \frac{\beta_c\left(\frac{\epsilon}{\epsilon_{cm}}\right)}{\beta_c - 1 + \left(\frac{\epsilon}{\epsilon_{cm}}\right)^{\beta_c}} \tag{4-1}$$

Using the initial tangent modulus, $E_{it}$, the value of $\beta_c$ is

$$\beta_c = \frac{1}{1 - \left(\frac{f_{cm}}{\epsilon_{cm} E_{it}}\right)} \tag{4-2}$$

Where, $E_{it}$ is the initial tangent modulus, which can be estimated, according to Hognestad (1951), as:

$$E_{it} = \frac{f_{cm}}{\varepsilon_{cm}}\left(\frac{24.82}{f_{cm}} + 0.92\right) \tag{4-3}$$

According to CEB-FIP Model Code (CEB-FIP, 1991), undamaged modulus of deformation, $E_0$ can be calculated as

$$E_0 = E_{it}(0.8 + 0.2\frac{f_{cm}}{88}) \tag{4-4}$$

Only one input parameter $f_{cm}$, is required to get the initial elastic, hardening and softening stress-strain behavior of concrete in uniaxial compression. Furthermore, the uniaxial stress strain behavior agrees satisfactorily with the experimental results, and shows more precise softening behavior.

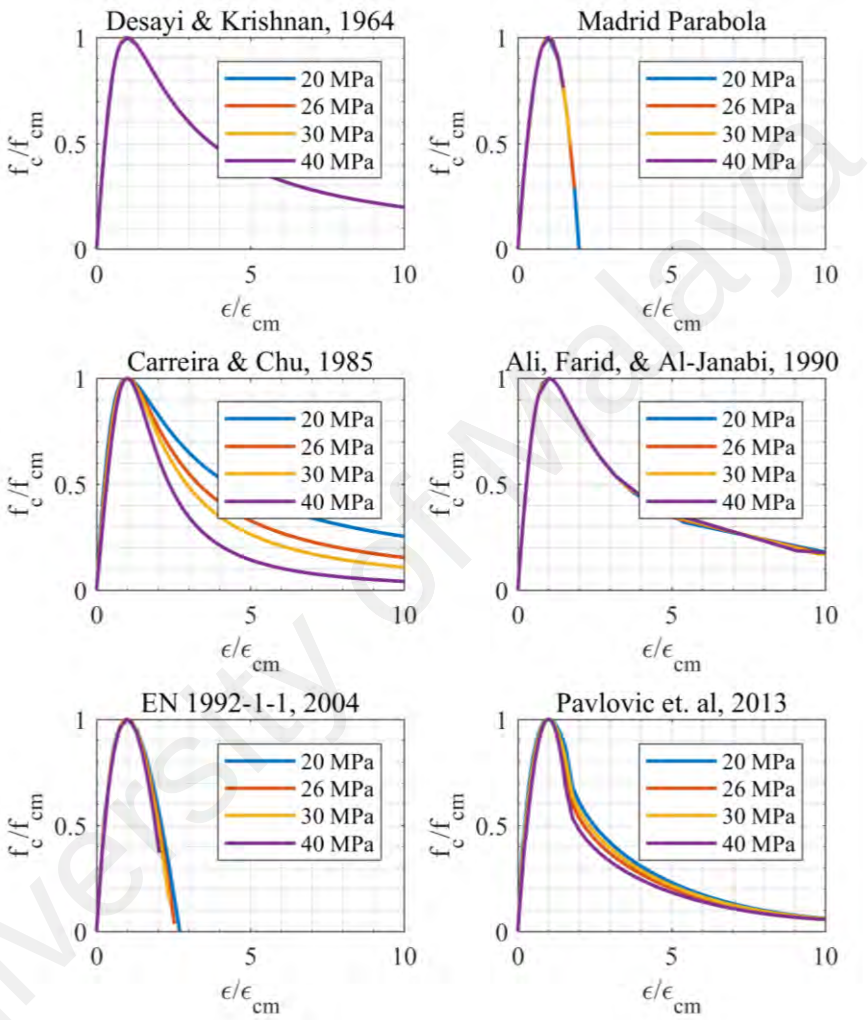


**Figure 4.5:** Concrete compressive stress-strain models

The model by Carreira & Chu (1985), showed good agreement with the experimental stress-strain behavior, as shown in Figure 4.6, for concrete strengths of 20 MPa, 26 MPa, 30 MPa and 40 MPa.

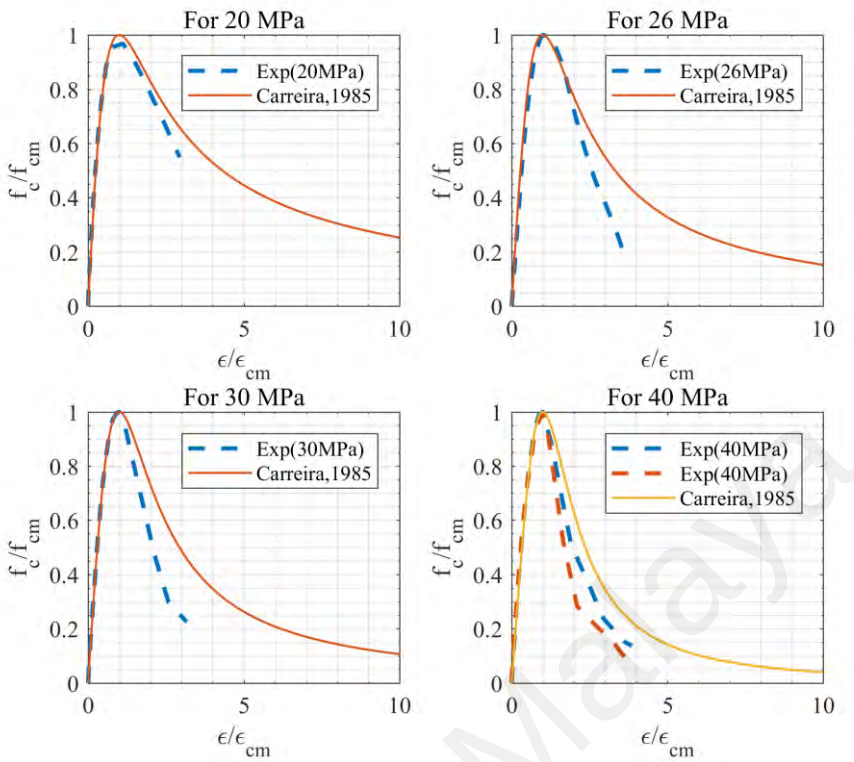


**Figure 4.6:** Carreira & Chu (1985) model comparison with experimental data

In short, the complete uniaxial stress-strain behavior of concrete in compression can be obtained by using Equation 4-1 using the value of compressive strength ($f_{cm}$) measured from compression test in the laboratory.

### 4.2.2 Concrete in uniaxial tension

Unlike in compression, the stress-strain behavior of concrete in tension cannot be easily reproduced experimentally. The onset of tensile crack formation can be observed with servo-controlled loading, as done by Hordijk (1991). Usually, in design practices, the split cylinder strength is used to represent the tensile strength. Or the tensile strength is also approximated as 10 percent of the compressive strength of concrete.

For studying concrete in tension, a small overview of the microstructure of concrete is presented here. Studies of microstructure of concrete show that the cracks initiate at the interfacial transition zone (ITZ); the zone that separates the aggregates from the cement paste. This zone is formed during the mixing of concrete, where the aggregate and the paste get separated by a fewer cement particles and more water molecules. Therefore, as the concrete makes its final set, micro-cracks are already present in this transition zone, which further penetrate into the paste where they merge to form a continuous crack (Hsu et al., 1963; Nemati & Monteiro, 1997; Ringot & Bascoul, 2001; Shah & Chandra, 1970). Figure 4.7 shows the cracks in ITZ by the procedure of etching, where the cracks are seen as the protruding surfaces in the image. These cracks are in random directions and the propagation of these cracks is the reason for presence of nonlinear behavior in concrete.

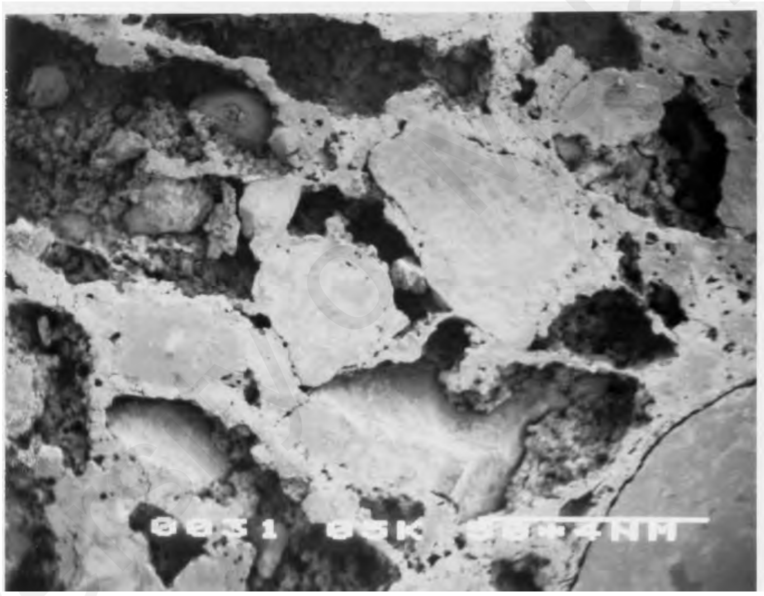

**Figure 4.7:** Cracks in interfacial transition zone (ITZ) (Nemati & Monteiro, 1997)

Accordingly, the tensile constitutive relation of concrete can be divided into two parts, a linear elastic ascending branch, and a softening branch (Figure 4.8). The softening branch is either modeled as linear or bilinear (CEB-FIP, 1991) for convenience in calculations. The concrete acts in almost linear way before reaching the tensile strength. When the maximum stress is reached, the micro-cracks develop into a concentrated zone. This implies that the further deformation will be caused in the micro-crack region while the rest of the region acts in elastic manner. At peak tensile strength, when the crack forms, the softening starts. There are cohesive stresses present in the fracture zone –

which is present at the crack tip and exhibits reduced stress concentration. This is more realistic representation of crack formation as compared to the linear elastic fracture mechanics (Petersson, 1981). From the point of representing the behavior, the stress-crack width (*w*) relation is used. Therefore, the combined stress-strain and stress-crack opening is termed as stress-displacement. According to experiments performed by Hordijk (1991); after the crack initiation, the stresses start reducing until they become zero, while the crack width (*w*) increases until it reaches the critical crack width ($w_c$). According to Hamad et al., (2013), the nonlinear vibration characteristics rely on this post-peak behavior, in which the transferrable stresses depend on crack opening. Unlike compressive stress-strain behavior, the slope of softening branch doesn't vary much with change in strength and can be generalized to the post-peak relation in tension, given by Equation 4-5.

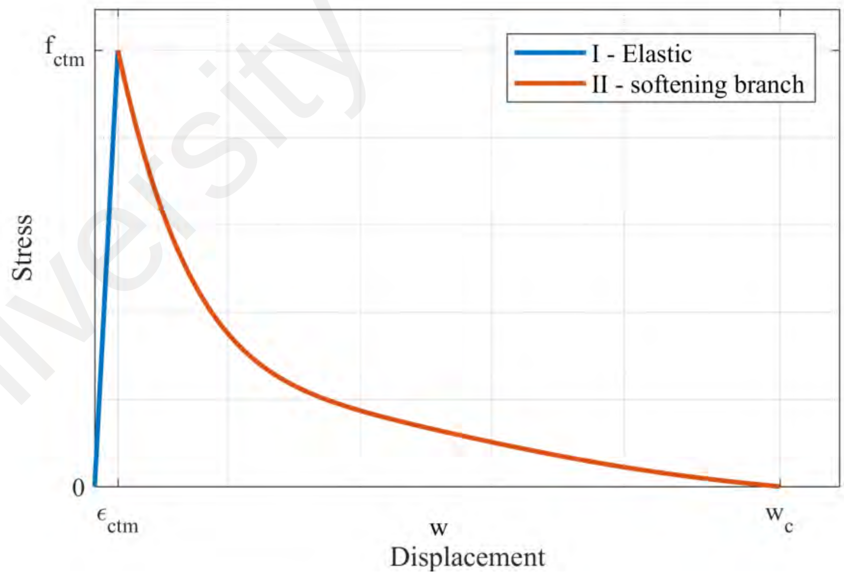


**Figure 4.8:** Tensile stress-displacement relation

Based on a number of tensile strength tests done on plain concrete, a non-linear fit was found which can give the post-peak response of concrete for any strength of concrete, as shown in Figure 4.9 (Hordijk, 1991). The relation for post-peak response is shown in Equation 4-5.

$$\frac{f_{ct}}{f_{ctm}} = [1 + \left(C_1 \frac{w}{w_c}\right)^3 ]e^{-C_2\frac{w}{w_c}} - \frac{w}{w_c}(1 + C_1^3)e^{-C_2} \tag{4-5}$$

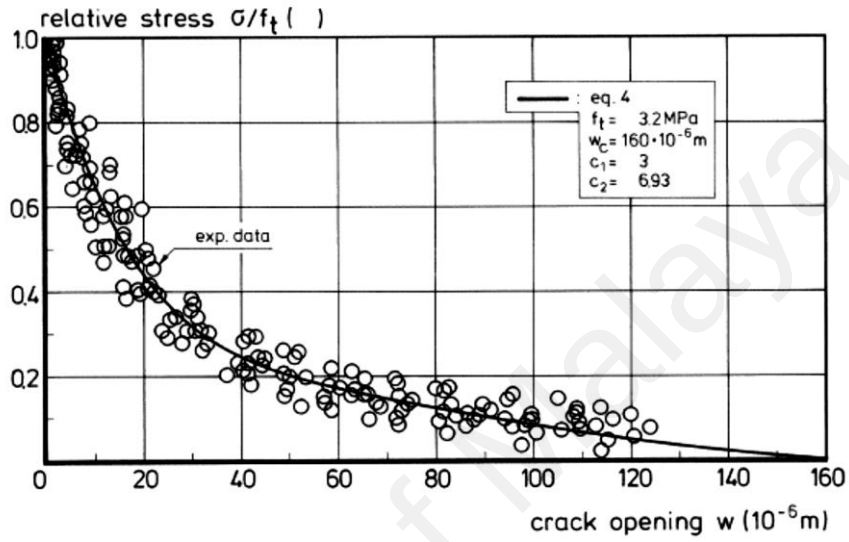


**Figure 4.9:** Tensile stress (*$f_{ct}$*) vs crack width *(w)* Relationship, from Hordijk (1991)

Where $C_1$ and $C_2$ are constants with values of 3 and 6.93 respectively. $f_{ctm}$ is concrete tensile strength, which can be calculated from CEB-FIP (1991). The critical crack width ($w_c$) is the maximum crack width where the tensile stress becomes zero. The value of $w_c$ can be calculated using fracture energy as presented in Equation 4-6.

$$w_c = 5.14 \times \frac{G_F}{f_{tm}} \tag{4-6}$$

The fracture energy ($G_F$), with units of N/mm can be calculated from by following equation (Phillips & Binsheng, 1993).

$$G_F = \frac{43.3 + 1.13 f_{cm}}{1000} \tag{4-7}$$

Therefore, the combined action of stress-strain and stress-crack width is called as stress-displacement relationship. While incorporating in finite element model, the respective displacements can be transformed into the respective strains, by dividing by the characteristic length ($l_{eq}$), to get a collective stress-strain constitutive relation in tension.

### 4.2.3 Reinforcing Steel

Reinforcing steel cyclic test results show the presence of stress redistribution after reaching the yield, point also called as Bauschinger's effect, as shown in Figure 4.10 (Thompson & Park, 1978). For isotropic model of concrete, the reinforcing steel contribution is kept mostly remains linear and the nonlinear behavior is the most prominent at lower damage levels (Hamad et al., 2015; Neild et al., 2002). Therefore, an elastic-perfectly plastic (bilinear) stress-strain curve was used for modeling reinforcement in the concrete beams, as elastic-perfectly plastic model generally gives acceptable response prediction of RC beams (Neale et al., 2005). Furthermore, the interaction between the concrete and the reinforcement was done using the embedded region constraint (Dassault Systèmes, 2013).

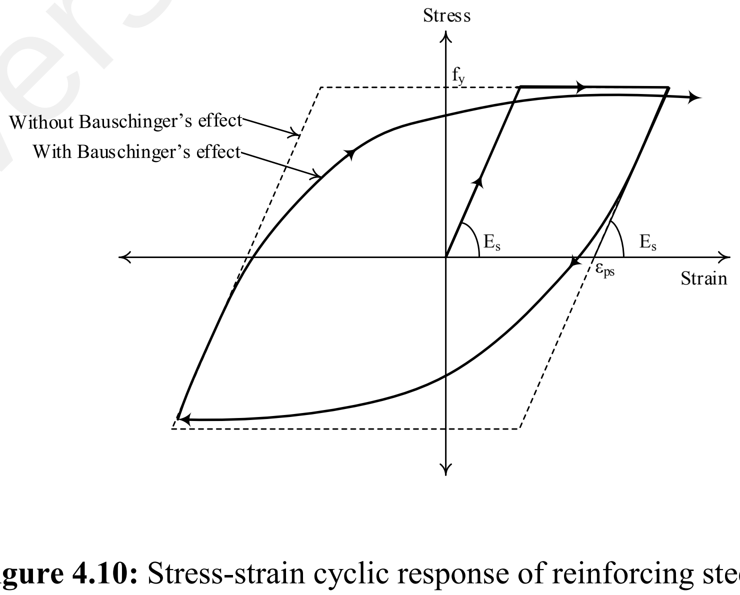


**Figure 4.10:** Stress-strain cyclic response of reinforcing steel

### 4.3 Concrete damaged plasticity model (CDPM)

The plasticity approach is a phenomenological approach in modeling concrete. Due to obtaining the mechanical behavior in different stress states without complicated modeling and comparatively lower computation cost, makes it very popular approach in modeling concrete. In this study, the uniaxial stress-strain relations from Carreira & Chu (1985) model in compression and fictitious crack model in tension were incorporated in the CDPM to represent the cyclic behavior of concrete. The components of CDPM are explained below

#### 4.3.1 The plasticity Theory

Generally, the theory of plasticity requires a yield criterion, a hardening rule and a flow rule. For plastic deformation, certain assumptions are made according to Ragab & Bayoumi (19989).

- Isotropy throughout the plastic deformation
- The material is incompressible (plastic incompressibility)
- The yield stress is independent of hydrostatic pressure, yielding is only influenced by the deviatoric stress components of the stress tensor
- Bauschinger's effect for cyclic loading is ignored
- Rate independent response

Out of all the models incorporating plasticity, elastic strain-hardening plastic model more accurately defines concrete. The components of this model, according to Hu & Schnobrich (1989), are (a) a yield function that defines the yield surface, (b) a hardening rule that defines the motion of yield surfaces, (c) a flow rule that non-linearly relates plastic strains to stresses, (d) a uniaxial stress-strain curve, and (e) a plastic hardening modulus. The model development, based on these components is explained below.

### 4.3.2 Yield Function

Yield function defines the initial and the subsequent yield surfaces. This stress function defines the initial yield function before the plastic deformations occur. Within the yield surface, the stress states are elastic. For a biaxial case, the biaxial compression, biaxial tension and the combined stress states are shown in Figure 4.11 (a). The respective idealized uniaxial stress-strain curve for the same stress states can be seen in Figure 4.11 (b). For the compressive stress reaching the failure uniaxial compressive strength ($f_{cm}$) and tensile stress reaches tensile strength ($f_{ctm1}$ and $f_{ctm2}$ in orthogonal principal directions), the failure curve forms similar to the outer-most curve shown in Figure 4.11 (b). A yield function of the form is shown in Equation (4-8).

$$f(\sigma_1, \sigma_2, \sigma_c, \sigma_{t1}, \sigma_{t2}) \tag{4-8}$$

Where, $\sigma_1$ and $\sigma_2$ are the stress point components on yield curve, $\sigma_c$ is the yield value in compression, and $\sigma_{t1}$ and $\sigma_{t2}$ are the yield values in tension in respective orthogonal principal directions. Therefore, the function $f$ can be used to obtain the failure conditions of two uniaxial limiting strengths (compressive and tensile) in a biaxial space. The experimental investigation of biaxial behavior of concrete has been done previously (Kupfer et al., 1969).

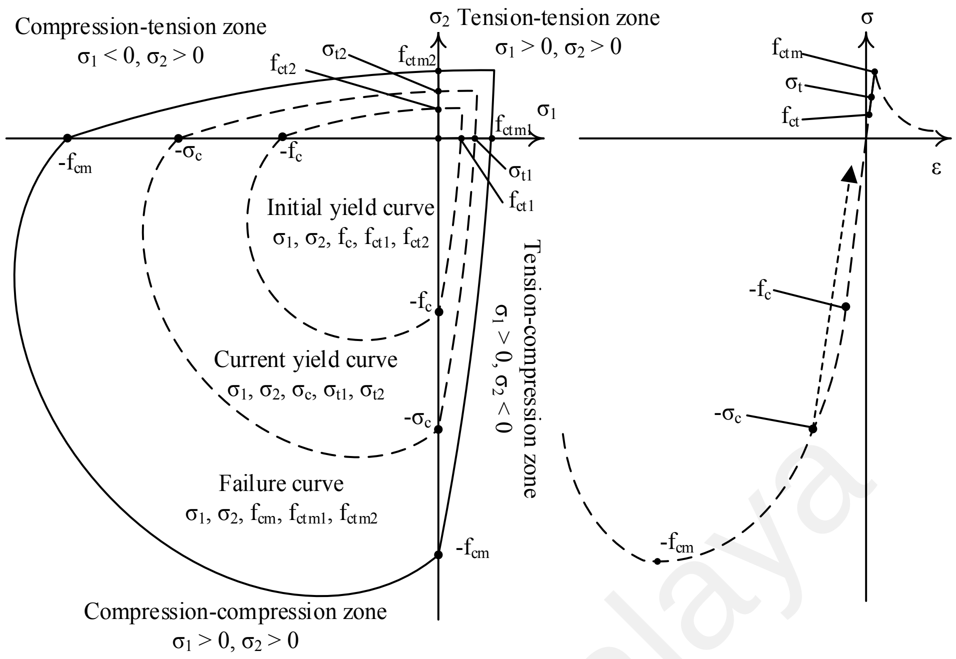


**(a) Biaxial case** **(b) Idealized uniaxial case**

**Figure 4.11:** Schematic yield surfaces, from Chen (2007)

In this study, the yield function proposed by Lubliner et al., (1989) and improved by Lee & Fenves (1998) was adopted. The generalized yield function ($F$) in terms of effective stresses ($\bar{\sigma}$) is detailed below

$$F = \frac{1}{1-\alpha}\left(\alpha I_1 + \sqrt{3J_2} + \beta(\hat{\sigma}_{max})\right) \qquad (4\text{-}9)$$

Which, according to (Alfarah et al., 2017; Lubliner et al., 1989), is given as

$$F = \frac{1}{1-\alpha}\left(q - 3\alpha p + \beta\langle -\sigma_{max}\rangle - \gamma\langle -\sigma_{max}\rangle\right) - \bar{\sigma_c} \leq 0 \qquad (4\text{-}10)$$

Where α, $\beta$ and γ are dimensionless material constants (Equations 4-14, 4-15 and 4-16), $\bar{\sigma_c}$ is the effective compressive cohesion stress ($\bar{\sigma_c} = \sigma_c(1 - d_c)$) and $\sigma_{max}$ is the maximum principal effective stress. The description of $d_c$ can be found in Section 4.3.5. The effective hydrostatic pressure ($p$) or the first effective stress invariant is given by

$$p = -\frac{1}{3}\bar{\sigma}: I \qquad (4\text{-}11)$$

And the second effective stress invariant is given as Mises equivalent effective stress ($q$) is given as

$$q = \sqrt{\frac{3}{2}(\bar{S}:\bar{S})} \tag{4-12}$$

$\bar{S}$ is the effective stress deviator, defined as

$$\bar{S} = \bar{\sigma} + pI \tag{4-13}$$

$$\alpha = \frac{{f_{b0}}/{f_{c0}} - 1}{2\left({f_{b0}}/{f_{c0}}\right) - 1} \tag{4-14}$$

Where $f_{b0}/f_{c0}$ is the ratio of biaxial compressive yield strength and uniaxial compressive yield strength. According to Lubliner et al., (1989), $\alpha$ values for concrete range between 0.08 and 0.12, and $f_{b0}/f_{c0}$ values lie between 1.10 and 1.16.

$$\beta = \frac{\overline{\sigma_c}}{\overline{\sigma_t}}(1-\alpha) - (1+\alpha) \tag{4-15}$$

Where $\overline{\sigma_c}$ and $\overline{\sigma_t}$ are effective cohesive compressive and tensile stresses, respectively. Their values can be found by $\overline{\sigma_c} = \sigma_c(1-d_c)$, and $\overline{\sigma_t} = \sigma_t(1-d_t)$.

$$\gamma = \frac{3(1-K_c)}{2K_c - 1} \tag{4-16}$$

Where $K_c$ is the ratio of the second stress invariant in the tensile meridian to that of compressive meridian for any value of the pressure invariant ($I_1$) such that the maximum principal stress is negative. A typical value of 2/3 of Kc gives the value of coefficient γ as 3 for concrete.

### 4.3.3 Hardening rule

After the formation of initial yield surface, the hardening rule describes the evolution of subsequent yield surfaces. Different hardening rules can be applied considering the hardening behavior of the material. Three types of hardening rules are available in literature: isotropic hardening (Chen & Chen, 1975; Hill, 1998), kinematic hardening (Prager, 1955; Ziegler, 1959) and mixed hardening (Hodge, 1957). A comparison of isotropic and kinematic hardening can be seen in Figure 4.12.

Isotropic hardening gives the expansion of the yield surface without any distortion or translation. Isotropic hardening rule (Grassl & Jirásek, 2006; Lu et al., 2016; Voyiadjis et al., 2008). In kinematic hardening, the yield surface just translates as a rigid body in the stress space (Menzel et al., 2005; Zhu et al., 2017). Kinematic hardening is popular in the modeling the reinforcing steel (Andriotis et al., 2016; Floros & Ingason, 2013; Frederick & Armstrong, 2007).

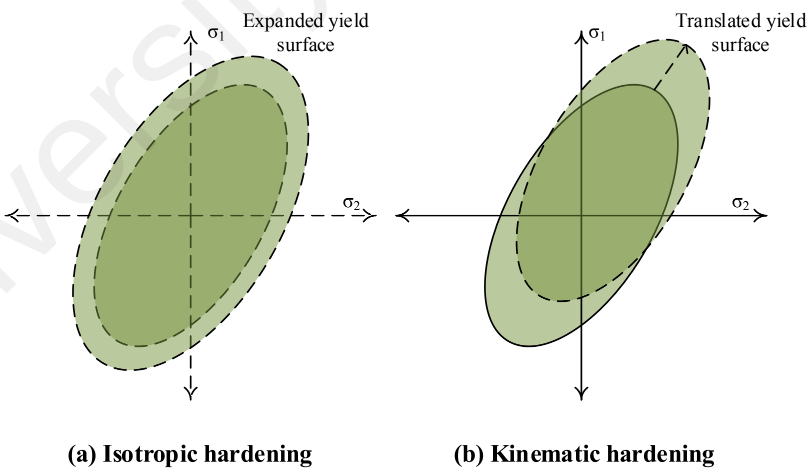


**Figure 4.12:** Hardening models in biaxial stress field (Zait et al., 2010)

The comparative study of the isotropic and kinematic hardening can be found in another research (Zait et al., 2010). The study indicates the influence of the hardening in cyclic or large amplitude single load-unload conditions. For the sake of simplification in calculation without compromising the mechanical behavior, isotropic hardening was used in this model.

### 4.3.4 Flow rule

The increment in strain can be divided into two parts, the elastic part ($d\varepsilon^{el}$) and the plastic part ($d\varepsilon^{pl}$). For isotropic materials, the principal plastic increments are proportional to principal deviatoric stresses ($s_{ij}$).

$$d\varepsilon_{ij}^{pl} = s_{ij} d\lambda \qquad (4\text{-}17)$$

This plastic stress-strain law is known as a flow rule, referred to as Levy Mises flow rule (Gratacos et al., 1992). Keeping in consideration the hardening rule, the flow rule can be written as:

$$d\varepsilon_{ij}^{pl} = d\lambda G_{ij} \qquad (4\text{-}18)$$

Where $G_{ij}$ is a function of stresses or hardening parameters. For symmetric strain, the function is symmetric.

$$d\varepsilon_{ij}^{pl} = d\lambda \frac{\partial g}{\partial \sigma_{ij}} \qquad (4\text{-}19)$$

The function $g$, when differentiated with respect to the stresses, yields plastic strains. This function is called plastic potential function, and the flow rule is called non-associated flow rule. While associated flow rule (normality rule) uses yield function instead of plastic potential and the plastic strain increment in normal to the yield surface. The associated flow rule does not represent concrete behavior in most of the cases and may lead to discrepancies, especially in cases when there is a combination of high compressive and low tensile stresses (Hu & Schnobrich, 1989).

The yield criterion uses non-associated flow rule with Drucker-Prager hyperbolic function, as shown in meridional plane in Figure 4.13. The plastic potential function is given by

$$g = \sqrt{(\epsilon\sigma_{t0}\ tan\psi)^2 + q^2} - p\ tan\psi \qquad (4\text{-}20)$$

Where $\psi$ is the dilation angle measured in p-q plane and is explained in Section 4.4.3. $\epsilon$ is the eccentricity that defines the rate at which the function approaches the asymptote. When eccentricity is zero, the flow potential tends to be a straight line.

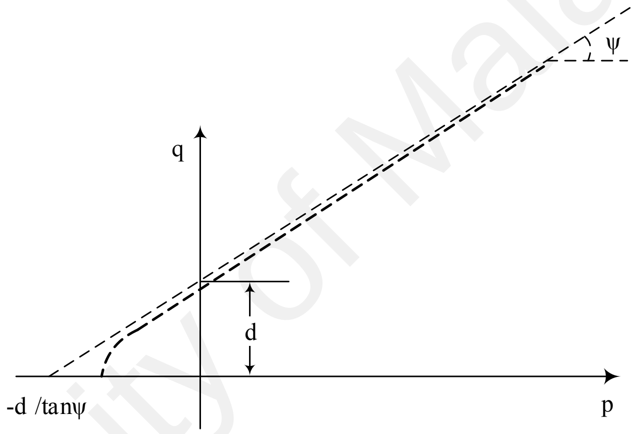


**Figure 4.13:** Example of yield criteria (CDPM) in the meridional (p-q) plane

### 4.3.5 Continuum damage mechanics (CDM)

As proposed by Lubliner et al. (1989), the compressive damage variable can be calculated using continuum damage mechanics model (CDM) from the equation given below

$$d_c = 1 - \frac{1}{2+a_c}\left[2(1+a_c)\exp\left(-b_c\varepsilon_c^{in}\right) - a_c\exp\left(-2b_c\varepsilon_c^{in}\right)\right] \qquad (4\text{-}21)$$

Where $a_c$ and $b_c$ are dimensionless coefficients, as given below.

$$a_c = 2\left(\frac{f_{cm}}{f_{c0}}\right) - 1 + 2\sqrt{\left(\frac{f_{cm}}{f_{c0}}\right)^2 - \left(\frac{f_{cm}}{f_{c0}}\right)} \qquad (4\text{-}22)$$

$$b_c = \frac{f_{c0} l_{eq}}{G_{ch}} \left(1 + \frac{a_c}{2}\right) \tag{4-23}$$

Where $f_{co}$ is the uniaxial compressive yield strength, $l_{eq}$ is the characteristic length or the mesh size, and $G_{ch}$ is the crushing energy per unit area. The crushing energy, $G_{ch}$ can be calculated from fracture energy $G_F$ by the following equations (Phillips & Binsheng, 1993).

$$G_F = \frac{43.3 + 1.13 f_{cm}}{1000} \quad \text{(N/mm)} \tag{4-24}$$

$$G_{ch} = \left(\frac{f_{cm}}{f_{ctm}}\right)^2 G_F \tag{4-25}$$

The plastic strains, in this case plastic compressive strain $\varepsilon_c^{pl}$, using the following relation.

$$\varepsilon_c^{pl} = \varepsilon_c^{in} - \frac{f_c d_c}{1 - d_c E_0} \tag{4-26}$$

The tensile parameters, $d_t$, $a_t$, $b_t$ and the plastic strain $\varepsilon_t^{pl}$, can similarly be calculated by Equations 4-27 to 4-30, respectively.

$$d_t = 1 - \frac{1}{2 + a_t}\left[2(1 + a_t)\exp\left(-b_t \varepsilon_c^{in}\right) - a_t \exp\left(-2 b_t \varepsilon_t^{in}\right)\right] \tag{4-27}$$

$$a_t = 2\left(\frac{f_{ctm}}{f_{t0}}\right) - 1 + 2\sqrt{\left(\frac{f_{ctm}}{f_{t0}}\right)^2 - \left(\frac{f_{ctm}}{f_{t0}}\right)} \tag{4-28}$$

$$b_t = \frac{f_{t0} l_{eq}}{G_F}\left(1 + \frac{a_t}{2}\right) \tag{4-29}$$

$$\varepsilon_t^{pl} = \varepsilon_t^{in} - \frac{\sigma_t d_t}{1 - d_t E_0} \tag{4-30}$$

After that, the inelastic strain, $\varepsilon_c^{in}$ can be calculated by subtracting maximum elastic strain, $\varepsilon_{co}$ from the total strain, $\varepsilon_c$

$$\varepsilon_c^{in} = \varepsilon_c - \varepsilon_{co} \tag{4-31}$$

The modulus of elasticity $E_{cm}$, can be estimated according to Pešić et al. (2015) and Noguchi et al. (2009) as:

$$E_{cm} = 33.5\mathrm{k}_1\mathrm{k}_2\left(\frac{\rho_c}{2400}\right)^2\left(\frac{f_{cm}}{60}\right)^{1/3} \tag{4-32}$$

This completes the constitutive model using CDPM model which is capable of representing the cyclic behavior of concrete in compression and tension. The elastic, plastic behavior in uniaxial and multiaxial stress states was later confirmed based on the simulations carried out on concrete specimens.

## 4.4 Calibration of CDPM

The concrete damaged plasticity model is can be implemented in any finite element subroutine (Dassault Systèmes, 2013). The following subsections give the review of previously used parameters, and based on that, the parameters have been selected. These parameters are the dilatancy angle ($\psi$), flow potential eccentricity ($\epsilon$), the ratio of initial equi-biaxial compressive yield stress to initial uniaxial compressive yield stress ($f_{b0}/f_{c0}$), ratio of the second stress invariant on the tensile meridian to that on the compressive meridian ($K_c$) and the viscosity parameter (or the relaxation time, $\mu$).

### 4.4.1 Compressive constitutive relations (Carreira's model)

The concrete damaged plasticity model is applicable in modeling concrete structures and will be used in this research as a constitutive model in observing damage under monotonic, cyclic and dynamic loading. The model assumes two main concrete failure mechanisms, crushing and cracking, which are assigned through the damage parameters.

The compression and tensile damage parameters can be used to visualize the respective failure mechanisms. The model utilizes stiffness degradation mechanisms (damage) with irrecoverable strains (plasticity).

The concrete damaged plasticity model has been incorporated and comprehensively explained in other researches (Alfarah et al., 2017; Ghaedi et al., 2016). The parameters used in this model include dilation angle ($\psi$), eccentricity ($\epsilon$), the ratio of compressive strength in multiaxial loading to uniaxial loading ($f_{bo}/f_{co}$), the ratio of the second stress invariant on the tensile meridian to that on the compressive meridian ($K_c$) and viscosity parameter ($\mu$). As there has been no explicit indication of using these parameters, hence, the parameters were reviewed based on the past studies. Based on simulations carried out on modeled concrete specimens, the values of 50, 0.1, 1.16, 0.67 and 0.0025 were used for $\psi$, $\epsilon$, $f_{bo}/f_{co}$, $K_c$ and $\mu$, respectively. The uniaxial response of the cyclic loading was compared with different compressive strengths from experimental values.

### 4.4.2 Tensile constitutive relations (fictitious crack model)

After the tensile strength of the concrete is reached, there is softening behavior in concrete. This softening regime is a fictitious crack, which has not formed yet, but it exists until the critical crack width ($w_c$) is reached, where the actual crack is formed. The investigation on crack formation has been recently carried out in modeling concrete cracking behavior (Hamad et al., 2015; Skar et al., 2017). Tensile stress $f_t$ (for crack width ($w$) can be calculated using Hordijk's fictitious crack model (Equation 4-5). The critical crack width, $w_c$, can be calculated using Equation 4-6.

To be on the same path with the recent developments of similar researches, the crack width values have been converted to tensile strains as given in Equation 4-33 (Alfarah et al., 2017).

$$\varepsilon_t = \varepsilon_{ctm} + w/l_{eq} \tag{4-33}$$

### 4.4.3 Dilation angle (ψ)

Vermeer & De Borst (1984) evaluated the existing test data of triaxial tests available to introduce equation for evaluation of the dilation angle. According to them, the behavior of granular materials can be improved by using a non-associated flow rule. A potential function used like Mohr-Coulomb yield surface is used in this model in which the angle of internal friction ($\varphi$) can be replaced by angle of dilation ($\psi$) (Babu et al., 2005; Oñate et al., 1988; Vermeer & De Borst, 1984). Typical Dilation angle values by different related researchers are 13° (Vermeer & De Borst, 1984) and between 8° and 15° (Oñate et al., 1988). Recently, while modelling the different reinforced concrete structural members (frames, beams), the dilation angle value of 13° was chosen (Alfarah et al., 2017).

Obaidat (2011) proposed a finite element modeling framework of investigating the retrofitting of FRP material. In modeling that situation, the dilation angle was used as 37° which is same as angle of internal friction mentioned for modified Coulomb's materials (Nielsen & Hoang, 2011).

It has been pointed out that despite the range assigned analytically, the dilation angle has been used differently in modeling structural situations which cannot be generalized for structural members. The summary of the $\psi$ values used in different researches have been summarized in Table 4.1. It can be seen that the dilation angle was more or less calibrated in these researches and does not necessarily fall in the range specified in the model damaged plasticity model proposed. As the current research focuses on investigating a four-point loading regime on RC beam-type structures, the past research shows the dilation angle values used between 35° and 38°, as shown in Table 4.1.

**Table 4.1:** Summary of usage of $\psi$ in different studies

| Type of simulation | Reference | ψ |
|---|---|---|
| Biaxial Compression test | Lubliner et al. (1989) | 15° |
| Notched Beam mixed fracture | | 32° |
| Simulating 3-point and 4-point bending in beam | Jankowiak & Lodygowski (2005) | 38° |
| RC Beam shear modeling | Birtel & Mark (2006) | 30° |
| Push-out tests of shear studs | Nguyen & Kim (2009) | 20° |
| FRP retrofitting model of RC beams | Obaidat (2011) | 37° |
| Push-out test simulation of bolted shear connectors and headed studs | Pavlović et al. (2013) | 36° |
| RCC slab bend test | Rodríguez et al. (2013) | 30° |
| Nonlinear FE analysis of damaged and repaired RC beams | Aktas & Sumer (2014) | 30° |
| Wedge splitting test for HS concrete | Sitek et al. (2014) | 30° |
| 4-point bending test of RC beams, Test case 1 | Sümer & Aktas (2015) | 37° |
| 4-point bending test of RC beams, Test case 2, 3 | Sümer & Aktas (2015) | 30° |
| - | - | 40° |
| - | - | 50° |
| RC frame modelling | Alfarah et al. (2017) | 13° |
| Precast segmental concrete column modeling for cyclic loading | Li et al. (2017) | 30° |
| Simply supported partially pre-stressed beam | Hafezolghorani et al. (2017) | 31° |

To investigate this, a standard reinforced concrete cylinder (100mm dia, 200mm height) was modeled using FE subroutine and loaded monotonically and the stress strain behavior was studied while keeping rest of the factors, constant (Figure 4.14). A displacement-controlled loading regime was applied on the modeled cylinder. The mesh size was kept at 10mm and the constitutive relations were implemented accordingly.

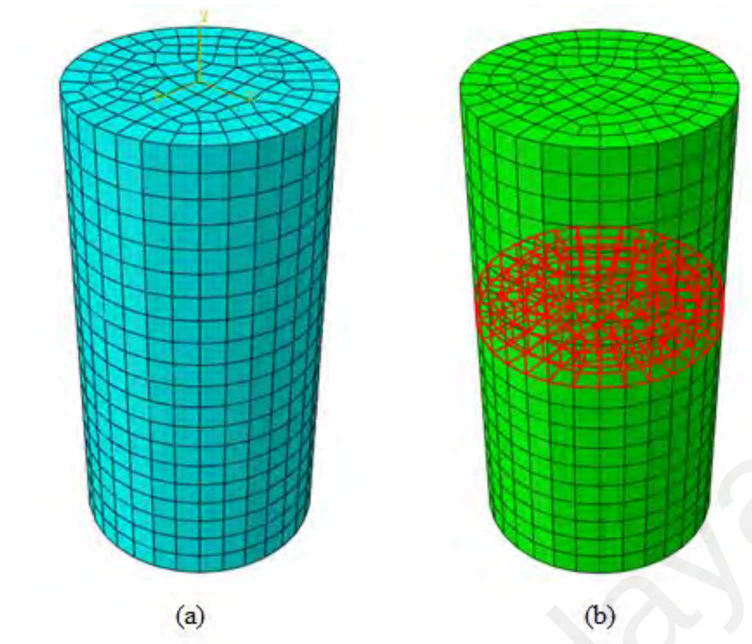


**Figure 4.14:** (a) Simulated Cylinder (b) selected elements for stress-strain behavior

For the desired compressive strength, and keeping rest of the parameters as constant, it can be seen that the post-peak behavior above 35° is not much affected by the dilation angle. The idea was to evaluate the output stress-strain behavior from the input uniaxial stress-strain by simulating the displacement controlled compressive loading on a concrete cylinder model. The stress-strain behavior against different dilation angle values can be seen in Figure 4.15. Based on the simulated stress-strain response, a higher value of dilation angle deviates the strain by 15%, but saves the computation costs. At lower values of dilation angle, the solution of the equations leads to more computation cost, as can be seen by a less smooth declining branch, which for higher values of dilation angle, is a smooth transition. Therefore, the value of dilation angle, for this study, was chosen as 50°.

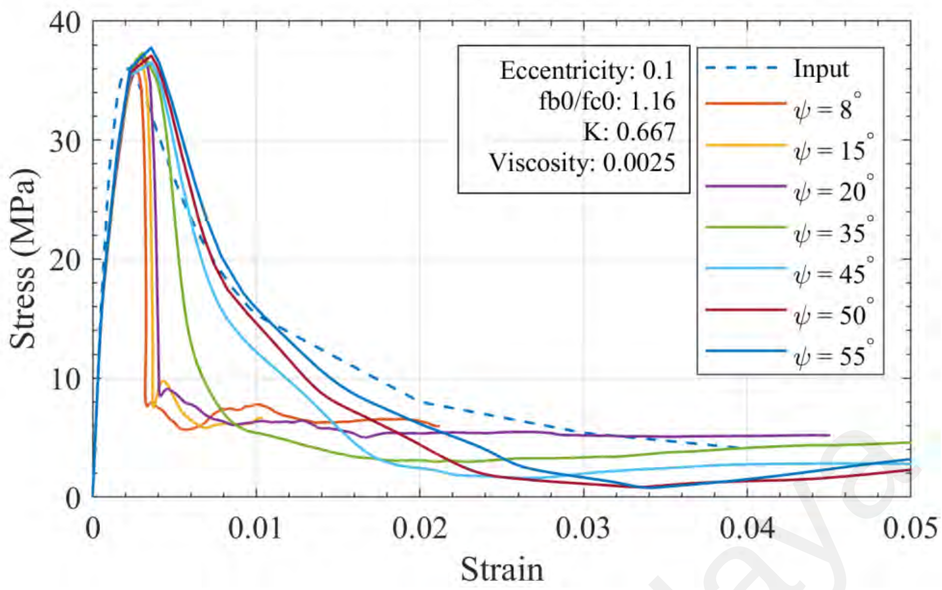


**Figure 4.15:** Effect of dilation angle ($\psi$) on stress-strain relation of concrete

### 4.4.4 Flow potential eccentricity ($\epsilon$)

As the non-associated flow rule is used with the plastic potential function (Equation 4-20), the value of 0.1 was used for the flow potential eccentricity.

### 4.4.5 Initial equi-biaxial compressive yield stress to initial uniaxial compressive yield stress ratio ($f_{b0}/f_{c0}$)

The ratio $f_{b0}/f_{c0}$, refers to the biaxial tests performed on plain concrete blocks by Kupfer et al. (1969). Concrete in biaxial behavior is 16% stronger than in uniaxial compression. For tensile case, the biaxial tensile strength is same as uniaxial tensile strength.

### 4.4.6 Ratio of the second stress invariant on the tensile meridian to that on the compressive meridian ($K_c$)

A typical value of 2/3 of $K_c$ gives the value of coefficient $\gamma$ as 3 for concrete. Therefore, the value of 0.667 was used in this study.

### 4.4.7 Viscosity parameter or Relaxation time ($\mu$)

Viscosity parameter, $\mu$, used for the visco-plastic regularization of the concrete constitutive equations in Abaqus/Standard analyses. The viscosity parameter is used in relation with the loading time. The trials performed for different values of viscosity parameter shows that a higher or lower value of relaxation time overestimates the tensile strength of concrete Figure 4.16.

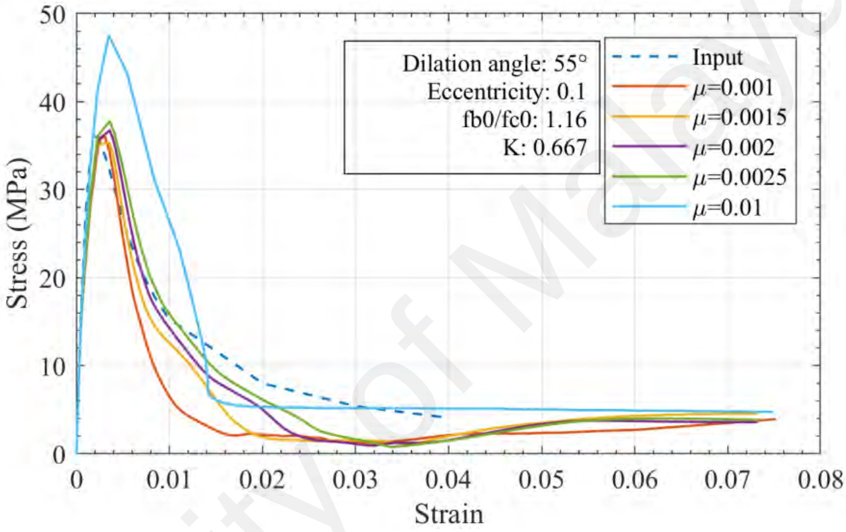


**Figure 4.16:** Effect of viscosity parameter ($\mu$) on stress-strain relation of concrete

A higher value saves the computation time but the stress-strain response deviates from the expected values. A study was carried out for calibrating this factor with respect to the loading time (Szczecina & Winnicki, 2017). Based on the study and the trial simulations run with different values, suitable values of 0.0025 was used for this study.

## 4.5 Model comparison with the past research

The currently developed model will be discussed for different combination of uniaxial cyclic and multiaxial stress-strain response in this section, as follows:

### 4.5.1 Uniaxial cyclic response

The uniaxial cyclic behavior was carried out on the model. It was based on calculation of plastic strains for compression (Equation 4-26) and tension (Equation 4-30). The uniaxial compressive stress-strain behavior, compared with the experimental data (Karsan & Jirsa, 1969; Okamoto et al., 1976; Sinha et al., 1964; Tanigawa & Uchida, 1979), is presented in Figure 4.17. The cyclic uniaxial stress-strain behavior reasonably replicates the experimental cyclic response for the broad range of normal-weight, normal strength concrete with compressive strengths of 20, 26, 30 and 40 MPa. The factor $\beta_c$ was calibrated to match the shape of the stress-strain curve.

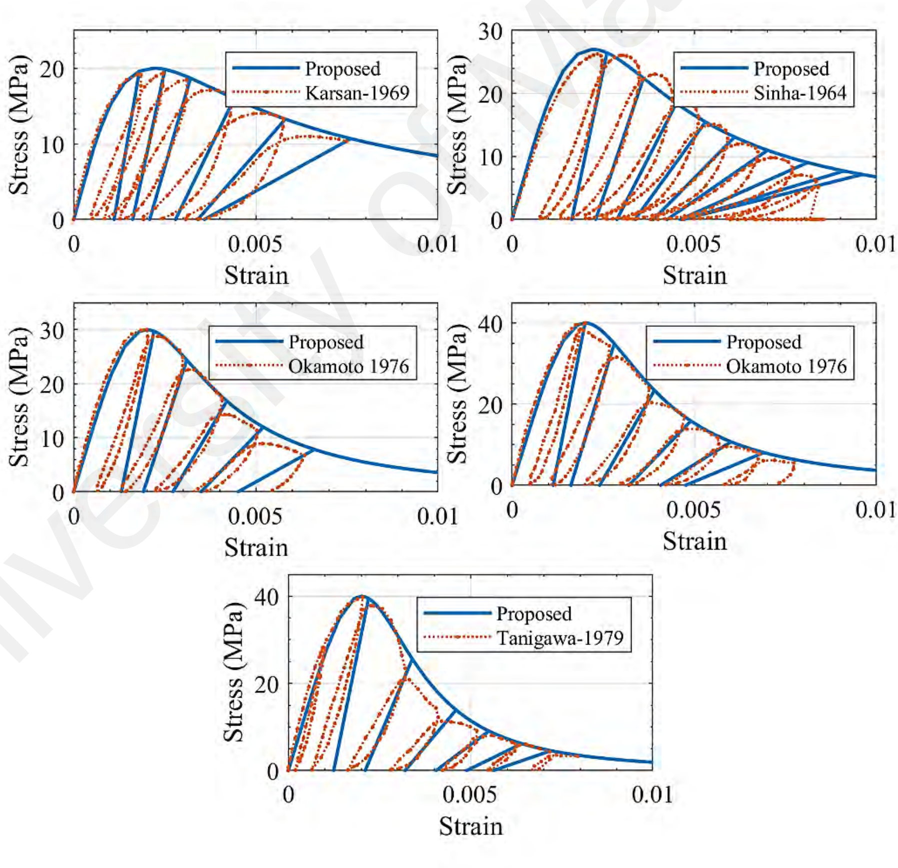


**Figure 4.17:** Comparison of proposed model in cyclic compression with test data

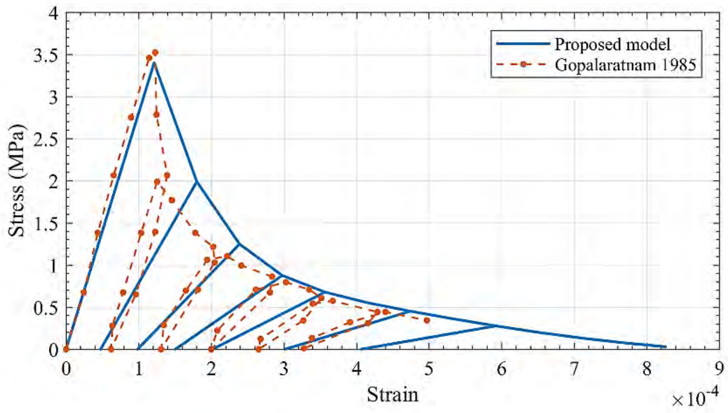


**Figure 4.18:** Comparison of proposed model in cyclic tension with test data

For tensile behavior, there is not significant effect on softening behavior of concrete, but the nonlinear softening behavior is important for the cracking behavior and the crack response to the dynamic loading. The tensile behavior was also compared with the experimental investigation of Gopalaratnam & Shah (1985), for concrete tensile strength of 3.48MPa, as shown in Figure 4.18.

### 4.5.2 Biaxial stress-strain response

The first validation of the proposed model was carried out by verifying the behavior of concrete using the 4-noded bilinear solid element (CPS4). A square shaped block with size 82.6mm x 82.6mm was modeled with mesh size of 20.65mm (Voyiadjis & Taqieddin, 2009). Displacement controlled loading was applied according to the loading conditions shown in Table 4.2. The loading conditions for -1:-1 biaxial compression loading is shown in Figure 4.19.

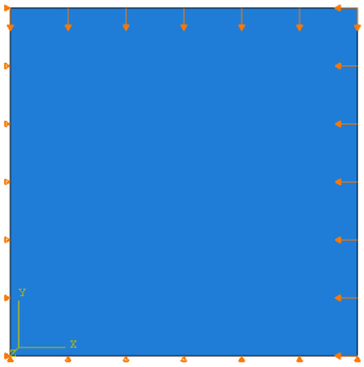

**Figure 4.19:** FE model for studying biaxial behavior (82.6x82.6mm$^2$)

The input material properties are shown in Table 4.2. There were three types of biaxial tests performed – biaxial compression, biaxial tension and combined compression-tension. The compressive stresses and strains are indicated by negative sign, while the tensile stresses and strains have positive values.

**Table 4.2:** Biaxial data from Kupfer et al., (1969)

| Sr. No. | $\sigma_1:\sigma_2$ | $f_{cm}$ (MPa) | $f_{ctm}$ (MPa) | $E_c$ (MPa) | $\varepsilon_{cm}$ | v |
|---|---|---|---|---|---|---|
| 1 | -1:-1 | 32.085 | 2.88765 | 28980 | 0.0022 | 0.2 |
| 2 | -1:-0.52 | 32.085 | 2.88765 | 28980 | 0.0022 | 0.2 |
| 3 | -1:0 | 32.085 | 2.88765 | 28980 | 0.0022 | 0.2 |
| 4 | -1:0.052 | 32.085 | 2.88765 | 28980 | 0.0022 | 0.19 |
| 5 | -1:0.103 | 32.085 | 2.88765 | 28980 | 0.0022 | 0.19 |
| 6 | -1:0.204 | 32.085 | 2.88765 | 28980 | 0.0022 | 0.19 |
| 7 | 1:0 | 28.98 | 2.6082 | 31395 | - | 0.18 |
| 8 | 1:0.55 | 28.98 | 2.6082 | 31395 | - | 0.18 |
| 9 | 1:1 | 28.98 | 2.6082 | 31395 | - | 0.18 |

The biaxial response of the simulation can be seen in Figure 4.20. The computed strains against the applied stress combinations are presented. It can be seen that the biaxial strength of concrete, in state -1:-1, is 16% more than the uniaxial compressive strength, agreeing with the experimental investigation (Kupfer et al., 1969). Similarly, the results of simulation in combined compression-tension and biaxial tension are presented in Figure 4.21 and Figure 4.22, respectively. For biaxial tension, there is no effect on the tensile strength of concrete.

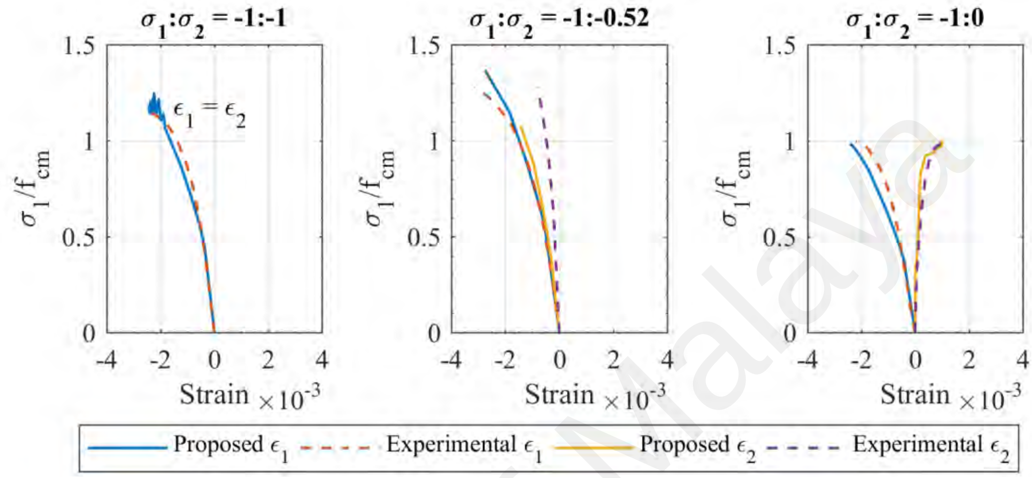


**Figure 4.20:** Model comparison with biaxial compression tests (Kupfer et al., 1969)

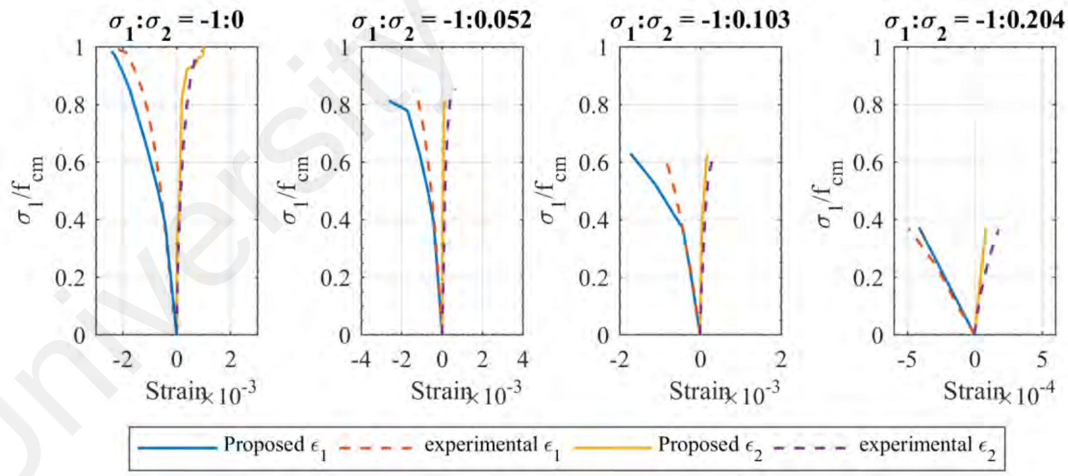


**Figure 4.21:** Model comparison with compression-tension tests (Kupfer et al., 1969)

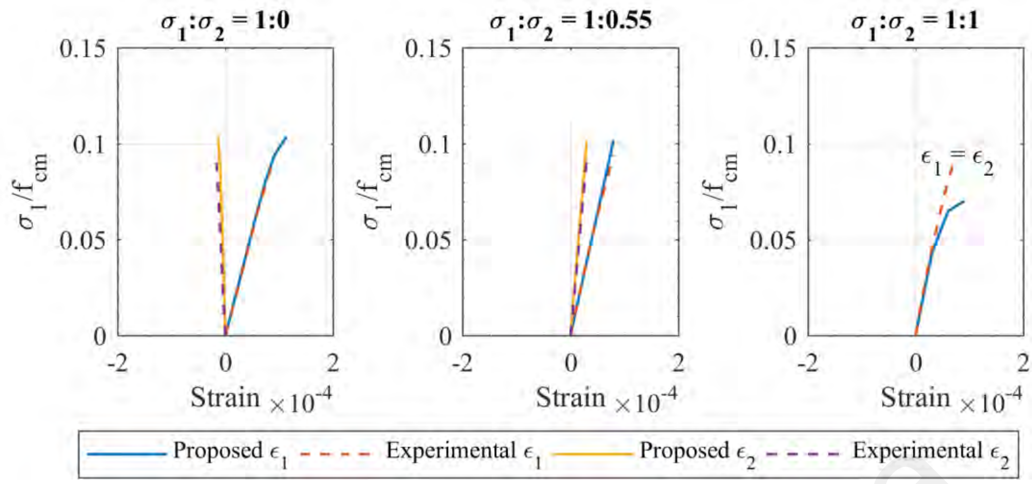


**Figure 4.22:** Model comparison with Biaxial tension tests (Kupfer et al., 1969)

Therefore, the modeling framework of concrete damaged plasticity model (CDPM) combines the plasticity, which captures the irrecoverable strain phenomenon, and the continuum damage mechanics (CDM) model, which captures the stiffness degradation due to increase in damage. The model has reasonably replicated the macroscopic behavior of concrete for uniaxial and biaxial tests performed by different researchers. The implementation of this model in simulating the nonlinear analysis is believed to represent the actual concrete behavior, and will be investigated in next chapter.

## 4.6 Summary

This chapter presents the material formulation for concrete using elastic strain-hardening plastic material using Carreira & Chu (1985) model and Hillerborg (1976) model for uniaxial compression and tension respectively. Plasticity was coupled with continuum damage mechanics (CDM) model for catering permanent strains and stiffness degradation in concrete modeling formulation, collectively called as concrete damaged plasticity model (CDPM). Reinforcing steel was modeled using the elastic perfectly plastic property. Different parameters, like dilation angle, flow potential eccentricity, ratio of biaxial compressive stress to uniaxial compressive stress and viscosity, were calibrated using concrete block simulations while keeping in line with the latest developments in the literature. The model developed in this study was found to be capable of replicating the reinforced concrete behavior quite reasonably. The dynamic capability of this model is explained in next chapter by modeling a finite element beam model and simulating the dynamic excitations.

# CHAPTER 5: IMPLEMENTATION OF MODEL

This chapter presents the implementation of the CDPM model proposed in Chapter 4 in modeling the nonlinear behavior for RC beams. The idea was to apply a harmonic excitation on the damaged RC beam to study the effects of damage on nonlinear behavior. Two types of approaches were used to detect nonlinear behavior - the restoring force surfaces (RFS) method and the formation of super-harmonics. This chapter also presents the solution procedures adopted for the nonlinear equations used in dynamic analysis. The modal analysis, which uses linear perturbation, was also carried out side by side to debate on the sensitivity of the nonlinear method.

The first and the foremost step for concrete modeling implementation was designing a scaled laboratory specimen. Reinforced concrete bridges are mostly pre-stressed or simply supported beam-slab structures. But for existing infrastructure, a major percentage of bridges constitutes of simply supported bridges. The fundamental frequencies of these simple bridges are said to lie between 1.5 and 12.5 Hz (Billing, 1984; Shepherd & Aves, 1973). To replicate a bridge in laboratory for modeling, a scaled model needs to be made. But based on the past researches, creating such a scaled specimen which has natural frequencies in the range of full-scale bridges makes it impractical. Designing such a laboratory test specimen will give a slender beam which is not possible to achieve in laboratory. Therefore, an RC beam was designed keeping in consideration the test equipment capabilities, casting facilities and the desired type of failure. The scaled beam in the current study had the first natural frequency approximately 60Hz.

The material modeling was done based on the ready-mix concrete ordered for beam casting. The procedure explained in Chapter 4 was adopted in developing the constitutive laws. For modeling reinforcing steel, the tensile strength was used for making elastic perfectly-plastic model. The bond between concrete and rebars was done by assigning the embedded region constraint to the reinforcement. Figure 5.1 shows the complete methodology involved for the nonlinear analysis carried out at each step for incremental static damage.

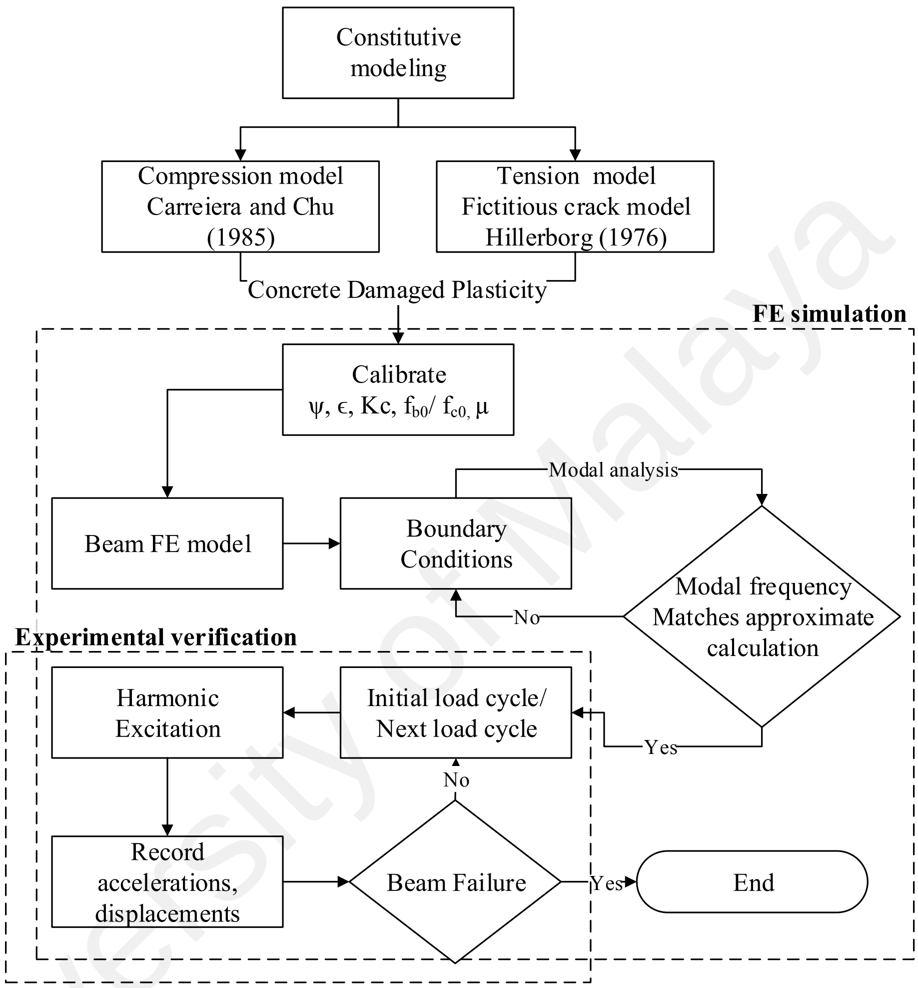


**Figure 5.1:** Detailed Flow chart of the methodology

Therefore, a beam was designed with reasonably less slenderness to accommodate the combination of flexural and shear failure mechanisms, as the investigations for flexural response have already been studied by Hamad et al. (2015). In previous similar research, the beams were designed to have a tensile failure by yielding of steel reinforcement, which may be influenced by bond failure and the inconsistencies in the rebar strengths.

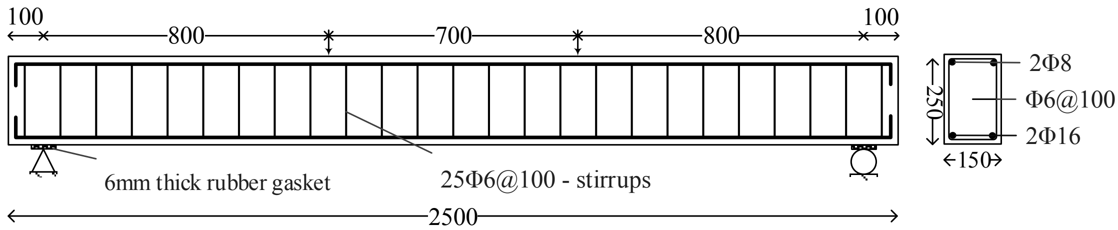


**Figure 5.2:** Design of RC Beam for investigation (all units are in mm)

For current research, the beam was modeled with lesser value of shear-to-span depth ratio (a/d) to study the effect of mix-mode cracking in RC beam. According to Obaidat (2011), the bond failure doesn't affect the overall strength significantly, the embedded region interaction was therefore considered suitable for the modeling. The geometric and reinforcement details of the designed beam are shown in Figure 5.2. These properties of beam were adopted for carrying out the simulation first and the laboratory testing later.

## 5.1 Finite Element Modeling of RC beams

The RC beam shown in Figure 5.2 was computationally modelled using commercial finite element software ABAQUS (Dassault Systèmes, 2013). For modelling concrete, C3D8R (Continuum, 3-D, 8-node, Reduced integration) element was used. For steel, T3D2 (Truss, 3-D, 2 nodes) element was used. The steel reinforcement was embedded in concrete using embedded region constraint. The maximum failure load of the beam (~110kN) was divided into 10 cycles in the increments of 10% of the failure load. At the end of each loading cycle, a harmonic excitation of 30Hz was applied on the beam at the rate of 0.0002 seconds to investigate the non-linear response. The static and dynamic loading points can be seen in Figure 5.5. Dynamic Implicit integration was used to run the nonlinear dynamic analysis. The material properties were taken from the average results of the 3 beams tested, as shown in Table 5.1.

**Table 5.1:** Experimental mechanical properties of concrete

| **Beam ID** | $\rho_c$ **(*kg/m³*)** | **$f_{cm}$ (*MPa*)** | **$f_{ctm}$ (*MPa*)** | **$E_{cm}$ (*GPa*)** |
|---|---|---|---|---|
| Beam-II | 2305.035 | 35.575 | 3.887 | 27.463 |
| Beam-III | 2316.353 | 35.097 | 3.830 | 26.984 |
| Beam-IV | 2289.945 | 37.570 | 3.978 | 28.617 |
| **Average** | **2303.778** | **36.080** | **3.898** | **27.688** |

For FE modeling, the tensile strength was estimated using Eurocode (EN1992-1-1, 2004), as below:

$$f_{ctm} = 0.30(f_{cm} - 8)^{2/3} \tag{5-1}$$

Where $k_1$ and $k_2$ are correction factors corresponding to coarse aggregates and mineral admixtures and have been detailed in Noguchi et al. (2009) for different constituents. The mechanical properties estimated from compressive strength are shown in Table 5.2.

**Table 5.2:** Calculated mechanical properties of concrete for FE modeling

| **P (*kg/m³*)** | **$f_{cm}$ (*MPa*)** | **$f_{ctm}$ (*MPa*)** | **$E_{cm}$ (*GPa*)** |
|---|---|---|---|
| 2303.778 | 36.080 | 3.898 | 27.349 |

Mesh sensitivity analysis was carried out for four configurations, as can be seen in cross-section in Figure 5.3. The load-deflection response, based on the mesh size, can be seen in Figure 5.4. The finer mesh converged the load deflection response at 25mm mesh size (6060 elements). For the current study, the 25mm mesh size was considered suitable because of the better visualization of cracks, which is also part of the study. However, the convergence of solution for this beam setup is not affected significantly by the mesh size, and coarser meshing can also be used considering the embedment of the rebars as discrete reinforcement.

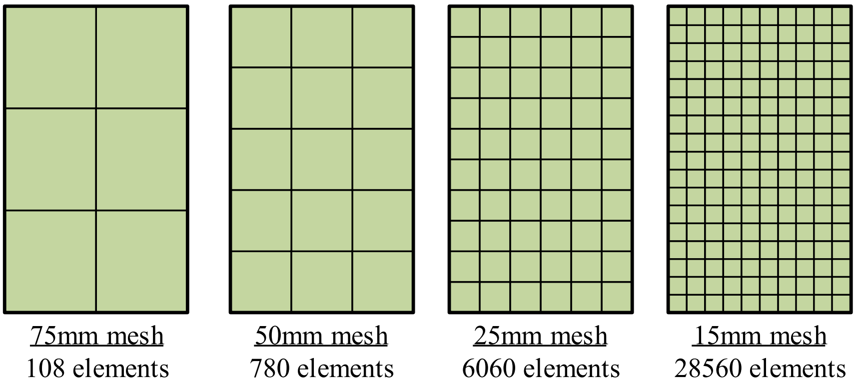


**Figure 5.3:** Different Mesh sizes for sensitivity analysis

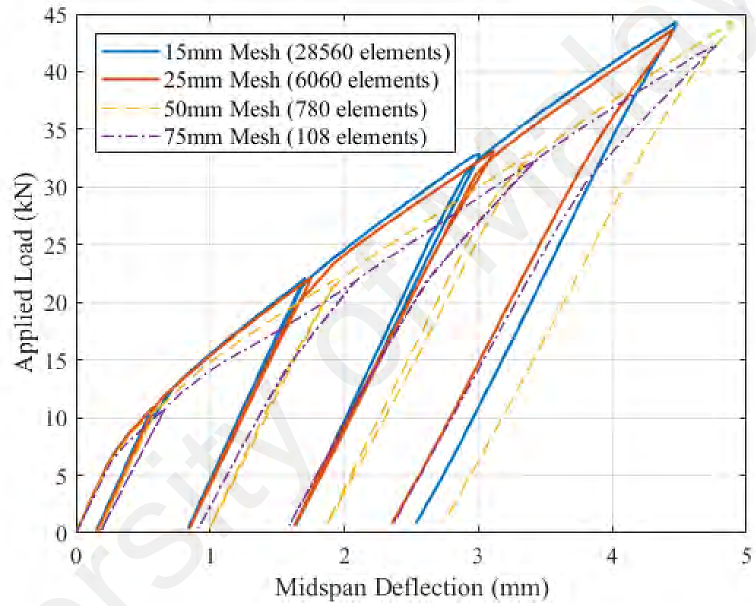


**Figure 5.4:** Load-Deflection Comparison for different meshing sizes

A complete FE model of RC beam can be seen in Figure 5.5. Four-point flexural loading was applied. The restraints of u1, u2 and u2 were used which are representation of a combination or hinge and roller support. This is the reason the symmetric conditions were not applied for saving calculations, and the complete model of the beam was used instead of half beam model.

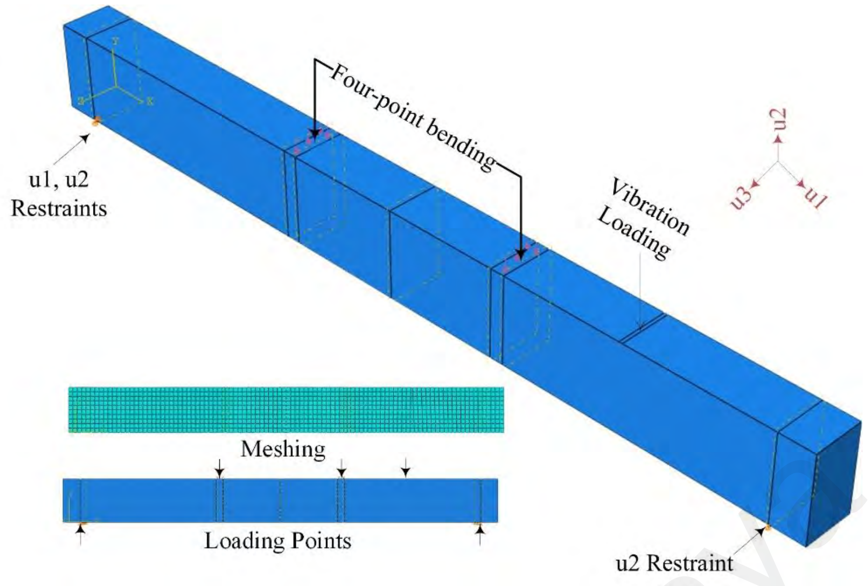


**Figure 5.5:** Beam sketch for computational Model (25mm mesh size)

The vibration loading was applied in the form of a sinusoidal wave form. The vibration loading was simulated on the beam for each damage level and the resulting displacements were recorded at the respective nodes for the dynamic analysis.

### 5.1.1 Solution procedures

The underlying solution procedures of the nonlinear equations for static and dynamic loading were used efficiently. For static loading and unloading, Newton's method was used to solve the set of nonlinear equations. For nonlinear dynamic analysis, the implicit integration scheme was used for solution of nonlinear equations at fixed time interval. The half-step residual calculation was suppressed to save the computation cost. A brief detail of both the solution procedures, the static and the dynamic analysis, is given below.

#### 5.1.1.1 Solution procedure for static loading

The loading was applied in the percentage increments of the failure loads. The set of linear equations was solved using Direct sparse solver (DSS) because of its suggested usage in analyzing 'block-type' models (Dassault Systèmes, 2013). For the solution of nonlinear equations, Newton's method was used. For the model under consideration, the equilibrium equations are symbolically given as

$$F^N(u^M) = 0 \tag{5-2}$$

Where $F^N$ is the component related to the N$^{th}$ variable and $u^M$ is the value of the M$^{th}$ variable. The solution of the symbolic Equation 5-3 is desired in terms of $u^M$. For an iteration $i$, the approximated value of solution is obtained as $u_i^M$. Let $c_{i+1}^M$ be the difference between this solution and the exact solution to the discrete equation (Equation 5-2), and is given by

$$F^N(u_i^M + c_{i+1}^M) = 0 \tag{5-3}$$

Expanding the above equation gives

$$F^N(u_i^M) + \frac{\partial F^N}{\partial u^P}(u_i^M)c_{i+1}^P + \frac{\partial^2 F^N}{\partial u^P \partial u^Q}(u_i^M)c_{i+1}^P c_{i+1}^Q + \cdots = 0 \tag{5-3}$$

If $u_i^M$ is the close approximated solution, the magnitude of each $c_{i+1}^M$ will be small. So, the terms after the first two terms are neglected giving a system of linear equations.

$$K_i^{NP} c_{i+1}^P = -F_i^N \tag{5-5}$$

where $K_i^{NP}$ is the Jacobian Matrix, given by

$$K_i^{NP} = \frac{\partial F^N}{\partial u^P}(u_i^M) \tag{5-6}$$

In a similar way, the next approximation is given by

$$u_{i+1}^M = u_i^M + c_{i+1}^M \tag{5-7}$$

The convergence is obtained by ensuring the small values of $F_i^N$ and $c_{i+1}^N$.

The stability is achieved by applying damping in case the increments become unstable or singular. For a stable model, the dissipated energies are very small, and the artificially induced damping has no effect. If the region goes unstable, the local velocities increase and the dissipated energy is then dissipated by the artificially applied damping. This damping is determined in such a way that the extrapolated dissipated energy is a small fraction of extrapolated dissipated strain energy. This fraction is called dissipated fraction energy, and a value of 0.0002 was used in the analysis procedure.

#### 5.1.1.2 Solution procedure for dynamic loading

For modal analysis, eigenvalue extraction was performed to calculate the natural frequencies and the mode shapes. It is a linear perturbation procedure, where this procedure provides the linear response of the system with reference to the base state (Figure 5.6). The base state can be the state at the end of the last nonlinear state.

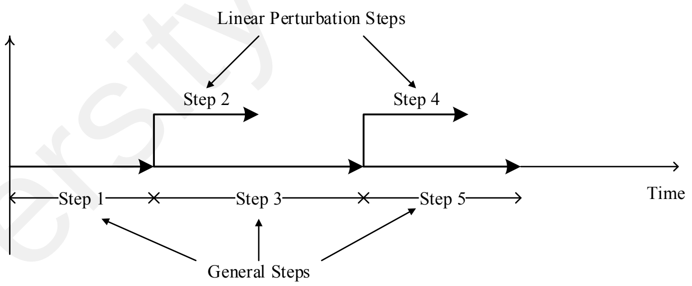


**Figure 5.6:** Linear perturbation procedure explained (Dassault Systèmes, 2013)

The eigenvalue problem for the natural frequencies of an undamped finite element model is:

$$(-\omega^2 M^{MN} + K^{MN})\phi^N = 0 \tag{5-8}$$

where $M^{MN}$ is the symmetric mass matrix, $K^{MN}$ is the stiffness matrix with initial stiffness included, $\phi$ is the mode of vibration (eigenvector) and $M$ and $N$ are the degrees of freedom.

The Lanczos eigensolver was used for eigenvalue extraction, and first four modal frequencies in bending were extracted. For solution of nonlinear equations (the harmonic response), implicit integration schemes were incorporated.

The solution procedure for dynamic implicit schemes can be obtained using the concept of 'half-step residual' (Hibbitt & Karlsson, 1979). The equilibrium equation for such procedure is the given equilibrium equation the d'Alembert force included, given below

$$f = F - \rho\ddot{u} \tag{5-9}$$

Where $f$ is the body force at a point, can be written in terms of F, the externally prescribed body force and the d'Alembert force. In terms of virtual work, the body force can be written as

$$\int_V f.\delta v \, dV = \int_V F.\delta v \, dV - \int_V \rho\ddot{u} . \delta v dV \tag{5-10}$$

The last term can be written in terms of reference density and reference volume as $\int_{V_0} \rho_0 \ddot{u} . \delta v dV_0$.

Where $\ddot{u}$ is the acceleration field, which is calculated from the time integration operator. The displacement at a point can be approximated as $u = N^N + u^N$ so that $\ddot{u} = N^N + \ddot{u}^N$, provided that $N^N$ are not displacement dependent. The finite element equilibrium equation can be written as

$$M^{NM}\ddot{u}^M + I^N - P^N = 0 \tag{5-11}$$

where $M^{NM} = \int_{V_0} \rho_0 N^N . N^M dV_0$ is the consistent mass matrix, $I^N =$

$\int_{V_0} \beta^N : \sigma dV_0$ is the internal force vector and $P^N = \int_S N^N . tdS + \int_S N^N . FdV$ is the external force vector.

The implicit operator defined by (Hilber & Hughes, 1978), which is an extension of trapezoidal rule, was used to solve the non-linear problem. This operator replaces Equation 5-12 by

$$M^{NM} \ddot{u}^M|_{t+\Delta t} + (1+\alpha)(I^N|_{t+\Delta t} - P^N|_{t+\Delta t}) - \alpha(I^N|_t - P^N|_t) + L^N|_{t+\Delta t} = 0 \quad (5\text{-}12)$$

where, $L^N|_{t+\Delta t}$ is the sum of Lagrange multiplier forces associated with degree of freedom (N). Newmark formulae for displacement and velocity integration completes the implicit operator, given, respectively, as:

$$u|_{t+\Delta t} = u|_t + \Delta t \dot{u}|_t + \Delta t^2 ( \left(\frac{1}{2} - \beta\right) \ddot{u}|_t + \beta \ddot{u}|_{t+\Delta t} \quad (5\text{-}13)$$

$$\dot{u}|_{t+\Delta t} = \dot{u}|_t + \Delta t((1-\gamma)\ddot{u}|_t + \gamma \ddot{u}|_{t+\Delta t} \quad (5\text{-}14)$$

where $\beta = 1/4(1-\alpha)^2, \gamma = 1/2 - \alpha$ and $-1/3 \leq \alpha \leq 0$. A value of -0.05 was used for $\alpha$, to give just enough artificial damping to allow time incrementation to work smoothly.

The system of simultaneous nonlinear dynamic equilibrium equations is solved at each time increment. The solution is achieved iteratively using Newton's method. A fixed time increment is used to sample the dynamic response at desired sampling frequency. The computation cost can be reduced significantly by suppressing the calculation of half-step residual. Therefore the half-step residual calculations are not discussed here and can be found in detail in ABAQUS Documentation (Dassault Systèmes, 2013).

### 5.1.2 Steps for FE analysis

The solution steps explained above are built-in functions available in the FE software ABAQUS. The complete procedure for constitutive modeling, FE modeling and the FE analysis is summarized below

1. Use the compressive stress ($f_{cm}$) and, if available, the tensile ($f_{ctm}$), from laboratory tests to obtain the uniaxial stress-strain behavior in compression and tension. The elasto-plastic stress-strain relation of reinforcing steel can be obtained from the experimental tensile strength ($f_y$).
2. Using the CDPM equations, calculate the inelastic/cracking strains, damage parameters and subsequently the plastic strains.
3. Model the RC beam using FE software ABAQUS.
4. Calibrate the boundary conditions to match the natural frequency of the model approximately with the structure by running trial simulations.
5. Apply first loading cycle of incremental static load using static analysis with load being 10% of the approximate ultimate failure load. Then unload the beam to the zero-load condition.
6. Obtain the natural frequency using frequency extraction tool in ABAQUS.
7. Apply the harmonic force having frequency approximately half the first natural frequency on the beam. Carry out time domain analysis using implicit dynamic analysis technique and obtain the results in the form of time histories of the displacement, velocity and acceleration.
8. The restoring force surfaces are obtained by subtracting inertial force from the exciting force (Equation 2-3). The restoring force surfaces are plotted against displacement to find modal stiffness. The modal stiffness doesn't change in linear systems.

9. Fast Fourier Transform (FFT) of the acceleration response gives the frequency domain response, with appearance of the super-harmonics as an indication of nonlinear behavior.
10. Repeat step 4 through step 9 for the next load increment and repeat until the beam reaches its ultimate strength.
11. The modal stiffness from RFS and the nonlinearity coefficient from super-harmonics are obtained, which when plotted with the damage, give the relation of nonlinearity with damage.

The above simulation steps show that the complete linear, nonlinear, damage response of the structure can be modeled accurately for the complete life-cycle of the structure. This can be a useful data which can be compared to the existing serviceable structure. The nodes chosen for recording the time domain response were chosen at same locations in the model as chosen in experiment. Therefore, the complete procedure is easily replicable experimentally.

## 5.2 Experimental Investigation

For experimental investigation, the sample sizes, accessibility of the equipment and the possibly constant ambient laboratory conditions were carefully incorporated for carrying out the testing. As the same beam samples were to be statically loaded-unloaded first, and later dynamically excited, there was frequent switching of equipment. During this switching of equipment, the load-deflection setup could easily be disrupted. Therefore, during the testing, the setting up of equipment was very carefully planned in order to preserve the results as close as possible to the developed model in the simulation.

### 5.2.1 Casting of Beam specimens

There were three beams cast, namely Beam-II, Beam-III and Beam-IV. Ready-mix Grade C40, normal weight concrete was ordered with the properties shown in Table 5.3.

Deformed bars were used for the bottom reinforcement and plain bars were used for top and transverse reinforcement. The casting was done on a single day and the demolding was done after 7 days of casting, during which the specimen top surface was cured constantly. The steps involved in casting of the beam specimens can be seen Figure 5.7, to Figure 5.9. Figure 5.7 shows the detailing of reinforcing steel. The attaching of strain gauges can be seen in Figure 5.8 and the casting of beams can be seen in Figure 5.9.

**Table 5.3:** Properties of Ready-mix concrete

| | |
|---|---|
| Type of Cement | Ordinary Portland Cement |
| CSA ratio | 1 : 2.36 : 2.81 |
| Cement | 370 kg |
| Sand | 873 kg |
| Coarse aggregate | 1040 kg |
| Water | 155 kg |
| w/c ratio | 0.42 |
| Slump | 85 mm |
| Average 28-day cube strength (CB 1-3) | 51.62 MPa |
| Average 28-day cylinder strength (CS 1-3) | 36.08 MPa |

**Figure 5.7:** Preparation of reinforcing steel

**Figure 5.8:** Fixing of strain gauges on rebars

**Figure 5.9:** Casting of RC beam specimens

To keep check on the concrete properties, there were 40 cylinders and 40 cubes cast. The casting was done on vibrating table to have adequate initial setting. For the best representation of the specimens, the test specimens were cured in the same location as the beams. For each test on the beam, compressive and tensile strengths were measured through specimen tests. There were few specimens that deviated from the desired values, but those disparities were due to improper pouring or due to damage in demolding. The compressive strength for the complete testing regime is shown in Figure 5.10.

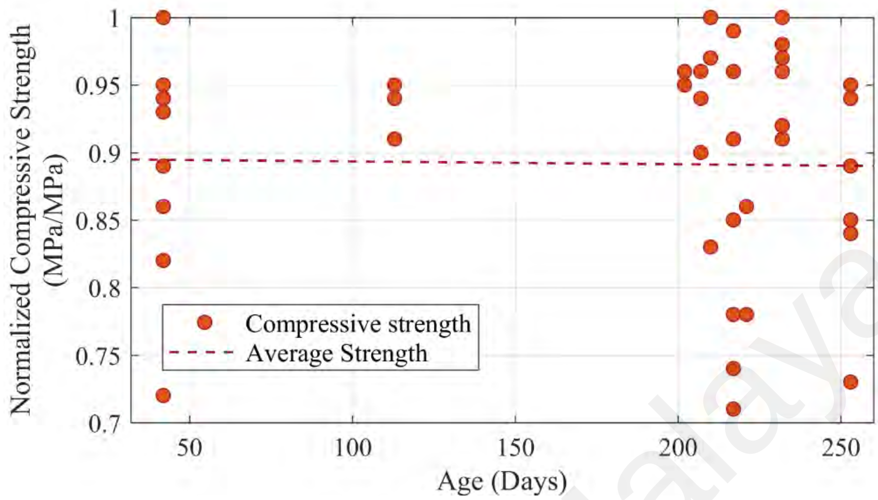


**Figure 5.10:** Normalized average compressive strength during the testing regime

The compressive strength was normalized with the highest values of the cylinder and the cube strengths, and were plotted together as normalized strengths. The difference in average compressive strength from maximum strength of the beams was 10% (Figure 5.10).

### 5.2.2 Test setup

The test setup was divided into three setups; static loading for inducing damage, impact hammer testing for natural frequency identification and harmonic vibration testing for nonlinear behavior identification. The modal testing of beams to the failure has been only reported by a few researchers (Benedetti et al., 2018; Hamad et al., 2015; Neild et al., 2003b). The setting up of instrumentation for each part of the test setup while keeping the LVDTs intact was difficult, as the midpoint deflection for four-point bending required an LVDT placed at the center span. The beams were placed on the support platform for the test setup as can be seen in Figure 5.11. There were 6mm thick rubber gaskets placed beneath the beams to account for uniform transfer of the contact between the beam and the support.


**Figure 5.11:** Beam test setup for static and dynamic testing

Due to the implications damage while transferring the beam, the free-free vibration analysis was not possible in the present testing arrangement. Therefore, the dynamic testing was performed while the beam was kept undisturbed in the testing machine. The incremental static loading was performed in 10 cycles. After each static loading cycle, impact hammer testing and harmonic testing were performed. The details of the equipment and the testing schemes are explained below.

### 5.2.2.1 Static Testing

For static testing, a spreader beam of 700 mm span was placed on the top of the beam under the loading head of the machine. SATEC 600kN Universal Testing Machine was used for the flexural cyclic loading. Flexural loading was applied in increments of 11kN of the failure load (~110kN) of the beam as shown in Figure 5.12.

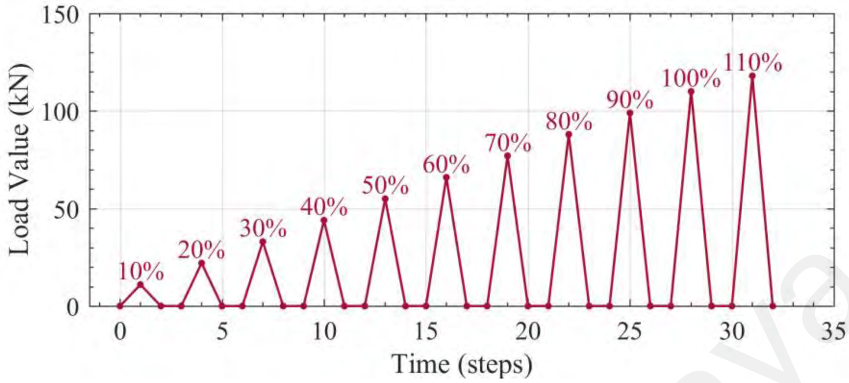


**Figure 5.12:** Incremental Static loading profile for beam testing

As the loading rate has different trends for different types of specimens (Fu et al., 1991), the chosen rate was kept constant for all the static testing to keep this parameter as a constant for all the tested specimens. The beam was loaded for each cycle at displacement-controlled rate of 0.75 mm/min and then unloaded at the same rate. The specimens failed at ~110kN load with crushing of the top concrete.

#### 5.2.2.2 Dynamic Testing

There were two types of vibration setups used for the dynamic testing, impact hammer for the modal frequency extraction and harmonic vibrations for identification of the presence of non-linearities. These dynamic tests were performed after each loading and unloading cycle of static loading. After each static load increment, the spreader beam was removed and the dynamic testing was performed in unloaded state.

First, the impact hammer testing was performed for obtaining natural frequencies. The impact hammer equipment can be seen in Figure 5.13. LIXIE 300H-HH-35 dead blow sledge was used for the impact. The impact hammer and the data logger can be seen in Figure 5.13. Kristler IEPE single axis accelerometers, type IEPE with measuring range of $\pm$ 25g and sensitivity of 193 mV/g, was fixed at 875mm from the right face of the beam.

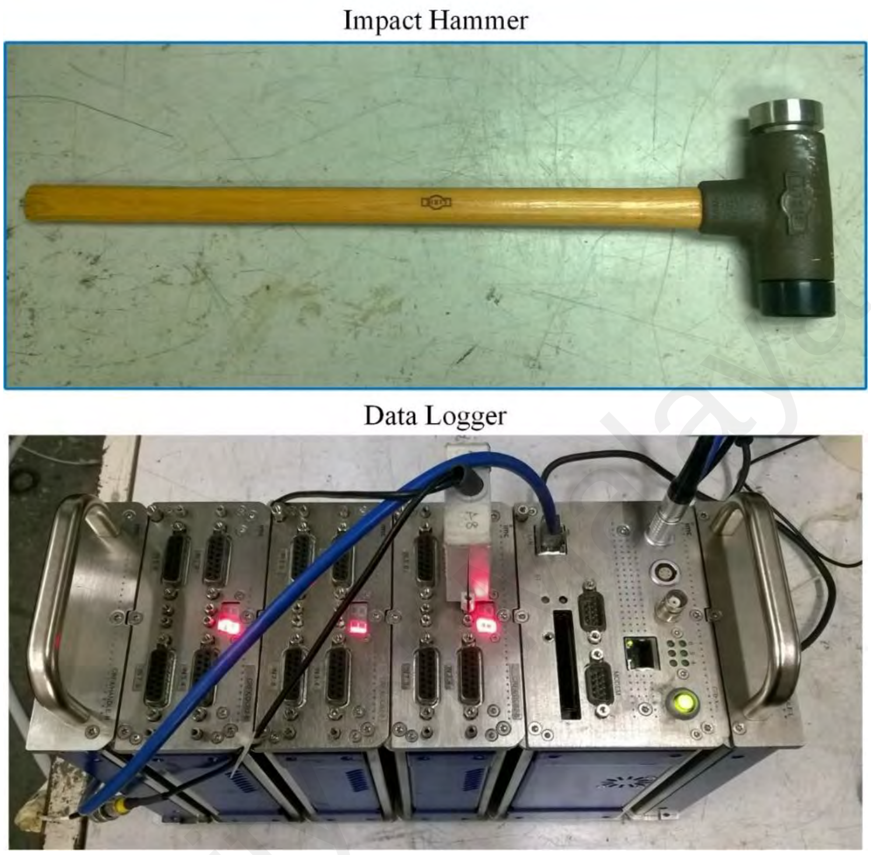


**Figure 5.13:** Modal testing equipment

The schematic diagram of impact hammer testing is shown in Figure 5.14. The impact hammer was struck five times at the six specified points on the top surface of the beam. The midpoint location was not accessible because of the lack of clearance between the beam top and the loading head of the universal testing machine. The impact hammer testing was carefully carried out for coherence values for each reading by using imc WAVE software.

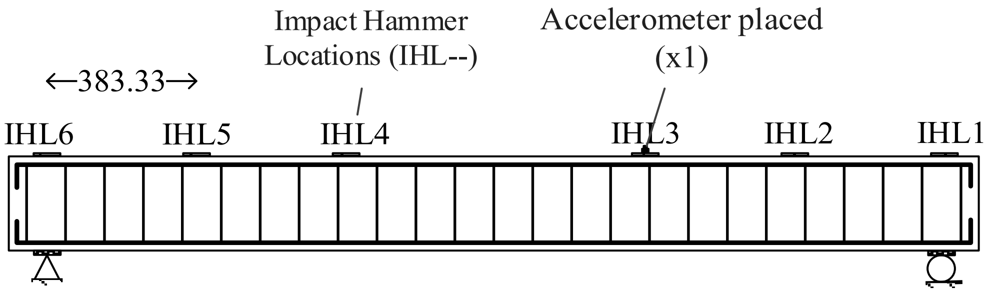


**Figure 5.14:** Schematic diagram of impact hammer testing

The data recorded using the impact hammer were frequency response functions, coherence values, phase and power spectral density. The results and analysis of the impact hammer test are discussed in Chapter 6.

The schematic diagram for the harmonic vibration test setup is shown in Figure 5.15. There were 7 accelerometers fixed on the top surface of the beam at equal distances. A harmonic excitation was applied on the top of the beam with a vibration shaker. The harmonic excitation was applied with a frequency of 30Hz at different amplitudes using a signal generator, an amplifier and the response was recorded using a data logger. The test equipment is briefly explained below.

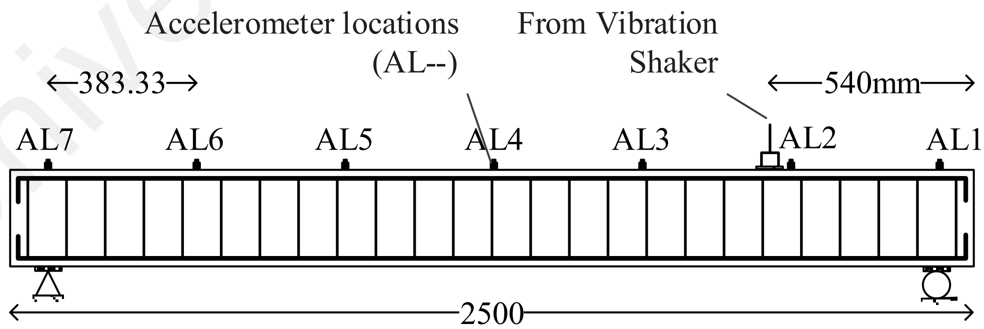


**Figure 5.15:** Schematic diagram of harmonic excitation test setup

The dynamic testing procedure was done using the equipment, as shown in Figure 5.16. The testing was conducted in such a way that a shaker (APS-113 Shaker) was fixed to apply excitations on the top surface of the beam, through an accessory connecting it to the top of the beam. The accelerometers (Kristler IEPE single axis accelerometers, Type IEPE 8702B25) were mounted to record the response of the beam. The shaker was connected to a signal generator (Model DS345 Synthesized Function generator) where the generated signals were amplified using a power amplifier (APS 125). The accelerometer data were digitized using Dewesoft Sirius 8-channel data logger.

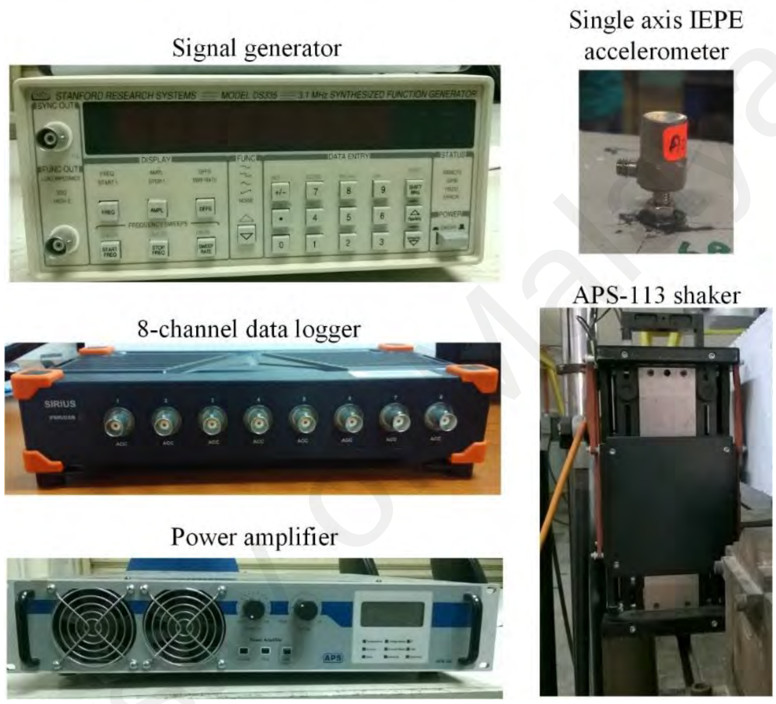


**Figure 5.16:** Non-linear vibration testing equipment

The excitation harmonic frequency was kept well below the first modal frequency but high enough that the filters (band pass, low pass, high pass) do not affect the results. The first modal frequency was estimated around 60 Hz. The input frequency was utilized as a harmonic signal with four different amplitudes (150N, 300N, 750N, 1500N) at 30Hz. There were 7 accelerometers installed on top of the beam at equal distances of 383.33 mm as shown in Figure 5.15.

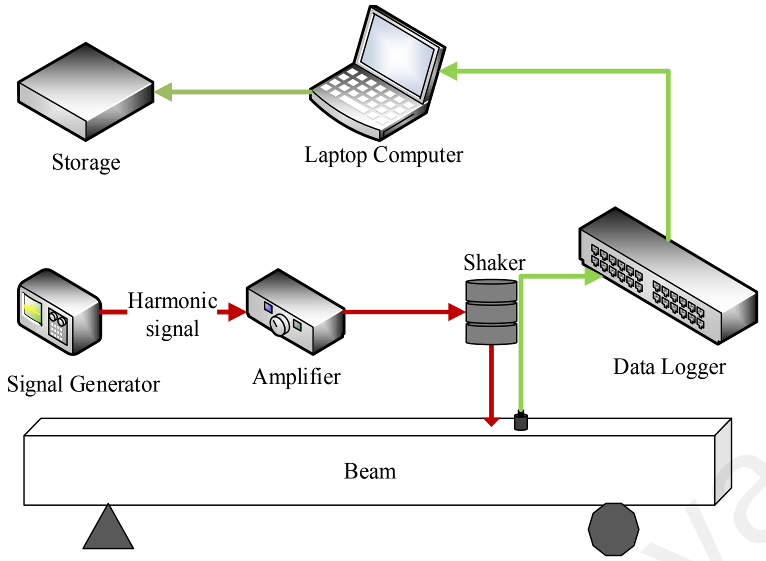


**Figure 5.17:** Schematic diagram of harmonic excitation testing procedure

The flowchart of the harmonic vibration procedure is demonstrated in Figure 5.17. The red lines represent input signal and the green lines represent the recorded response data. A sinusoidal harmonic signal with constant frequency of 30 Hz was passed through amplifier for different amplitude values. The amplified signal was fed into the shaker which excited the beam at the point 383.33mm from the support. The signal was allowed to stabilize while being monitored in the recording software (DEWESoft X2) and was recorded for 10 seconds through a data logger. The signal response was monitored during the recording to check for any discrepancy or unusual spike in the signal. The response was stored in the computer as accelerations and displacements for the analysis at sampling rate of 0.0002 seconds.

## 5.3 Summary

The constitutive model developed in Chapter 4 was implemented on an RC beam. The beam was modeled using FE software ABAQUS. The static and dynamic analysis schemes were carried out on the FE model to obtain linear and nonlinear vibration characteristics. The procedure was replicated experimentally to obtain the same set of data. There were three beams tested to validate the FE model. The casting and testing of these beams in context of the model have been explained step by step. The results were recorded in terms of load-deflection response, crack formation, modal frequencies and the time domain response of the harmonic excitation.

# CHAPTER 6: RESULTS AND DISCUSSION

## 6.1 Overview

An RC beam was modeled using CDPM model. The incremental static loading was carried out on the beam to simulate the life-cycle of the structure, and the linear and non-linear characteristics were recorded at each damage level to observe the dynamic behavior at different damage levels. Three types of investigations were performed; incremental static load testing, modal analysis (for natural frequency identification) and harmonic signal analysis (non-linear behavior assessment). The finite element modeling was done using commercial finite element software, ABAQUS, to simulate the aforementioned nonlinear behavior. This investigation was supported by experimental tests on 3 RC beams. This chapter presents the results of the model implemented in Chapter 5.

## 6.2 Environmental influences

The environmental conditions are very important in the testing carried out, especially the humidity and the ambient temperature. Liu et al. (2009) established a baseline for the temperature for the modal frequency variations for a complete year cycle from ~0℃ to ~38℃. For the complete temperature range, the change in natural frequency of an RC bridge was 4% for first mode and 2% for the second and third. Therefore, the temperature does affect the modal frequencies, but not significantly. In this study, the temperature variation was kept under observation.

Throughout the testing regime, the environmental conditions were kept in check so that the experimental results match with the model without any unknown influence. The specimens after casting were kept in their molds for 28 days. Later the specimens (prisms, cylinders and cubes) were cured at the location of specimens to have the best representative values of compressive and tensile strengths. While the tests were being carried out on the concrete beams, the temperature and humidity variations were recorded throughout the testing regime.

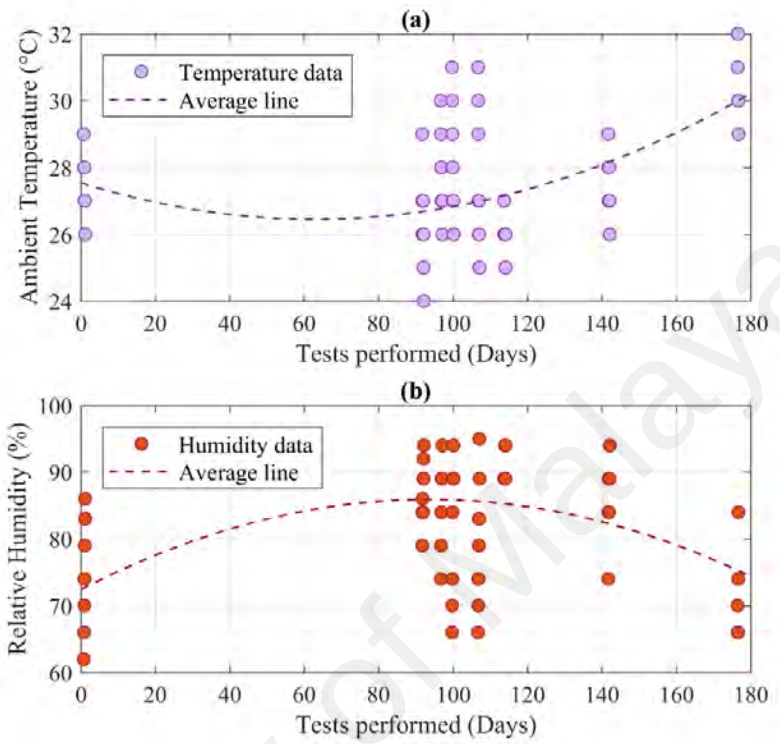


**Figure 6.1:** Environmental effects (a) temperature (b) relative humidity

Figure 6.1 shows the temperature and humidity variation with the time for different testing carried out. The testing was carried out with the mean temperature as 27.4°C and the relative humidity as 82.75%. Dynamic testing was performed after office hours to avoid additional noise from the surroundings (traffic), as the accelerometers used are sensitive to small disturbances in the vicinity of the laboratory. After every static loading cycle, the loading machine was turned off, the wires of the equipment were kept as straight as possible without any bends to avoid any interference during the signal recording.

Generally, the temperature difference deviated around 5°C during the complete testing procedure and the relative humidity varied up to 20% (Figure 6.1). For the complete testing regime (almost 3 months) the maximum temperature difference noted was 8°C. According to Xia et al., (2011), for every 10°C temperature change, the first two modal frequencies change by 2 to 3%. A change in 15°C of temperature while doing modal testing on a reinforced concrete bridge had 4-5% change in natural frequencies (Wahab & De Roeck, 1997). Natural frequencies are highly mode dependent, and the change in temperature affects the stiffness of the structures. Therefore, the environmental effects were within the limits of without affecting the natural frequencies of the beams.

## 6.3 Static Response

A four-point bend testing was performed on three reinforced concrete beams. The loading profile was applied in increments of 10% of the failure load for 10 cycles. The static test was performed majorly to evaluate the effectiveness of the developed model with the RC beam behavior. In the proceeding subsections, the analysis of load-deflection response and crack formations will be discussed.

### 6.3.1 Load-Deflection Response

The load-deflection results of the simulated beam are compared with that of experimentation, as presented in Figure 6.2.

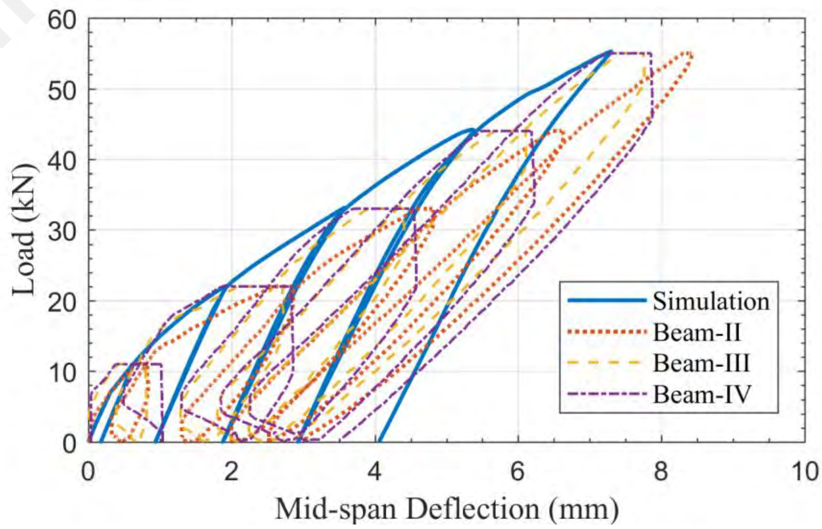


**Figure 6.2:** Experimental and computation load-deflection response of 5 cycles

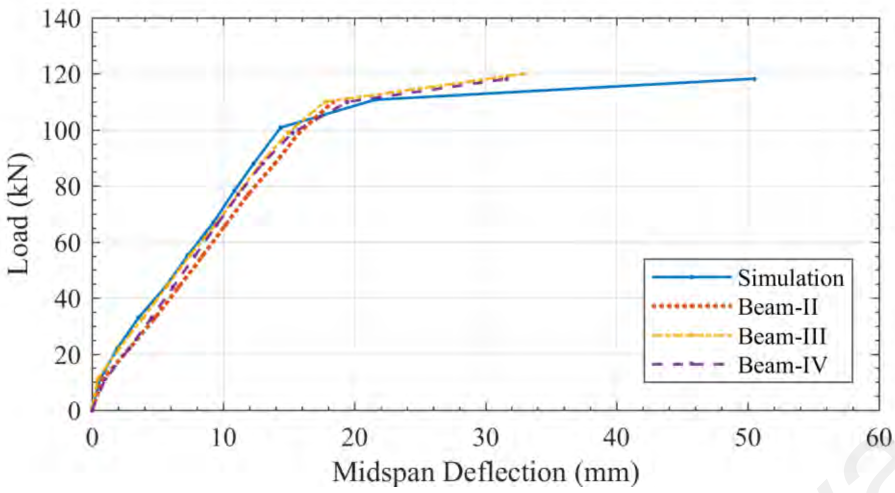


**Figure 6.3:** Monotonic Load-deflection response (peak picking)

The model reasonably replicates the load-deflection behavior, as it can be seen that the crack formation starts at the first loading cycle (11kN), as shown in Figure 6.2. The load deflection response was compared by peak picking method for better visualization (Figure 6.3). The beam load increased as a stable loading until ~110kN where the excessive deflections started, which was considered as the failure load. This agrees well with the experimental results, as the onset of excessive deflection in beams Beam-II, Beam-III and Beam-IV, was at ~110kN. In terms of cyclic loading (Figure 6.2), the unloading deflections varied by 25% on average, which may be significant, but does not affect the maximum failure load and the respective deflection. The slightly stiffer response of the simulation may attribute to the perfect bonding assumption in the finite element model. Although there was no bond failure observed, and beams crushed at the mid-span. The details of the failure of the specimens can be seen in Appendix-A.

### 6.3.2 Crack Formation

The tensile behavior of concrete is linear up to the maximum tensile strength beyond which the irrecoverable deformations occur. The damage variable in tension ($d_t$ in Equation 4-27) is dependent on inelastic strains and the tensile strength. Therefore, right after the crack formation, the value increases nonlinearly from 0 to 1. This can be used as a good tool to visualize crack formation. Figure 6.4 shows such visualization of crack from the simulation, compared with the respective crack formation from the laboratory tests. The complete details of the crack formation from simulation and the experimentation are given in Appendix A.

The flexural cracks started appearing after the first loading cycle (11kN). These flexural cracks propagated vertically until the 5$^{th}$ cycle (55kN), after which the inclined cracks started to appear on the shear span. The shear cracks propagated with the onset of flexural cracks, indicating the increased contribution of shear effects. The failure load for the modeled beam as well as the tested beams was around 110kN, which was the estimated value while designing the beam specimen.

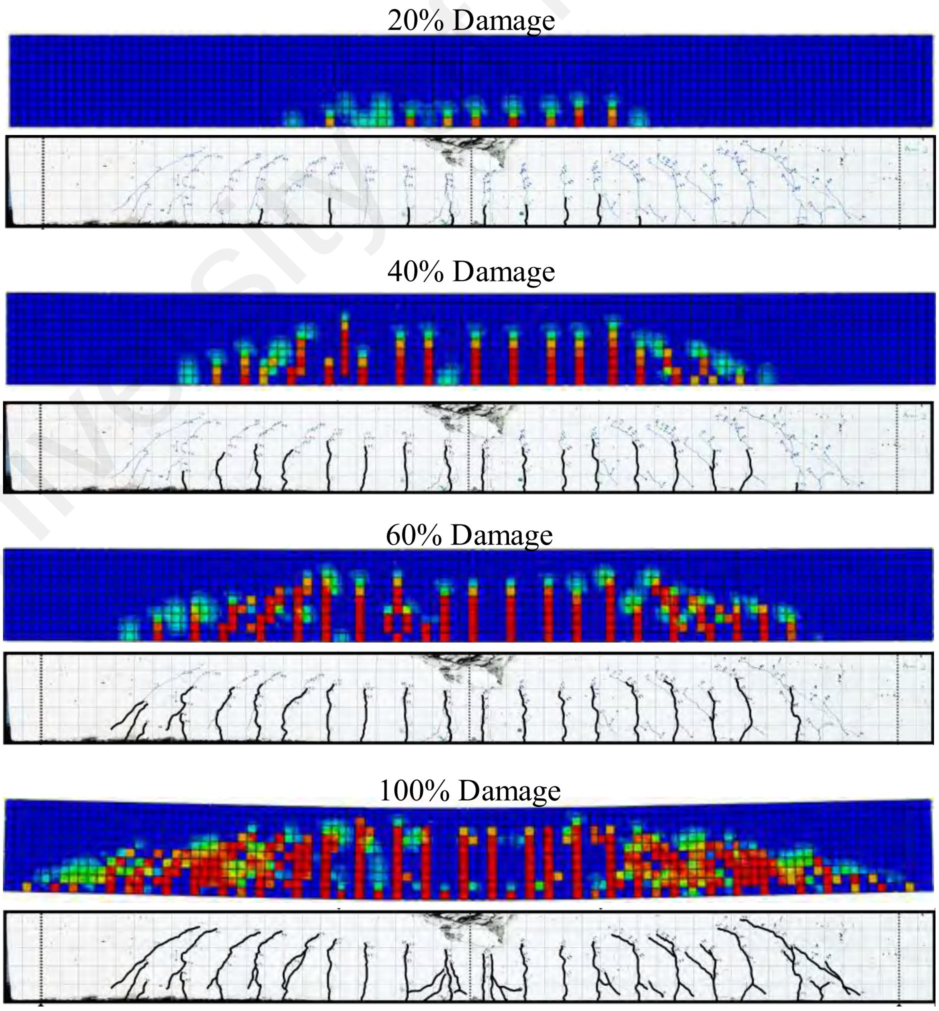


**Figure 6.4:** Crack formation comparison of simulation and experimental setup

With a reasonable confidence developed in the crack visualization from the three beams tested, the average crack height was measured at each loading cycle using LED light as a source. as the crack width measurement below 0.2mm was not possible to be measured by naked eye (Hamad et al., 2013). For computation model, as the tensile strength was reached, the damage occurred and the cracks started visualizing, as can be seen in Figure 6.4. A relation of average crack height and the damage was developed, as can be seen in Figure 6.5. It can also be seen through the slope of arrows that the crack propagation is more at initial damage levels, until 40% damage (44kN load).

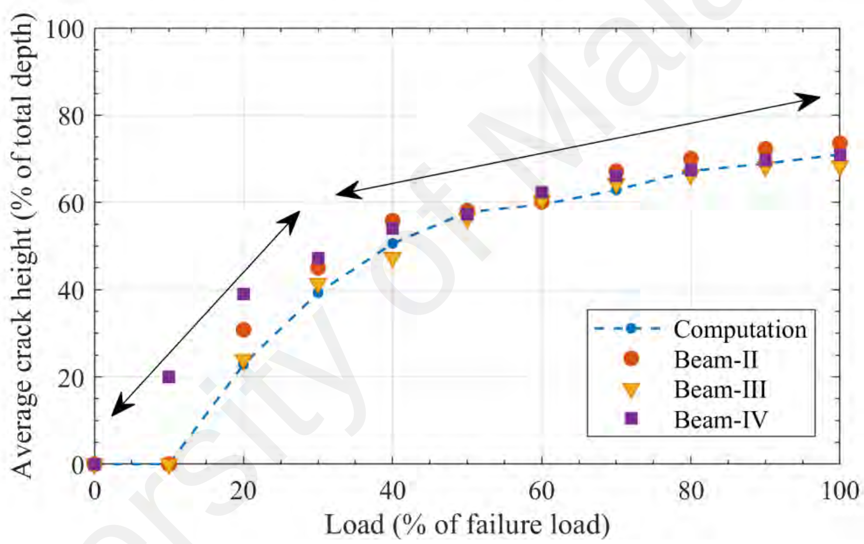


**Figure 6.5:** Comparison of Load and average crack height

The crack mouth opening displacement or crack widths were measured from images taken using a digital microscope. The crack widths at mid-span and at the location beneath loading point can be seen in Appendix B. The crack widths were plotted against the length of the beam for different damage levels. Figure 6.6 (a) shows the crack widths when the beam is fully loaded at each damage level, and Figure 6.6 (b) shows the crack widths when the beam was unloaded. The loaded and unloaded cracks at higher loads show more CMOD, as the shear cracks start to propagate. Furthermore, the CMOD values at the midspan started to reduce while the respective values at the shear span increased normally. This observation may suggest that the inclined cracks may contribute differently to the nonlinear behavior. However, the agreement between experiment and simulation shows that the mechanical behavior of RC beam can been reasonably replicated through FE model.

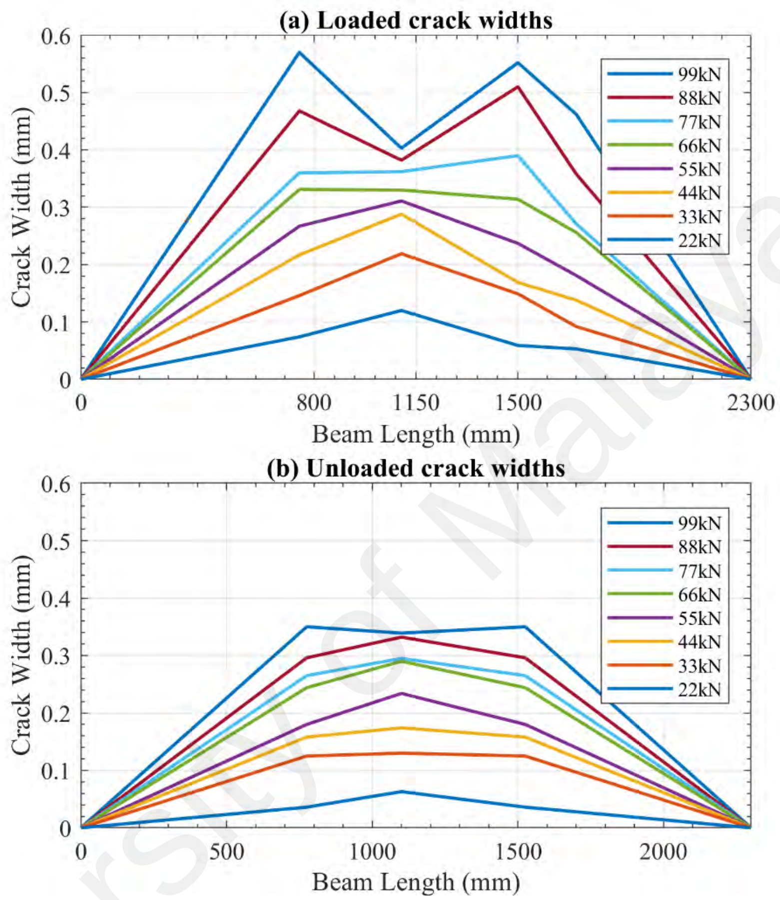


**Figure 6.6:** Experimental evolution of Crack widths with increasing load

## 6.4 Dynamic Response

The dynamic response is divided into three sub-sections; modal analysis, restoring force surfaces and formation of super-harmonics; as explained below.

### 6.4.1 Modal analysis

The modal analysis for the FE model was carried out by using Lanczos eigensolver; and the mode shapes and their respective modal frequencies were extracted. The support conditions in the experimental setup were 6mm thick rubber gaskets, which were calibrated with the finite element model boundary conditions. The boundary conditions were varied in terms of stiffness and a good agreement in fundamental frequencies was achieved for the boundary conditions, as shown previously in Figure 5.5.

To obtain experimental modal frequencies, impact hammer testing was performed at 6 locations, according to Figure 5.14. An accelerometer (Kristler IEPE single axis) was fixed at location IHL3. Figure 6.7 shows a typical recorded response for 5 strikes of impact hammer. The coherence plot presents the power transfer between the input and the output with value 1 indicating the complete transfer of the energy, as shown in Figure 6.7 (a). First three modal frequencies can be seen in the frequency response function in Figure 6.7 (b) and the phase shift at each natural frequency shift can be seen in Figure 6.7 (c). The power spectral density is also plotted in Figure 6.7 (d). At each mode, there is a phase shift. The response of the beam was recorded using recording software imc WAVE structural analyzer. The modal analysis was performed on recorded data using commercial signal processing software called ME'scope (ME'scope, 2009).

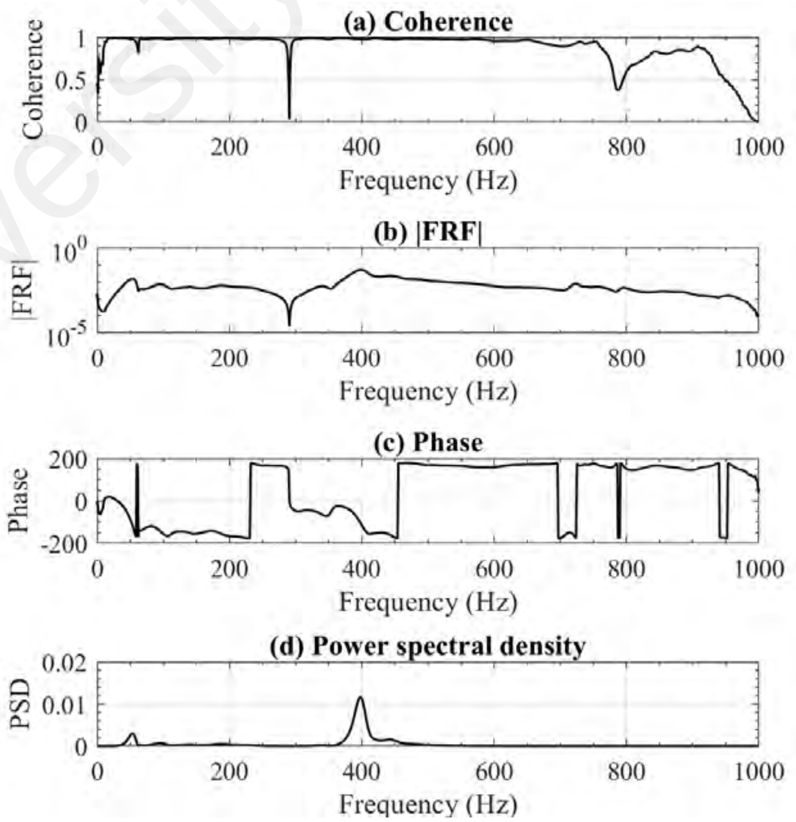


**Figure 6.7:** Typical **r**esponse of Impact hammer test at location IHL3

First four modes in bending were identified in the investigation. The identified mode shapes and their respective natural frequencies for the modal dynamic simulation and the impact hammer testing for Beam-III in undamaged state are shown in Figure 6.8. The undamaged computational natural frequencies were 61.738 Hz, 480.33 Hz, 725.80 Hz and 1042.70 Hz, whereas the natural frequencies identified from beam testing were 57.90 Hz, 400.00 Hz, 720.00 Hz and 1090 Hz. There was a good agreement found in the first four natural frequencies.

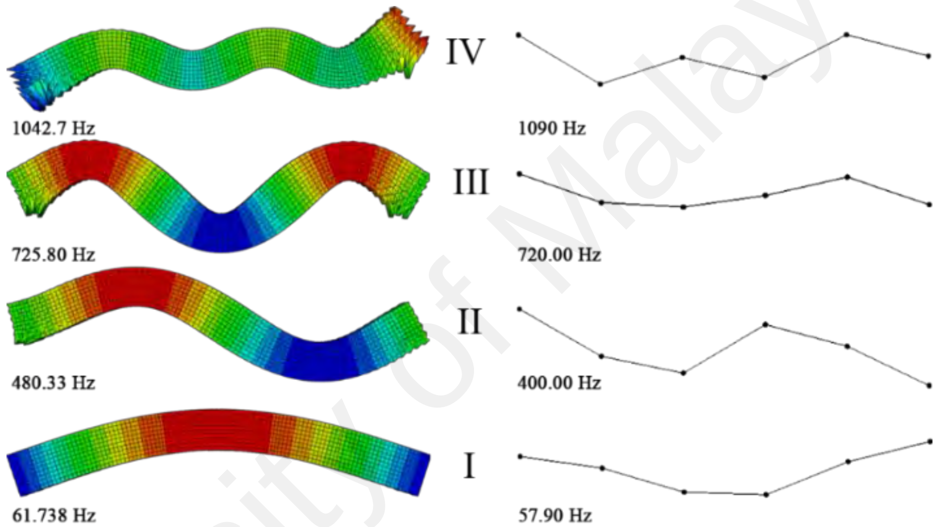


**Figure 6.8:** Computational (left) and Experimental (right) mode shapes

The reasons for carrying out modal analysis were; to calibrate the computational model with the test specimen, and, to analyze the sensitivity of the linear dynamic procedure to different damage stages. It was found that there is not much reduction in natural frequencies with the progression of damage.

The comparison of the first four natural frequencies for simulation and impact hammer testing on Beam-III can be seen in Figure 6.9. There was an average of 10% decrease in natural frequencies in simulation and 14% decrease in the impact hammer testing at complete failure. These results agree with the results of Hamad et al. (2015), which was

12%. The resonant frequency degradation, therefore, is not significantly affected by the damage.

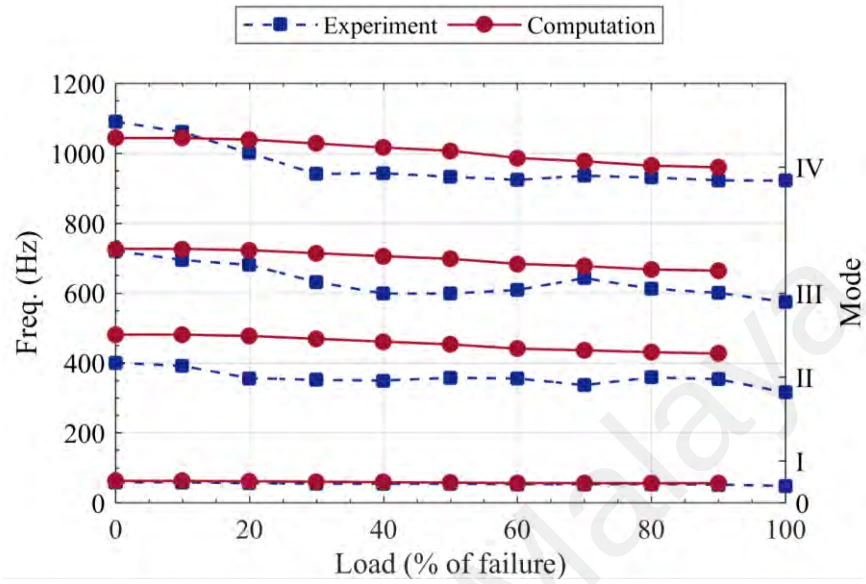


**Figure 6.9:** Experimental and computational values of first four modal frequencies

Now that a reasonable match was made between mode shapes and natural frequencies, the mechanical behavior of the beam was investigated in further detail. As there is not significant difference in the degradation of the modal frequencies (Figure 6.10), only first modal frequency was used for the further analysis.

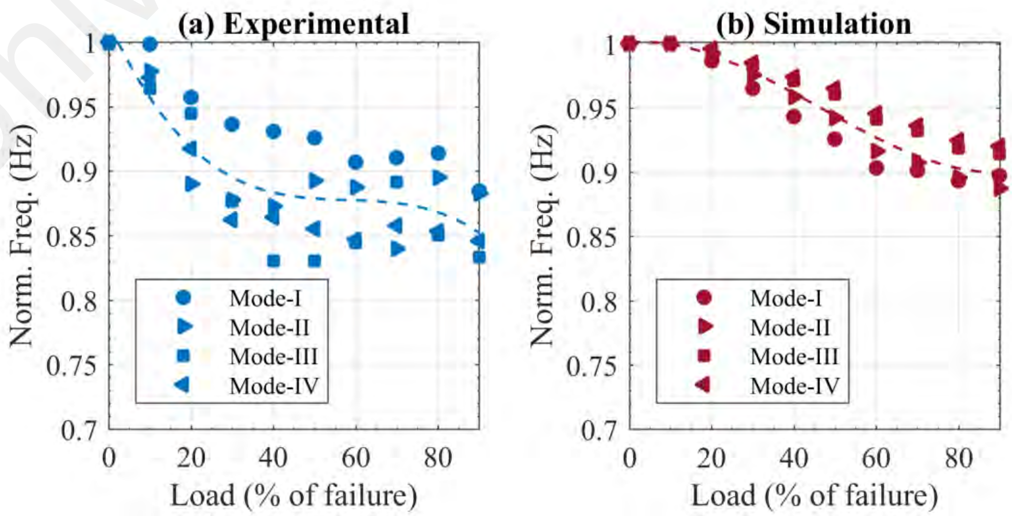


**Figure 6.10:** Normalized frequency degradation for first four modes

The normalized first natural frequency at each cycle was compared with the damage level (represented as the percentage load of the failure load) and the average crack height (calculated by averaging the crack heights formed at different damage levels). The relation between the damage load and the first natural frequency can be seen in Figure 6.11 (a). It can be seen that there is a significant decrease in first natural frequency with crack height increasing up to the 60% of the damage load. This relates with the flexural damage, as cracks propagate the most during initial loading stages (Figure 6.5). The relation between natural frequency and crack height was also attempted, as shown in Figure 6.11 (b). It can be seen that there is a gradual decrease in natural frequencies with crack propagation up to 60 percent of overall depth of the beam. The gradient varies abruptly afterwards, but the drop in natural frequency is maximum 15% even at complete failure.

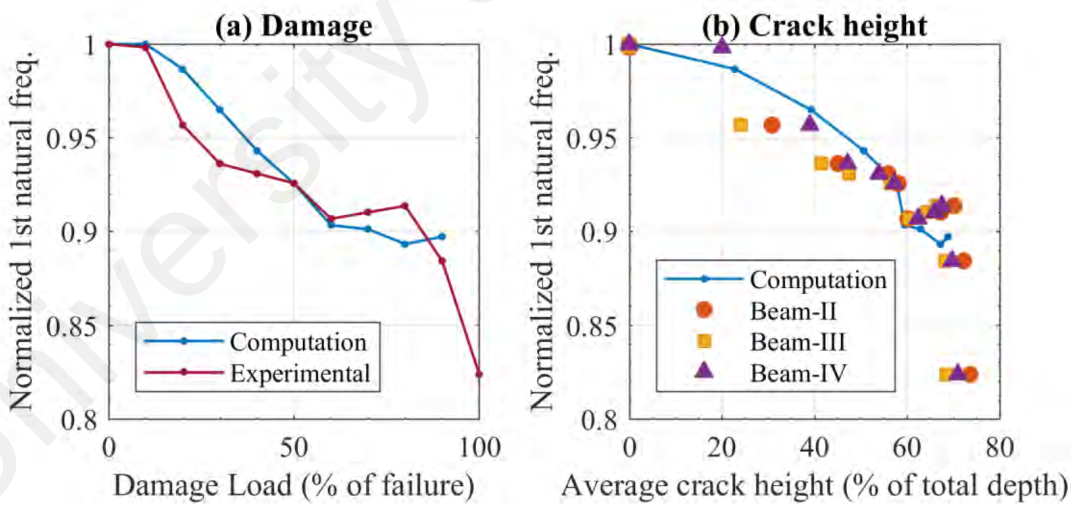


**Figure 6.11:** Natural frequency comparison with damage and crack height

Summing it up, the flexural crack formation is most significant at initial damage levels up to 60% of the damage load, and the natural frequency reduction is also smooth during this damage. But with the formation of inclined cracks, the trend seems to change; the flexural crack formation slows down and the frequency drop also reduces. However, the modal response can be used for determining the approximate fundamental frequency, as it does not vary significantly; and with an approximate value, the excitation frequency of harmonic excitation can be determined.

### 6.4.2 Restoring Force surfaces

Restoring force surface method is a very efficient way to identify nonlinear behavior. In terms of linear systems, the restoring force surfaces do not change their slope. But for nonlinear systems, the restoring force surfaces change their slope with change in the level of nonlinearity.

The formation of restoring force surfaces requires the acceleration, the displacement, the velocity as well as the input force. The model in this study was simulated with a harmonic excitation of 30 Hz for 10 seconds, sampled at 200Hz. The simulation values of the displacement, velocity, acceleration and the excitation force can be shown in Figure 6.12. Usually, the velocity response is integrated and differentiated to obtain displacement and acceleration, respectively.

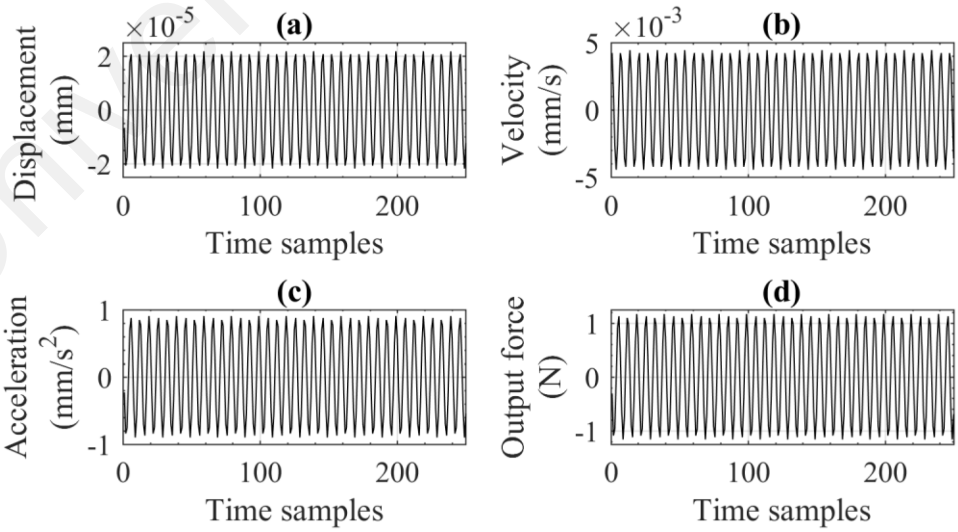


**Figure 6.12:** Typical response of the beam to a harmonic excitation

Restoring force surface can be visualized as a relation between restoring force and modal displacement in the phase plane. The values of restoring force were calculated by subtracting inertial forces from the applied forces, where the modal mass was taken as half the mass of the beam according to Hamad et al., (2015). The plots of restoring force with the response can be seen in Figure 6.13. In the figure, there are two data sets presented, the response at 10% damage and at 60% damage. For linear case, there is no difference in the slope of the curve fit. However, for nonlinear case, the slope of the restoring force decreases with increasing damage. The slope of the fit is referred to as modal stiffness.

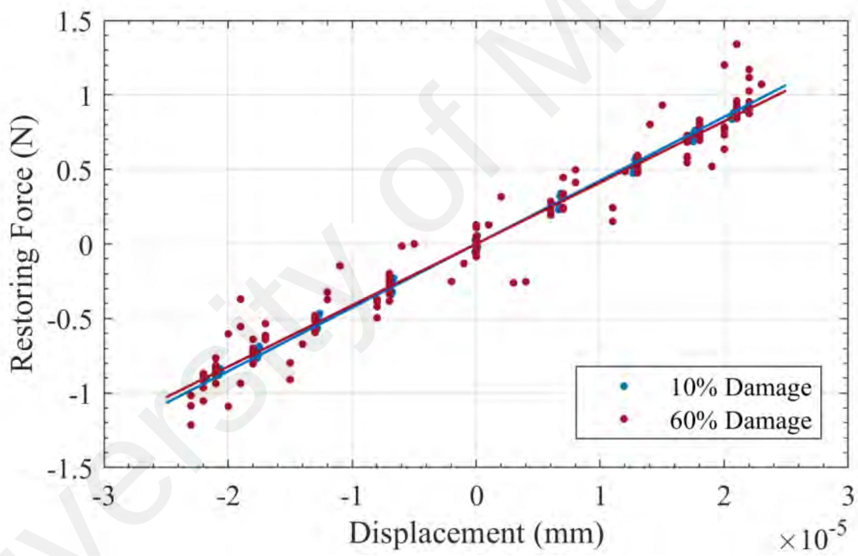


**Figure 6.13:** Curve fit for restoring force vs displacement plot

The complete restoring force displacement relation for the beam at different levels has been plotted in Figure 6.14. The modal stiffness calculation was also made for each damage level. The modal stiffness reduction was attempted at different amplitudes of harmonic excitation. The modal stiffness remains same for different damage levels except the magnitude of force increases. Experimentally, the restoring force is not dependent on the stiffness or the damping. But these factors have been incorporated in the concrete model. The stiffness reduction and damping were incorporated during nonlinear equation solution using implicit dynamic solution procedures.

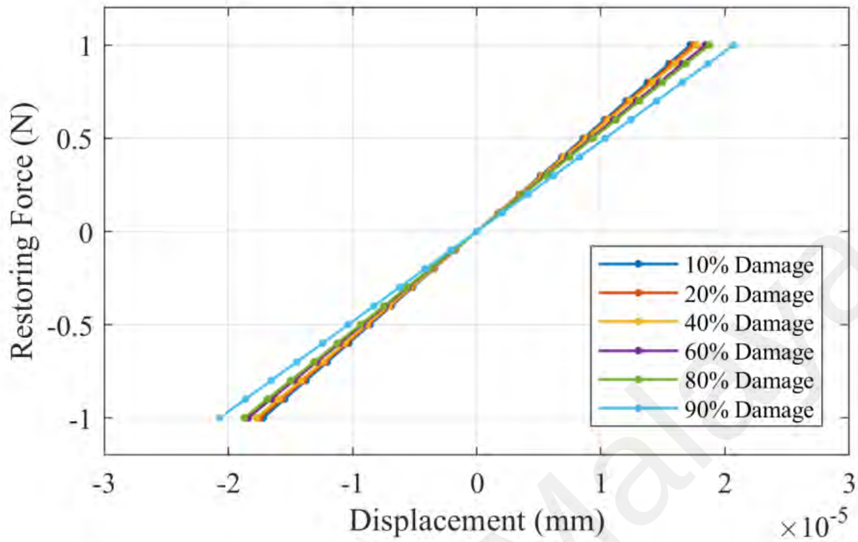


**Figure 6.14:** Restoring force vs displacement (response) at different damage levels

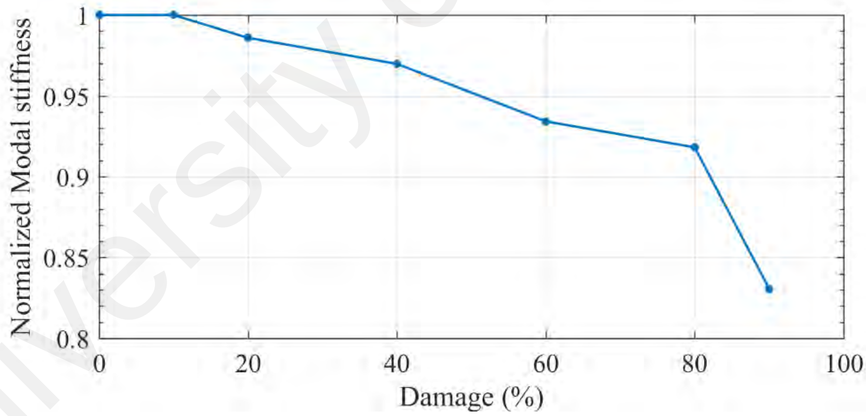


**Figure 6.15:** Simulated modal stiffness response to damage

From the above analysis of the harmonic response of the simulated specimen in terms of restoring force-displacement relationships, the maximum reduction in modal stiffness was 17% (Figure 6.15) which is stiff response as compared to the 45% observed in the other research (Hamad et al., 2015), and can be attributed to the stiffer beam (a/d = 3.55) as compared to slender beam (a/d=5.55). The restoring force surfaces are not reliant on the type of signals, so the formation of restoring force surfaces can be a good aid in partial modal stiffness calculation and the extent of non-linearity present. The model presented by Hamad et al., (2015) for flexural loading on slender beam is more sensitive to damage, as the modal stiffness reduction is up to 45 percent of the original modal stiffness. And the restoring force surfaces have also been used to identify the current condition of the structures (Tan, 2003). In this study, the formation of restoring force surfaces shows the capability of this model to detect the nonlinear behavior, which can be used as a useful tool in real-time health monitoring situations.

### 6.4.3 Formation of Super-harmonics

Formation of super-harmonics is the indication of damage. The cracks, present in the form of micro-cracks or generated through damage, constrain the structure to vibrate in a sinusoidal way, and that is why super-harmonics form, as the structure does not vibrate in a perfect harmonic manner. This can be attributed to the presence of micro-cracks, which merge at higher damage load to become macro-cracks. These micro-cracks are the reason for not propagating the sinusoidal vibration through the beam. These micro-cracks are already present in the structure even in its undamaged state, that is the reason – there may be formation of super-harmonics in undamaged state.

To investigate the presence of nonlinear behavior, a harmonic excitation of 30 Hz was applied at a point 440mm from the support at different amplitudes in the finite element simulation. This was achieved by applying implicit integration schemes for the solution of nonlinear set of equations. Fast Fourier transform (FFT) was performed on the simulation result to get the response to the acceleration in frequency domain.

For harmonic excitation a at frequency of 30Hz, the formation of super-harmonics was studied. The simulated beams response can be seen through Figure 6.16 to Figure 6.19. There were four types of forces applied 150N, 300N, 750N and 1500N. It can be seen in the magnified views of Figure 6.16 (b) to Figure 6.19 (b) that the magnitude of the $2^{nd}$

harmonic (60Hz) increases up to 60% damaged load, and then reduces. The effect was observed in case of all the amplitudes of the applied force. However, the frequency domain response shows the excited first mode. But there was no effect on the magnitude of the super-harmonics formed at the integer multiple of the excitation frequency.

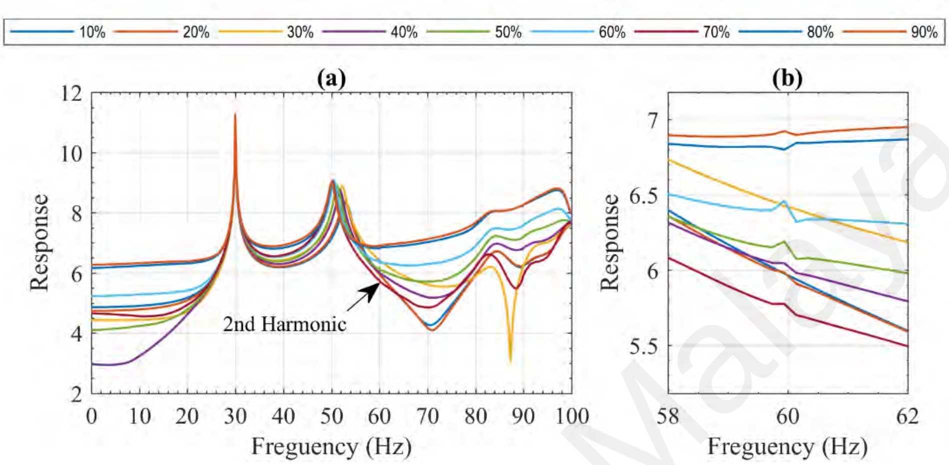


**Figure 6.16:** (a) Formation of super-harmonics at 150N force, (b) magnified view

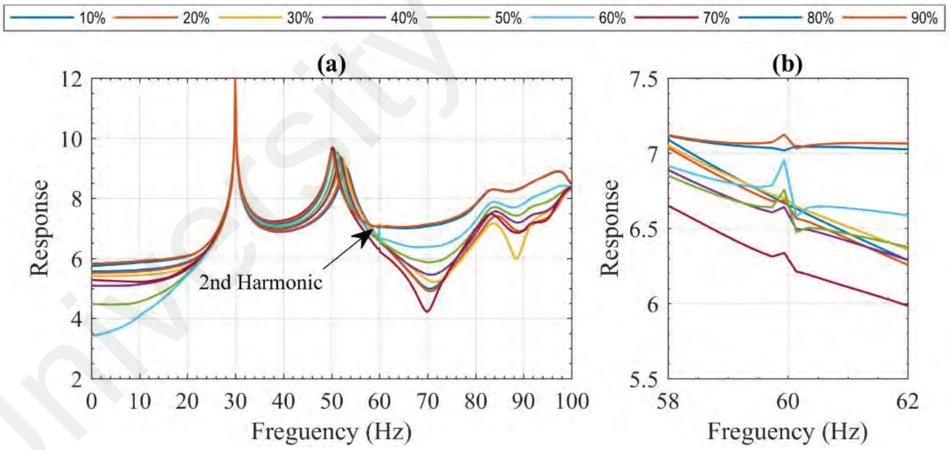


**Figure 6.17:** (a) Formation of super-harmonics at 300N force, (b) magnified view

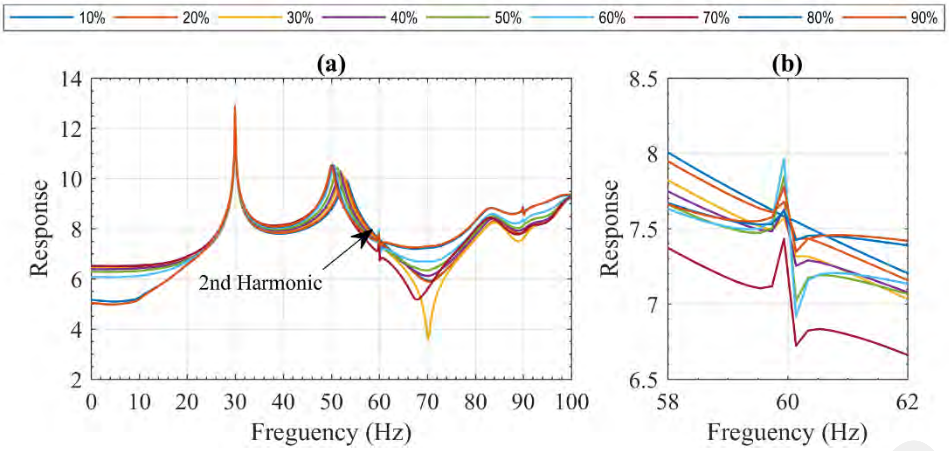


**Figure 6.18:** (a) Formation of super-harmonics at 750N force, (b) magnified view

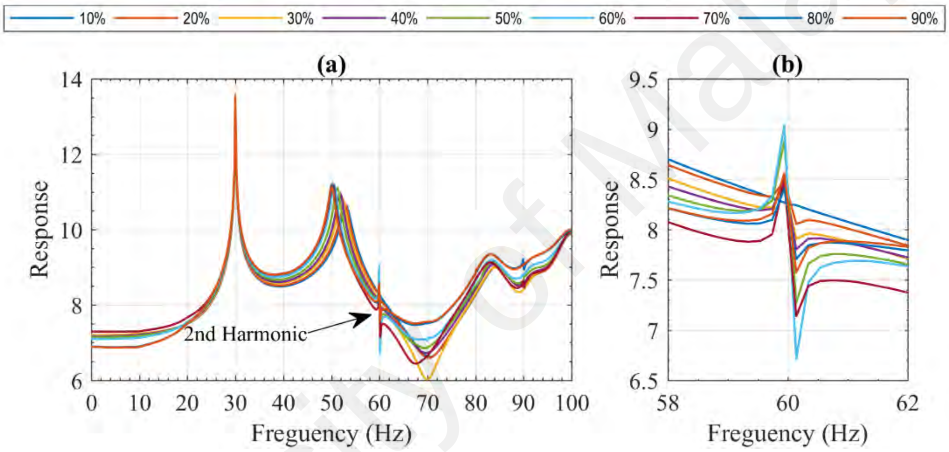


**Figure 6.19:** (a) Formation of super-harmonics at 1500N force, (b) magnified view

In case of experimental setup, the harmonic excitation was applied on top of the beam by using a vibration shaker. Because there was lack of signal conditioner, the response signal had noise in it. To reduce the noise in the output signal, the acceleration response data were down-sampled by a factor of 10, to obtain a smoother signal. The peaks of the down-sampled response were calculated and the Fast Fourier Transform (FFT) was performed to obtain the response of acceleration with reduced noise and clearer formation of 2$^{nd}$ harmonic (60Hz). A typical experimental response can be observed in Figure 6.20 for different damage levels. The second harmonic (60Hz) magnitude increases with the increase in damage, and is maximum at 60 percent damage load, from where the magnitude starts decreasing with further damage. Super-harmonics can be the direct indicative of the crack presence in concrete structures. The sensitivity to damage, translated as the magnitude of harmonic, increases up to initial damage levels, and then reduces. The sensitivity to super-harmonics for slender beams with flexure damage has been said to be maximum at 27% of damage (Neild, 2001) and 40% according to Hamad et al., (2015). In case of stiffer beam, the sensitivity was observed between 50-60% of the failure load, at higher magnitudes of excitation force.

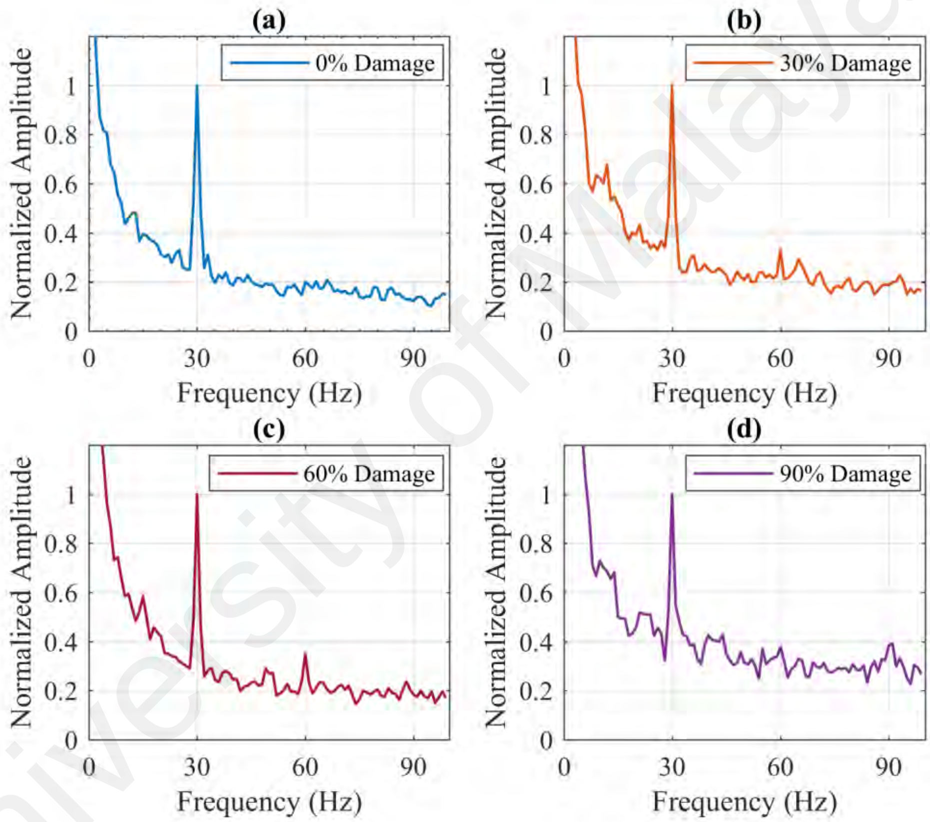


**Figure 6.20:** Experimental Super-harmonics at different damage levels

The nonlinear behavior detection from formation of super-harmonics is more sensitive to damage, but it does not follow monotonic trend with increasing damage. This limitation was addressed using a relation which involved super-harmonics, excitation force and damage load.

## 6.5 Baseline for damage detection

It has been seen that the model presented in this study is capable of reproducing the nonlinear behavior in RC beams from restoring force surfaces and the formation of super-harmonics, which has been in reasonable agreement with experiments. The nonlinear characteristics were investigated in terms of non-linearity coefficient. The ratio of the 2$^{nd}$ harmonic and the respective excitation force was termed as non-linearity coefficient. Polynomial curve fitting for simulation and experimental data was applied to the relation between the damage and the nonlinearity coefficient. The computational and the experimental curve fits of nonlinearity coefficient can be seen in Figure 6.21 and Figure 6.22, respectively. The nonlinearity coefficient was maximum at approximately 50-60 percent of the damage. It was found that nonlinearity is 5 times more sensitive to damage as compared to the modal frequency, which was only reduced 10% at 60% of the load.

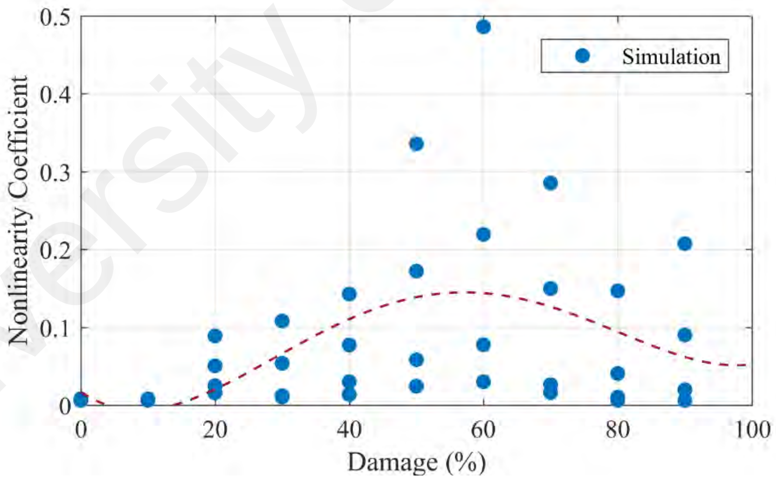


**Figure 6.21:** Effect of damage on nonlinearity coefficient (Simulation)

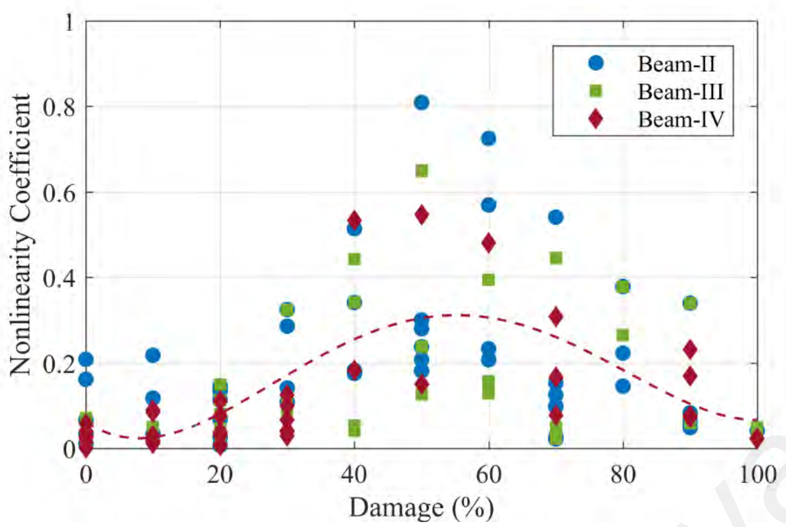


**Figure 6.22:** Effect of damage on nonlinearity coefficient (Experiment)

As there was an increase in the nonlinearity coefficient with increase in excitation force, the damage vs nonlinearity coefficient plots were separated according to the excitation forces at different amplitudes. The parameter of excitation force was plotted along with the nonlinearity coefficient and the damage level, as shown in the waterfall plot (Figure 6.23). Cubic interpolation was then applied using '*fit*' command in MATLAB for three parameters of damage, excitation force and nonlinearity, coefficients; in x, y and z directions, respectively. Resultantly, a surface was formed among these three parameters, as can be seen in Figure 6.24. This surface can be used in estimating the any of the three parameters from the corresponding known parameters. For instance, the nonlinearity coefficient has been estimated from the known values of damage and excitation force in Figure 6.25. A code was written in MATLAB for mapping the unknown parameter, as given in Appendix-C.

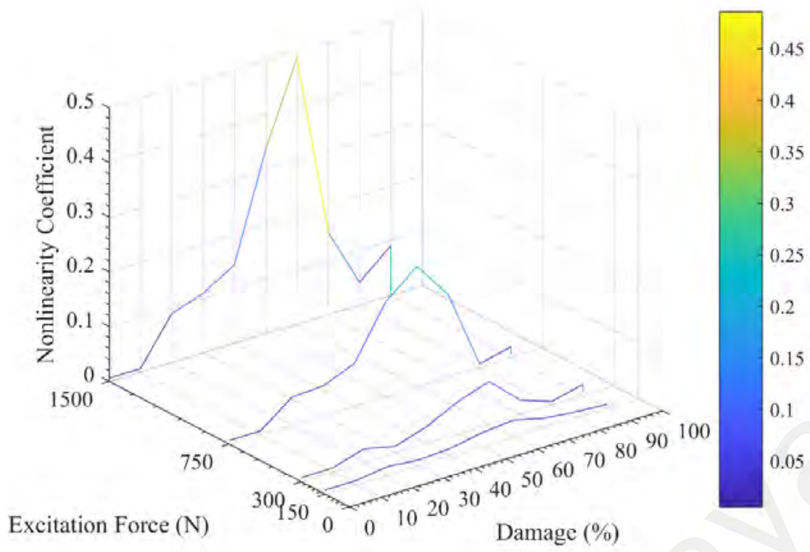


**Figure 6.23:** Waterfall plot of the simulated parameters

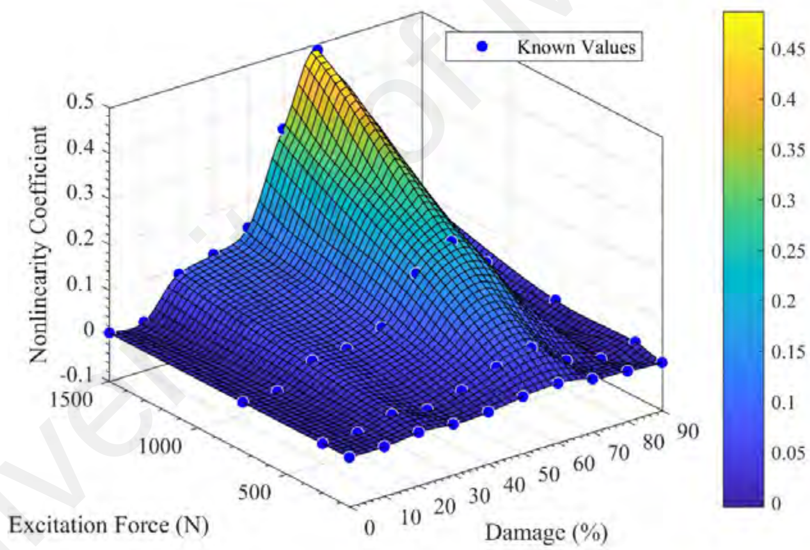


**Figure 6.24:** Interpolated surface for known parameters from simulation

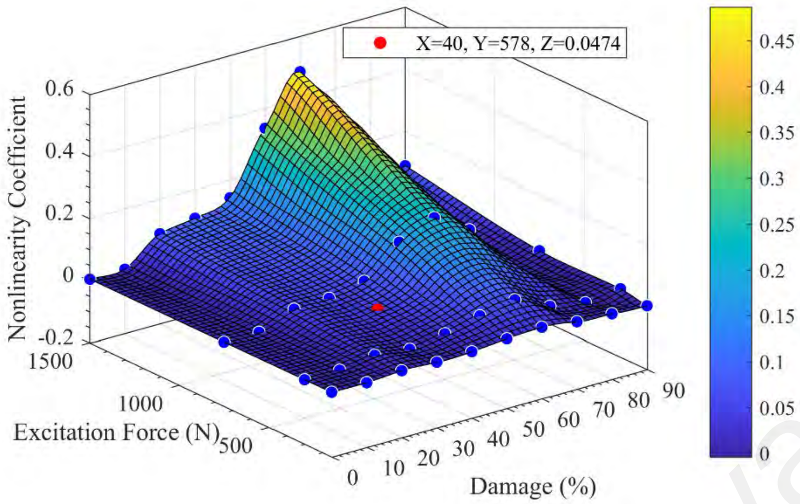


5

**Figure 6.25:** Calculating the unknown value from other two unknown values

This relation between the 3 parameters (damage, excitation force and nonlinearity coefficient) can be used to calculate any of the three parameters while the other two are known. In simpler words, the 3-parameter surface is developed based on the simulated model and can be used as a reference to calculate the unknown parameters from any two known values from experiment. For example, the input values of excitation force were estimated from the 3-parameter surface plot from the simulation results. The known values of damage and the nonlinearity coefficient were used to estimate the experimental values of excitation force. A set of mapped values on the surface from experimental values can be seen in Table 6.1. An estimate of the ranges of predicted force for three different amplitude ranges can be separated as roughly around ~400, ~800 and ~1000 N.

**Table 6.1:** Estimation of excitation force

| Input Damage, % (Simulation) | Input NL coefficient (Simulation) | Predicted force, N (Experiment) |
|---|---|---|
| 50 | 0.237 | 1069 |
| 60 | 0.233 | 793 |
| 70 | 0.153 | 773 |
| 20 | 0.026 | 335 |
| 70 | 0.098 | 541 |
| 40 | 0.047 | 578 |

The procedure explained above, eliminates the dependence on baseline data of the structure through model updating. This method is based on developing a complete damage regime and the effect of that damage on nonlinear behavior. The current condition of the structure can be predicted by overlaying the known on the 3-parameter surface.

Based on the investigation on baseline, a damage detection algorithm is proposed in the following steps

1. Calculate the super-harmonics and the respective nonlinearity coefficients based on the simulation from steps explained in Section 5.1.2
2. Repeat the simulation for at least two or more data set for different excitation forces (similar to Figure 6.23). This will give the range of excitation forces for the formation of surface.
3. Using the three set of data, plot the damage, nonlinearity coefficient and excitation force in 3d axis to form a surface (similar to Figure 6.24), which can be referred to as a reference surface.
4. Excite the actual structure with excitation force between the range of simulated excitation forces and record the response using an accelerometer. Calculate the experimental value of nonlinearity coefficient using FFT.
5. Use MATLAB code (Appendix C) to map the unknown value of damage from the other two known parameters. The tolerance can be calibrated with error in the code until the convergence is reached. This MATLAB code can be used to calculate any unknown of the three parameters while the corresponding other parameters are known.

To examine the possibility of generalization in using this methodology, the material data from another similar research (Hamad et al., 2015) were used to model and analyze the beam for nonlinearity coefficients. These nonlinearity coefficients were used to create the 3-parameter surface. The beam under consideration in the other research was a slender beam and experienced tension failure, in contrast to the beam setup utilized in this research.

Out of all the experimental and simulation aspects, the excitation force was unknown in the data presented in the reference paper. This methodology was used to predict the unknown data of the excitation force. To confirm the consistency of the nonlinear behavior from super-harmonics, the experimental data from Hamad et al. (2015) were used to model the beam using the currently applied model. The super-harmonics were used to calculate the nonlinearity coefficient for 100 and 1000N excitation forces, to observe the exaggerated response. It was revealed that the nonlinear behavior was maximum at 24.6kN loading cycle, which constitutes 59% of the damage load. This consistency in the results for a reasonably slender beam and a stiffer beam shows that at comparatively higher excitation forces for beam-type structures, the nonlinear behavior generally becomes maximum around 60 percent of the failure load. The surface fitting from the simulated FE model is presented in Figure 6.26.

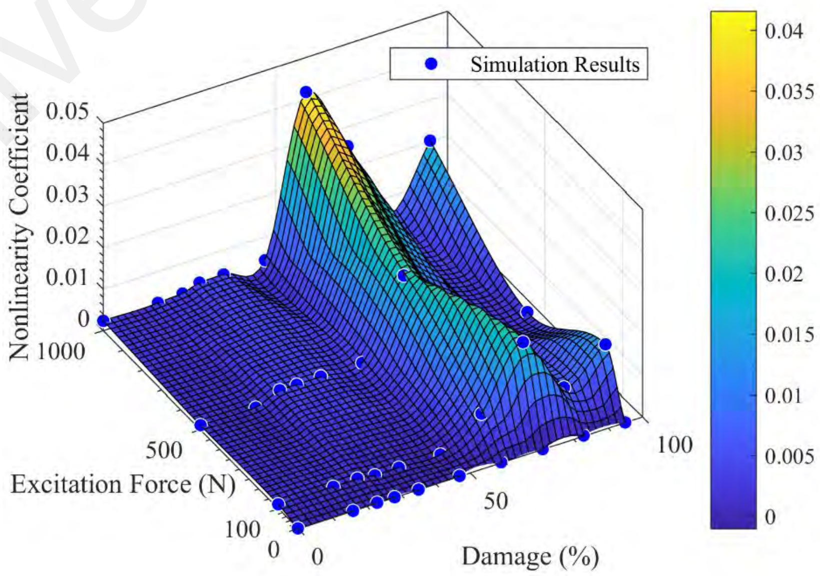


**Figure 6.26:** Interpolated surface values for data from Hamad et al. (2015)

The predicted values of the excitation force can be seen in Figure 6.27. There were few data utilized from Hamad et al. (2015) for estimating excitation force. The force comes out to be 2N, as the excitation response is very low. The predicted values of a few data can be seen in Table 6.2.

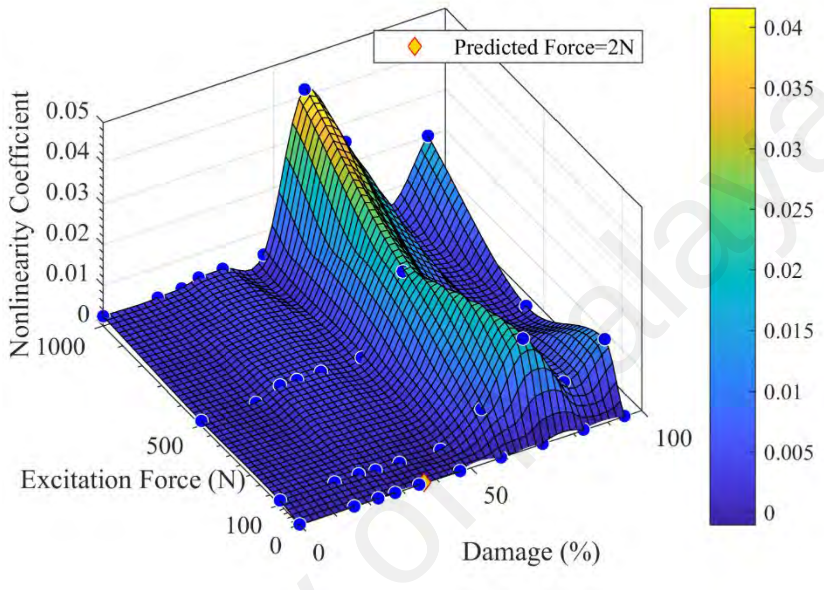


**Figure 6.27:** Predicted excitation force (2N) from Hamad et al. (2015)

It can also be seen in Figure 6.26 that the gradient of the surface at initial damage levels is not much significant. This can give false results while predicting the damage level from excitation force and the nonlinearity coefficient. To cater this, the tolerance of the error has to be calibrated for finding the correct values in the MATLAB code (Appendix-C), as less tolerance can generate error in results. It is suggested to use the tolerance values in the curve fitting almost similar to the significant figures of the excitation force.

**Table 6.2:** Estimated excitation force from Hamad et al. (2015)

| Input Damage, % (Simulation) | Input NL coefficient (Simulation) | Predicted force, N (Experiment) |
|---|---|---|
| 15.708 | 5.45E-06 | 2.000 |
| 23.014 | 7.51E-06 | 2.000 |
| 28.128 | 9.55E-06 | 2.000 |
| 34.795 | 9.7E-06 | 2.000 |
| 46.210 | 9.84E-06 | 2.000 |

From the above analysis on damage detection using nonlinearity coefficients, the reliance on baseline data of the structure can be eliminated. The method proposed is very straightforward and convenient for damage identification, as long as the values of excitation force and nonlinearity coefficient are known. The FE model can be created from the material properties and subsequently the 3-parameter surfaces can be formed. The experimental values of excitation force and nonlinearity coefficients can be used to map the unknown value of the damage on the 3-parameter surface. The type of gradient of the surface can give the indication that how much tolerance is required. For flat surfaces, more sensitivity is required and vice versa. It is therefore suggested to use excitation harmonic forces with higher magnitude to get a better accuracy of the data.

The non-linearity coefficients calculated for the two data sets show that the nonlinearity is maximum at 50-60% of the damage load which, at this level of current research, seems too strong a statement to propose this method to be generally applicable to the bridges. This needs to be further investigated on full scale bridges to validate the general applicability of the nonlinear behavior. As findings from the current study and Hamad et al. (2015) have majorly focused on the flexural dominant damage, the effects of shear (3-point loading) needs to be investigated also to validate the non-monotonicity of the nonlinear behavior.

The aforementioned limitations or the undiscovered aspects of this model, if validated, can make this method which is global, generally applicable and does not rely on baseline data of the structure. The damaged plasticity (CDPM) approach has been successfully applied in the reproducing the nonlinear behavior in RC beams. The improvements in the model and the capabilities in mesh-free analysis can further enhance the efficiency of the model (Alfarah et al., 2017).

# CHAPTER 7: CONCLUSIONS

## 7.1 Summary of the work

A constitutive model for concrete was presented by coupling of plasticity and continuum damage mechanics model to capture the plastic irreversible phenomenon and stiffness degradation due to damage increase, respectively. Carreira and Chu's (1985) compressive uniaxial constitutive relations and Hillerborg's (1976) tensile constitutive relations were incorporated to model the cyclic behavior of concrete behavior. The model was implemented by modeling an RC beam using finite element software ABAQUS. The beam was damaged incrementally by applying four-point flexural load. After every increment of damage, the harmonic excitation was simulated on the beam using implicit dynamic integration schemes at different amplitudes to characterize the nonlinear behavior. The response was investigated using formation of super-harmonics and restoring force surfaces, which was also validated experimentally. A damage assessment method was proposed which addresses the inverse engineering problem faced in structural health monitoring of RC structures.

## 7.2 Conclusions drawn

A sensitive damage detection method was proposed in this study. The constitutive modeling, finite element modeling and the characterization of nonlinear behavior has been used to propose a damage assessment method which addresses the constraints which have not been resolved yet. The model formulation makes it convenient for engineers and researchers to investigate the damage of concrete in more detail and gain more insights incorporating the existing simplified research. Based on the aforesaid explanations, the following conclusions can be drawn.

1. A constitutive model using concrete damaged plasticity model (CDPM) was successfully developed in modeling mechanical behavior of concrete. The proposed model used conventional laboratory test results to construct complete stress-strain behavior of concrete.
2. The model was implemented on an RC beam and it was found to be capable of reproducing the vibration behavior in cracked RC beams. Restoring force surface method and formation of super-harmonics were used to characterize the nonlinear behavior.
3. The sensitivity of nonlinear behavior with damage was compared with the natural frequency reduction and it was found that the nonlinear methods are more sensitive to damage than the modal methods and the proposed methodology does not require model updating.
4. The findings of the model were validated experimentally. It was found that the nonlinear behavior by the formation of super-harmonics tend to increase up to 50 to 60% of the damage load and then decrease gradually.
5. A damage detection method was proposed which uses the 3-parameter relation (damage, nonlinearity and the excitation force) to detect damage in RC beams. The proposed methodology uses progressive damage modeling and eliminates the baseline data during the damage detection.

In the summing, the proposed methodology reproduces the mechanical behavior of concrete accurately and can be efficiently used in SHM of the existing inventory of bridges while saving time and cost.

### 7.3 Recommendation for future research

Finally, the currently applied procedure can provide a major breakthrough in damage detection in realistic damage scenarios (e.g. mix mode crack formation) without the need of baseline structural data. Improved tension and compression models along with damage parameters, can be used to enhance the modeling efficiency in the future. A few advancements in plastic damage model are suggested to be studied for this model, like kinematic hardening and anisotropic damage (Menzel et al., 2005), isotropic damage (Jason et al., 2006) and partially associative plasticity (Wu & Crawford, 2015). Recent advancements can be also studied, a few suggested studies are (Xenos & Grassl, 2016), (Zhu et al., 2017) and (Piscesa et al., 2017).

To be deployed on real life structures, the size effect also needs to be incorporated, as suggested in fracture studies of deterministic strength size effect (Karihaloo et al., 2006). The effect of bond-slip on the dynamic behavior of concrete beams is also suggested (Floros & Ingason, 2013; Inoue et al., 2004).

It is also suggested to investigate this approach while incorporating prestressing effects, as most of the beam-type structures are pre-stressed or post-tensioned. Studies suggest that the pre-stressing enhances the fatigue life of the structures. The bond between reinforcement and concrete also influences the overall dynamic response. It is also suggested that the effects of bond can be studied in line with (Taqieddin, 2008). The nonlinear behavior was recently investigated by (Kim et al., 2017). The dynamic response due to pre-stressing force cannot be reliably detected, a few suggested loading conditions can help in crack detection (Limongelli et al., 2016). It is suggested that this study be deployed on pre-stressed beams to investigate the dynamic behavior of cracks.

The mesh size dependency is a major issue in finite element modeling of RC beams, as it significantly governs the computation cost. It is suggested that the use of fracture energy concept in constitutive modeling can prevent from mesh-size dependency (Nakamura & Higai, 2001). Alfarah et al. (2017) has proposed a model which is not sensitive to characteristic length. The efficiency of the proposed model can be optimized incorporating the mesh insensitivity. The mesh insensitivity, when incorporated can help in efficiency of the model. It is also suggested that the accuracy of model once achieved, can be exploited in modeling different damage scenarios to be incorporated in deep learning or machine learning (Lin et al., 2017), which is the technology SHM can evolve into. The computational efficiencies can be used based on the FE models to extract features for damage detection.

With all said, the model proposed uses the coupling of plasticity and continuum damage mechanics approach. It is possible to study the nonlinear behavior present in the RC structures for any concrete models with the aid of finite element software packages. The optimization of this methodology may lead to a vital contribution in structural health monitoring paradigm of civil engineering structures.

# REFERENCES


AASHTO. (2010). *AASHTO LRFD Bridge Design Specifications*.

ACI 318-14. (2014). *Building Code Requirements for Structural Concrete (ACI 318-14) and Commentary*. *American Concrete Institute*.

Adams, D. E., & Allemang, R. J. (1998). Survey of Nonlinear Detection and Identification Techniques for Experimental Vibrations. *Proceedings on the 23rd International Seminar on Modal Analysis, September 1998, Lueven, Belgium*.

Aktas, M., & Sumer, Y. (2014). Nonlinear finite element analysis of damaged and strengthened reinforced concrete beams. *Journal of Civil Engineering and Management*, *20*(2), 201–210.

Alam, S. Y., Saliba, J., & Loukili, A. (2014). Fracture examination in concrete through combined digital image correlation and acoustic emission techniques. *Construction and Building Materials*, *69*, 232–242.

Alfarah, B., López-Almansa, F., & Oller, S. (2017). New methodology for calculating damage variables evolution in Plastic Damage Model for RC structures. *Engineering Structures*, *132*, 70–86.

Ali, A. M., Farid, B. J., & Al-Janabi, A. I. M. (1990). Stress-Strain Relationship for concrete in compression made of local materials. *Engineering Sciences*, *2*(1), 183–194.

Andriotis, C., Gkimousis, I., & Koumousis, V. (2016). Modeling Reinforced Concrete Structures Using Smooth Plasticity and Damage Models. *Journal of Structural Engineering*, *142*(2), 04015105.

Arafa, M., & Mehlhorn, G. (1998). A modified discrete model in the nonlinear finite element analysis of prestressed and reinforced concrete structures. In *2nd International PhD Symposium in Civil Engineering, Budapest*.

Aslani, F., & Jowkarmeimandi, R. (2012). Stress-strain model for concrete under cyclic loading. *Magazine of Concrete Research*, *64*(8), 673–685.

Babu, R. R., Benipal, G. S., & Singh, A. K. (2005). Constitutive modelling of concrete: an overview. *Asian Journal of Civil Engineering (Building and Housing)*, *6*(4), 211–246.

Barenblatt, G. I. (1962). The mathematical theory of equilibrium cracks in brittle fracture. *Advances in Applied Mechanics*, *7*(1), 55–129.

Benedetti, A., Pignagnoli, G., & Tarozzi, M. (2018). Damage identification of cracked reinforced concrete beams through frequency shift. *Materials and Structures*, *51*(6), 147.

Billing, J. R. (1984). Dynamic loading and testing of bridges in Ontario. *Canadian Journal of Civil Engineering*, *11*(4), 833–843.

Birtel, V., & Mark, P. (2006). Parameterised finite element modelling of RC beam shear failure. In *Proceedings of the 19th Annual International ABAQUS Users' Conference. Boston:[sn]* (pp. 95–108).

Bouboulas, A., & Anifantis, N. (2011). Finite element modeling of a vibrating beam with a breathing crack: observations on crack detection. *Structural Health Monitoring: An International Journal*, *10*(2), 131–145.

Breccolotti, M., Bonfigli, M. F., D'Alessandro, A., & Materazzi, A. L. (2015). Constitutive modeling of plain concrete subjected to cyclic uniaxial compressive loading. *Construction and Building Materials*, *94*, 172–180.

Çalık, İ., Bayraktar, A., Türker, T., & Karadeniz, H. (2014). Structural dynamic identification of a damaged and restored masonry vault using Ambient Vibrations. *Measurement*, *55*, 462–472.

Cao, H., Li, B., & He, Z. (2013). Finite Element Model Updating of Machine-Tool Spindle Systems. *Journal of Vibration and Acoustics*, *135*(2), 024503.

Capozucca, R., & Magagnini, E. (2017). Analysis of cracked RC beams under vibration. In *Journal of Physics: Conference Series* (Vol. 842, p. 12076).

Carden, E. P. (2004). Vibration Based Condition Monitoring: A Review. *Structural Health Monitoring*, *3*(4), 355–377.

Carpinteri, A., Carmona, J. R., & Ventura, G. (2007). Propagation of flexural and shear cracks through reinforced concrete beams by the bridged crack model. *Magazine of Concrete Research*, *59*(10), 743–756.

Carreira, D. J., & Chu, K.-H. (1985). Stress-Strain Relationship for Plain Concrete in Compression. *American Concrete Institute Journal Proceedings*, *82*(6), 797–804.

Çatbaş, F. N., Kijewski-Correa, T., & Aktan, A. E. (Eds.). (2013). *Structural Identification of Constructed Systems - Approaches, Methods and Technologies for Effective Practice of St-Id. American Society of Civil Engineers*. Reston, VA: American Society of Civil Engineers.

Cavadas, F., Smith, I. F. C., & Figueiras, J. (2013). Damage detection using data-driven methods applied to moving-load responses. *Mechanical Systems and Signal Processing*, *39*(1–2), 409–425.

Cawley, P., & Adams, R. D. (1979). The location of defects in structures from measurements of natural frequencies. *The Journal of Strain Analysis for Engineering Design*, *14*(2), 49–57.

CEB-FIP, C. (1991). Model Code 1990. *Comite Euro-International Du Beton, Paris*, 87–109.

Cervera, M., Hinton, E., & Hassan, O. (1987). Nonlinear analysis of reinforced concrete plate and shell structures using 20-noded isoparametric brick elements. *Computers & Structures*, *25*(6), 845–869.

Chae, M. J., Yoo, H. S., Kim, J. Y., & Cho, M. Y. (2012). Development of a wireless sensor network system for suspension bridge health monitoring. *Automation in Construction*, *21*, 237–252.

Chen, A. C. T., & Chen, W. F. (1975). Constitutive Relations for Concrete. *Journal of Engineering Mechanics*, *101*(4), 465–481.

Chen, W.-F. (2007). *Plasticity in reinforced concrete*. J. Ross Publishing.

Cherepanov, G. P. (1967). The propagation of cracks in a continuous medium. *Journal of Applied Mathematics and Mechanics*, *31*(3), 503–512.

Chondros, T. G., Dimarogonas, A. D., & Yao, J. (2001). Vibration of a beam with a breathing crack. *Journal of Sound and Vibration*, *239*(1), 57–67.

Comité euro-international du béton. (1996). *RC Elements Under Cyclic Loading: State of the Art Report* (Vol. 230). Thomas Telford.

Cusatis, G., Mencarelli, A., Pelessone, D., & Baylot, J. (2011a). Lattice Discrete Particle Model (LDPM) for failure behavior of concrete. II: Calibration and validation. In *Cement and Concrete Composites* (Vol. 33, pp. 891–905). Elsevier.

Cusatis, G., Pelessone, D., & Mencarelli, A. (2011b). Lattice Discrete Particle Model (LDPM) for failure behavior of concrete. I: Theory. In *Cement and Concrete Composites* (Vol. 33, pp. 881–890). Elsevier.

Daly, A. F. (2000). Bridge management in Europe (BRIME): Modelling of deteriorated structures. In *Bridge Management 4-Inspection, Maintenance, Assessment and Repair*.

Daneshyar, A., & Ghaemian, M. (2017). Coupling microplane-based damage and continuum plasticity models for analysis of damage-induced anisotropy in plain concrete. *International Journal of Plasticity*, *95*, 216–250.

Dassault Systèmes. (2013). *ABAQUS Analysis User's Manual*. *Dassault Systemes Simulia Corp., Providence, RI*.

De Maesschalck, R., Jouan-Rimbaud, D., & Massart, D. L. (2000). The Mahalanobis distance. *Chemometrics and Intelligent Laboratory Systems*, *50*(1), 1–18.

Desayi, P., & Krishnan, S. (1964). Equation for the Stress-Strain Curve of Concrete. *ACI Journal Proceedings*, *61*(3).

Dharmaraju, N., Tiwari, R., & Talukdar, S. (2004). Identification of an open crack model in a beam based on force-response measurements. *Computers and Structures*, *82*(2–3), 167–179.

Dilena, M., & Morassi, A. (2011). Dynamic testing of a damaged bridge. *Mechanical Systems and Signal Processing*, *25*(5), 1485–1507.

Dilena, M., Morassi, A., & Perin, M. (2011). Dynamic identification of a reinforced concrete damaged bridge. *Mechanical Systems and Signal Processing*, *25*(8), 2990–

3009.

Doebling, S. W., Farrar, C. R., Prime, M. B., & others. (1998). A summary review of vibration-based damage identification methods. *Shock and Vibration Digest*, *30*(2), 91–105.

Du, X.-L., Lu, D.-C., Gong, Q.-M., & Zhao, M. (2010). Nonlinear unified strength criterion for concrete under three-dimensional stress states. *Journal of Engineering Mechanics*, *136*(1), 51–59.

Dugdale, D. S. (1960). Yielding of steel sheets containing slits. *Journal of the Mechanics and Physics of Solids*, *8*(2), 100–104.

Elices, M., & Planas, J. (1996). Fracture mechanics parameters of concrete. *Advanced Cement Based Materials*, *4*(3–4), 116–127.

EN1992-1-1. (2004). *Eurocode 2: Design of concrete structures-Part 1-1: General rules and rules for buildings*. *European Committee for Standardization*. Brussels, 2004.

Ewins, D. J. (1984). *Modal testing: theory and practice* (Vol. 15). Research studies press Letchworth.

Farrar, C. R., & Cone, K. M., Farrar, C. R. C., & Cone, K. K. M. (1994). *Vibration testing of the I-40 bridge before and after the introduction of damage*. *Report: LA-UR-94-3470, CONF-950240-3*.

Farrar, C. R., & Doebling, S. W. (1997, June). An overview of modal-based damage identification methods. In *Proceedings of DAMAS conference* (pp. 269-278).

Farrar, C. R., & Jauregui, D. A. (1998). Comparative study of damage identification algorithms applied to a bridge: I. Experiment. *Smart Materials and Structures*, *7*(5), 720–731.

Farrar, C. R., & Worden, K. (2007). An introduction to structural health monitoring. *Philosophical Transactions. Series A, Mathematical, Physical, and Engineering Sciences*, *365*(1851), 303–15.

Feenstra, P. H., & De Borst, R. (1996). A composite plasticity model for concrete. *International Journal of Solids and Structures*, *33*(5), 707–730.

FHWA. (2013). *Status of the Nation's Highways, Bridges, and Transit: Conditions and Performance*. Washington, DC: Federal Highway Administration. http://www. fhwa. dot. gov/policy.

Floros, D., & Ingason, O. A. (2013). *Modeling and simulation of reinforced concrete beams*. *Master's Thesis*. Chalmers University of Technology. Sweden.

Follen, C. W., Sanayei, M., Brenner, B. R., & Vogel, R. M. (2014). Statistical Bridge Signatures. *Journal of Bridge Engineering*, 04014022.

Frederick, C. O., & Armstrong, P. J. (2007). A mathematical representation of the multiaxial Bauschinger effect. *Materials at High Temperatures*, *24*(1), 1–26.

Fröjd, P., & Ulriksen, P. (2018). Detecting damage events in concrete using diffuse ultrasound structural health monitoring during strong environmental variations. *Structural Health Monitoring*, *17*(2), 410–419.

Fu, H. C., Erki, M. A., & Seckin, M. (1991). Review of Effects of Loading Rate on Concrete in Compression. *Journal of Structural Engineering*, *117*(12), 3645–3659.

Fu, Y., & DeWolf, J. T. (2004). Effect of Differential Temperature on a Curved Post-Tensioned Concrete Bridge. *Advances in Structural Engineering*, *7*(5), 385–397.

Fujino, Y., & Siringoringo, D. M. (2008). Structural health monitoring of bridges in Japan: An overview of the current trend. In *Proc. 4th Int. Conf. FRP CICE*.

Geiger, D., Wells, P., Bugas-Schramm, P., Love, L., McNeil, S., Merida, D., … others. (2005). *Transportation Asset Management in Australia, Canada, England, and New Zealand*.

Ghaedi, K., Ibrahim, Z., Adeli, H., & Javanmardi, A. (2017). Recent developments in vibration control of building and bridge structures. *Journal of Vibroengineering*, *19*(5), 3564–3580.

Ghaedi, K., Jameel, M., Ibrahim, Z., & Khanzaei, P. (2016). Seismic analysis of Roller Compacted Concrete (RCC) dams considering effect of sizes and shapes of galleries. *KSCE Journal of Civil Engineering*, *20*(1), 261–272.

Global Times. (2017). Construction boom brings China 805,300 road bridges. Retrieved from http://www.globaltimes.cn/content/1073693.shtml

Gomez, H. C., Fanning, P. J., Feng, M. Q., & Lee, S. (2011). Testing and long-term monitoring of a curved concrete box girder bridge. *Engineering Structures*, *33*(10), 2861–2869.

Gopalaratnam, V. S., & Shah, S. P. (1985). Softening response of plain concrete in direct tension. In *American Concrete Institute Journal Proceedings* (Vol. 82, pp. 310–323).

Gounaris, G., & Dimarogonas, A. (1988). A finite element of a cracked prismatic beam for structural analysis. *Computers and Structures*, *28*(3), 309–313.

Grassl, P., & Jirásek, M. (2006). Damage-plastic model for concrete failure. *International Journal of Solids and Structures*, *43*(22–23), 7166–7196.

Grassl, P., Xenos, D., Nyström, U., Rempling, R., & Gylltoft, K. (2013). CDPM2: A damage-plasticity approach to modelling the failure of concrete. *International Journal of Solids and Structures*, *50*(24), 3805–3816.

Gratacos, P., Montmitonnet, P., & Chenot, J. L. (1992). An integration scheme for Prandtl-Reuss elastoplastic constitutive equations. *International Journal for Numerical Methods in Engineering*, *33*(5), 943–961.

Guan, H. (2006). *Vibration-based structural health monitoring of highway bridges* (Doctoral dissertation, UC San Diego).

Hafezolghorani, M., Hejazi, F., Vaghei, R., Jaafar, M. S. Bin, & Karimzade, K. (2017). Simplified Damage Plasticity Model for Concrete. *Structural Engineering International*, *27*(1), 68–78.

Hamad, W. I., Owen, J. S., & Hussein, M. F. M. (2011a). A flexural crack model for damage detection in reinforced concrete structures. *Journal of Physics: Conference Series*, *305*(1), 012037.

Hamad, W. I., Owen, J. S., & Hussein, M. F. M. (2011b). The use of fictitious crack model in modelling the vibration behaviour of cracked reinforced concrete beams. *The 8th International Conference on Structural Dynamics (EURODYN)*.

Hamad, W. I., Owen, J. S., & Hussein, M. F. M. (2013). An efficient approach of modelling the flexural cracking behaviour of un-notched plain concrete prisms subject to monotonic and cyclic loading. *Engineering Structures*, *51*, 36–50.

Hamad, W. I., Owen, J. S., & Hussein, M. F. M. (2015). Modelling the degradation of vibration characteristics of reinforced concrete beams due to flexural damage. *Structural Control and Health Monitoring*, *22*(6), 939–967.

Hamed, E., & Frostig, Y. (2004). Free vibrations of cracked prestressed concrete beams. *Engineering Structures*, *26*(11), 1611–1621.

Hanif, M. U., Ibrahim, Z., Jameel, M., Ghaedi, K., & Aslam, M. (2016). A new approach to estimate damage in concrete beams using non-linearity. *Construction and Building Materials*, *124*(C), 1081–1089.

Hartle, R. A., Amrhein, W. J., Wilson III, K. E., Baughman, D. R., & Tkacs, J. J. (1995). *Bridge inspector's training manual/90*.

Hearn, G. (2007). *Bridge inspection practices* (Vol. 375). Transportation Research Board.

Hibbitt, H. D., & Karlsson, B. I. (1979). Analysis of pipe whip (No. EPRI-NP--1208). Hibbitt and Karlsson.

Hilber, H. M., & Hughes, T. J. R. (1978). Collocation, dissipation and [overshoot] for time integration schemes in structural dynamics. *Earthquake Engineering & Structural Dynamics*, *6*(1), 99–117.

Hill, R. (1998). *The mathematical theory of plasticity* (Vol. 11). Oxford university press.

Hillerborg, A. (1983). Analysis of one single crack. *Fracture Mechanics of Concrete (Developments in Civil Engineering)*, 223–249.

Hillerborg, A., Modéer, M., & Petersson, P.-E. (1976). Analysis of crack formation and crack growth in concrete by means of fracture mechanics and finite elements. *Cement and Concrete Research*, *6*(6), 773–781.

Hiwarkar, V. (2010). Nonlinear dyamics of cracked structures for non-destructive evaluation (Doctoral dissertation, Loughborough University, © Vikrant Hiwarkar).

Hodge, P. G. (1957). A general theory of piecewise linear plasticity based on maximum shear. *Journal of the Mechanics and Physics of Solids*, *5*(4), 242–260.

Hordijk, D. A. (1991). *Local approach to fatigue of concrete*. (Doctoral dissertation, TU Delft, Delft University of Technology).

Hsu, T. T. C., Slate, F. O., Sturman, G. M., & Winter, G. (1963). Microcracking of Plain Concrete and the Shape of the Stress-Strain Curve. *ACI Journal Proceedings*, *60*(2), 209–224.

Hu, H. T., & Schnobrich, W. C. (1989). Constitutive modeling of concrete by using nonassociated plasticity. Journal of Materials in Civil Engineering, 1(4), 199-216.

Hu, H.-T., & Schnobrich, W. C. (1990). Nonlinear Analysis of Cracked Reinforced Concrete. *Structural Journal*, *87*(2), 199–207.

Huszár, Z. (2001). Linear and non-linear modelling of dynamic behaviour of cracked reinforced concrete beams. In 1th Albert Caquot International Conference, Párizs (pp. 3-5).

Huszár, Z. (2006). Vibrations of Cracked Reinforced and Prestressed Concrete Beams. In *IABSE Symposium Report* (Vol. 92, No. 19, pp. 89-96). International Association for Bridge and Structural Engineering.

Inoue, K., Kikuchi, M., Ueda, M., & Koshikawa, T. (2004). Vibration analysis of reinforced concrete beam members including bond-slip of reinforcement. In *13th World Conference on Earthquake Engineering*.

Irwin, G. R. (1957). Relation of stresses near a crack to the crack extension force. *9th Cong. App. Mech., Brussels*.

Jankowiak, T., & Lodygowski, T. (2005). Identification of parameters of concrete damage plasticity constitutive model. *Foundations of Civil and Environmental Engineering*, *6*(1), 53–69.

Jason, L., Huerta, A., Pijaudier-Cabot, G., & Ghavamian, S. (2006). An elastic plastic damage formulation for concrete: Application to elementary tests and comparison with an isotropic damage model. *Computer Methods in Applied Mechanics and Engineering*, *195*(52), 7077–7092.

Jáuregui, D. V., & Barr, P. J. (2004). Nondestructive Evaluation of the I-40 Bridge over the Rio Grande River. *Journal of Performance of Constructed Facilities*, *18*(4), 195–204.

Kachanov, L. M. (1958). On the creep fracture time. *Izv Akad, Nauk USSR Otd Tech*, *8*, 26–31.

Karihaloo, B. L., Abdalla, H. M., & Xiao, Q. Z. (2006). Deterministic size effect in the strength of cracked concrete structures. *Cement and Concrete Research*, *36*(1), 171–188.

Karsan, I. D., & Jirsa, J. O. (1969). Behavior of Concrete Under Compressive Loadings. *Journal of the Structural Division, ASCE*, *95*(12), 2543–2564.

Kim, G.-J., Park, S.-J., & Kwak, H.-G. (2017). Experimental characterization of ultrasonic nonlinearity in concrete under cyclic change of prestressing force using Nonlinear Resonant Ultrasonic Spectroscopy. *Construction and Building Materials*, *157*, 700–707.

Kim, G. J., Park, S. J., & Kwak, H. G. (2017). Experimental characterization of ultrasonic nonlinearity in concrete under cyclic change of prestressing force. *Computers and Concrete*, *19*(5), 599–607.

Kim, S., Pakzad, S., Culler, D., Demmel, J., Fenves, G., Glaser, S., & Turon, M. (2007). Health Monitoring of Civil Infrastructures Using Wireless Sensor Networks. *2007 6th International Symposium on Information Processing in Sensor Networks*, 254–263.

King, N. S. (1999). Malaysian Bridges—Status and Condition. *Lecture Notes for Special Course on Bridge Assessment and Rehabilitation, Civil Engineering Department. Universiti Putra Malaysia*, 2–4.

Kong, X., Cai, C.-S., Hu, J., Kong, X., Cai, C.-S., & Hu, J. (2017). The State-of-the-Art on Framework of Vibration-Based Structural Damage Identification for Decision Making. *Applied Sciences*, *7*(5), 497.

Krätzig, W. B., & Pölling, R. (2004). An elasto-plastic damage model for reinforced concrete with minimum number of material parameters. *Computers & Structures*, *82*(15–16), 1201–1215.

Krauss, R., W., N., & H., A. (1999). Comparison of experimental identification techniques for a nonlinear SDOF system. In Anon (Ed.), *Proceedings of the International Modal Analysis Conference - IMAC* (Vol. 2, pp. 1182–1187). SEM, Bethel, CT, United States.

Kupfer, H., Hilsdorf, H. K., & Rusch, H. (1969). Behavior of Concrete Under Biaxial Stresses. *ACI Journal Proceedings*, *66*(8), 656–666.

Law, S. S., Ward, H. S., Shi, G. B., Chen, R. Z., Waldron, P., & Taylor, C. (1995a). Dynamic Assessment of Bridge Load-Carrying Capacities. I. *Journal of Structural Engineering*, *121*(3), 478–487.

Law, S. S., Ward, H. S., Shi, G. B., Chen, R. Z., Waldron, P., & Taylor, C. (1995b). Dynamic Assessment of Bridge Load-Carrying Capacities. II. *Journal of Structural Engineering*, *121*(3), 488–495.

Law, S. S., & Zhu, X. Q. (2004). Dynamic behavior of damaged concrete bridge structures under moving vehicular loads. *Engineering Structures*, *26*(9), 1279–1293.

Lee, J., & Fenves, G. L. (1998). Plastic-Damage Model for Cyclic Loading of Concrete Structures. *Journal of Engineering Mechanics*, *124*(8), 892–900.

Lee, P. K. K., Ho, D., & Chung, H. (1987). Static and Dynamic Tests of Concrete Bridge. *Journal of Structural Engineering*, *113*(1), 61–73.

Lee, U., & Shin, J. (2002). A frequency response function-based structural damage identification method. *Computers and Structures*, *80*(2), 117–132.

Li, C., Hao, H., & Bi, K. (2017). Numerical study on the seismic performance of precast segmental concrete columns under cyclic loading. *Engineering Structures*, *148*, 373–386.

Li, H.-N., Yi, T.-H., Ren, L., Li, D.-S., & Huo, L.-S. (2014). Reviews on innovations and applications in structural health monitoring for infrastructures. *Structural Monitoring and Maintenance*, *1*(1), 1.

Limongelli, M. P., Siegert, D., Merliot, E., Waeytens, J., Bourquin, F., Vidal, R., … Cottineau, L.-M. (2016). Damage detection in a post tensioned concrete beam--Experimental investigation. *Engineering Structures*, *128*, 15–25.

Lin, Y. Z., Nie, Z. H., & Ma, H. W. (2017). Structural Damage Detection with Automatic Feature-Extraction through Deep Learning. *Computer-Aided Civil and Infrastructure Engineering*, *32*(12), 1025–1046.

Liu, C., DeWolf, J. T., & Kim, J.-H. (2009). Development of a baseline for structural health monitoring for a curved post-tensioned concrete box–girder bridge. *Engineering Structures*, *31*(12), 3107–3115.

Lomborg, B. (2003). *The skeptical environmentalist: measuring the real state of the world* (Vol. 1). Cambridge University Press Cambridge.

Lu, D., Du, X., Wang, G., Zhou, A., & Li, A. (2016). A three-dimensional elastoplastic constitutive model for concrete. *Computers and Structures*, *163*, 41–55.

Lubliner, J. (2008). *Plasticity theory*. Courier Corporation.

Lubliner, J., Oliver, J., Oller, S., & Oñate, E. (1989). A plastic-damage model for concrete. *International Journal of Solids and Structures*, *25*(3), 299–326.

Magalhães, F., Cunha, A., & Caetano, E. (2012). Vibration based structural health monitoring of an arch bridge: From automated OMA to damage detection. *Mechanical Systems and Signal Processing*, *28*, 212–228.

Maguire, J., & Severn, R. (1987). Assessing the Dynamic Properties of Existing Bridge Structures by Hammer Testing. *ICE Proceedings*, *83*(4), 769–784.

Majewski, S. (2003). The mechanics of structural concrete in terms of elasto-plasticity. *Publishing House of Silesian University of Technology, Gliwice*.

Masri, S. F., & Caughey, T. (1979). A nonparametric identification technique for nonlinear dynamic problems. *Journal of Applied Mechanics*, *46*(2), 433–447.

ME'scope, T. M. (2009). Version 5.0 Operating Manual. *Vibrant Technology, Inc., Jamestown, California*.

Menzel, A., Ekh, M., Runesson, K., & Steinmann, P. (2005). A framework for multiplicative elastoplasticity with kinematic hardening coupled to anisotropic damage. *International Journal of Plasticity*, *21*(3), 397–434.

Meruane Naranjo, V., & Heylen, E. (2010). Damage Assessment of a Bridge under Varying Environmental Conditions. In *International Conference on Noise and Vibration Engineering-ISMA2010* (pp. 1463-1476).

Moreu, F., LaFave, J., & Spencer, B. (2012). Structural health monitoring of railroad bridges—Research needs and preliminary results. In *Structures Congress 2012* (pp. 2141–2152).

Mottershead, J. E., & Friswell, M. I. (1993). Model Updating In Structural Dynamics: A Survey. *Journal of Sound and Vibration*, *167*(2), 347–375.

Nakamura, H., & Higai, T. (2001). Compressive fracture energy and fracture zone length of concrete. *Modeling of Inelastic Behavior of RC Structures under Seismic Loads*, 471–487.

Nandi, A., & Neogy, S. (2002). Modelling of a Beam with a Breathing Edge Crack and Some Observations for Crack Detection. *Journal of Vibration and Control*, *8*(5), 673–693.

Neale, K. W., Ebead, U. A., Abdel Baky, H. M., Elsayed, W. E., & Godat, A. (2005). Modelling of debonding phenomena in FRP-strengthened concrete beams and slabs. *International Institute for FRP in Construction*.

Neild, S. A. (2001). *Using non-linear vibration techniques to detect damage in concrete bridges* (Doctoral dissertation, University of Oxford).

Neild, S. A., McFadden, P. D., & Williams, M. S. (2003a). Damage Assessment in Concrete Beams Using Non-Linear Analysis of Vibration Measurements. *Key Engineering Materials*, *245–246*, 557–564.

Neild, S. A., Williams, M. S., & McFadden, P. D. (2002). Non-linear behaviour of reinforced concrete beams under low-amplitude cyclic and vibration loads. *Engineering Structures*, *24*(6), 707–718.

Neild, S. A., Williams, M. S., & McFadden, P. D. (2003b). Nonlinear Vibration Characteristics of Damaged Concrete Beams. *Journal of Structural Engineering*, *129*(2), 260–268.

Nemati, K. M., & Monteiro, P. J. M. (1997). A new method to observe three-dimensional fractures in concrete using liquid metal porosimetry technique. *Cement and Concrete Research*, *27*(9), 1333–1341.

Nguyen, H. T., & Kim, S. E. (2009). Finite element modeling of push-out tests for large stud shear connectors. *Journal of Constructional Steel Research*, *65*(10–11), 1909–1920.

Nielsen, M. P., & Hoang, L. C. (2011). *Limit analysis and concrete plasticity*. CRC Press.

Noguchi, T., Tomosawa, F., Nemati, K. M., Chiaia, B. M., & Fantilli, A. P. (2009). A practical equation for elastic modulus of concrete. *ACI Structural Journal, 106*(5), 690.

Obaidat, Y. (2011). *Structural retrofitting of concrete beams using FRP-debonding issues* (Doctoral dissertation, Lund University).

Okamoto, S., Shiomi, S., & Yamabe, K. (1976). Earthquake resistance of prestressed concrete structures. In *Proceedings of AIJ annual convention* (pp. 1251–1252).

Oñate, E., Oller, S., Oliver, J., & Lubliner, J. (1988). A constitutive model for cracking of concrete based on the incremental theory of plasticity. *Engineering Computations*, *5*(4), 309–319.

Owen, J. S. (2003). Monitoring the degradation of reinforced concrete beams under cyclic loading. In *Key Engineering Materials* (Vol. 245, pp. 307–314).

Papanikolaou, V. K., & Kappos, A. J. (2007). Confinement-sensitive plasticity constitutive model for concrete in triaxial compression. *International Journal of Solids and Structures*, *44*(21), 7021–7048.

Pavlović, M., Marković, Z., Veljković, M., & Buđevac, D. (2013). Bolted shear connectors vs. headed studs behaviour in push-out tests. *Journal of Constructional Steel Research*, *88*, 134–149.

Pešić, N., Živanović, S., Dennis, J., & Hargreaves, J. (2015). Experimental and finite element dynamic analysis of incrementally loaded reinforced concrete structures. *Engineering Structures*, *103*, 15–27.

Petersson, P.-E. (1981). *Crack growth and development of fracture zones in plain concrete and similar materials*. *Report TVBM 1006*. Division of Building Materials, LTH, Lund University.

Phillips, D. V., & Binsheng, Z. (1993). Direct tension tests on notched and un-notched plain concrete specimens. *Magazine of Concrete Research*, *45*(162), 25–35.

Piscesa, B., Attard, M. M., Samani, A. K., & Tangaramvong, S. (2017). Plasticity constitutive model for stress-strain relationship of confined concrete. *ACI Materials Journal*, *114*(2), 361–371.

Prager, W. (1955). The theory of plasticity: a survey of recent achievements. *Proceedings of the Institution of Mechanical Engineers*, *169*(1), 41–57.

Pugno, N., Surace, C., & Ruotolo, R. (2000). Evaluation of the non-linear dynamic response to harmonic excitation of a beam with several breathing cracks. *Journal of Sound and Vibration*, *235*(5), 749–762.

Ragab, A.-R., & Bayoumi, S. E. (2018). *Engineering solid mechanics* (1st Editio). New York: Routledge.

Rashid, Y. R. (1968). Ultimate strength analysis of prestressed concrete pressure vessels. *Nuclear Engineering and Design*, *7*(4), 334–344.

Ren, W., Blandford, G. E., & Harik, I. E. (2004a). Roebling Suspension Bridge . I : Finite-Element Model and Free Vibration Response, (April), 110–118.

Ren, W., Harik, I. E., Blandford, G. E., Lenett, M., & Baseheart, T. M. (2004b). Roebling Suspension Bridge . II : Ambient Testing and Live-Load Response, (April), 119–126.

Rice, J. R. (1968). A path independent integral and the approximate analysis of strain concentration by notches and cracks. *Journal of Applied Mechanics*, *35*(2), 379–386.

Ringot, E., & Bascoul, A. (2001). About the analysis of microcracking in concrete. *Cement and Concrete Composites*, *23*(2–3), 261–266.

Rodríguez, J., Martínez, F., & Martí, J. (2013). Concrete constitutive model, calibration and applications. *2013 SIMULIA Community Conference (SCC)*.

Rucevskis, S., Janeliukstis, R., Akishin, P., & Chate, A. (2016). Mode shape-based damage detection in plate structure without baseline data. *Structural Control and Health Monitoring*, 23(9), 1180-1193.

Rytter, A. (1993). *Vibrational based inspection of civil engineering structures* (Doctoral dissertation, Dept. of Building Technology and Structural Engineering, Aalborg University).

Sadrnejad, S. A. (2010). Numerical modelling for the evaluation of progressive damage to plain concrete structures. *Journal of the South African Institution of Civil Engineering*, *52*(2), 19–30.

Saiidi, M., Douglas, B., & Feng, S. (1994). Prestress Force Effect on Vibration Frequency of Concrete Bridges. *Journal of Structural Engineering*, *120*(7), 2233–2241.

Salawu, O. S. (1997). Assessment of bridges: use of dynamic testing. *Canadian Journal of Civil Engineering*, *24*(2), 218–228.

Salawu, O. S., & Williams, C. (1995). Bridge Assessment Using Forced-Vibration Testing. *Journal of Structural Engineering*, *121*(2), 161–173.

Kamrujjaman Serker, N. H. M., Wu, Z., & Li, S. (2010). A nonphysics-based approach for vibration-based structural health monitoring under changing environmental conditions. *Structural Health Monitoring*, 9(2), 145-158.

Shah, A. A., & Ribakov, Y. (2009). Non-linear ultrasonic evaluation of damaged concrete based on higher order harmonic generation. *Materials & Design*, *30*(10), 4095–4102.

Shah, S. P., & Chandra, S. (1970). Fracture of Concrete Subjected to Cyclic and Sustained Loading. *ACI Journal Proceedings*, *67*(10), 816–827.

Shan, W., Wang, X., & Jiao, Y. (2018). Modeling of Temperature Effect on Modal Frequency of Concrete Beam Based on Field Monitoring Data. *Shock and Vibration*, *2018*, 1–13.

Shepherd, R., & Aves, R. J. (1973). Impact factors for simple concrete bridges. *Proceedings of the Institution of Civil Engineers*, *55*(1), 191–210.

Silva, J. M. M., & Maia, N. M. M. (1999). *Modal analysis and testing*. (J. M. M. Silva & N. M. M. Maia, Eds.). Dordrecht: Springer.

Sima, J. F., Roca, P., & Molins, C. (2008). Cyclic constitutive model for concrete. *Engineering Structures*, *30*(3), 695–706.

Simoen, E., De Roeck, G., & Lombaert, G. (2015). Dealing with uncertainty in model updating for damage assessment: A review. *Mechanical Systems and Signal Processing*, *56–57*, 123–149.

Sinha, B. P., Gerstle, K. H., & Tulin, L. G. (1964). Stress-Strain Relations for Concrete Under Cyclic Loading. *ACI Journal Proceedings*, *61*(2), 195–211.

Sitek, M., Adamczewski, G., Szyszko, M., Migacz, B., Tutka, P., & Natorff, M. (2014). Numerical Simulations of a Wedge Splitting Test for High-strength Concrete. *Procedia Engineering*, *91*, 99–104.

Skar, A., Poulsen, P. N., & Olesen, J. F. (2017). General cracked-hinge model for simulation of low-cycle damage in cemented beams on soil. *Engineering Fracture Mechanics*, *175*, 324–338.

Sohn, H., Farrar, C. R., Hemez, F. M., Shunk, D. D., Stinemates, D. W., Nadler, B. R., & Czarnecki, J. J. (2003). A review of structural health monitoring literature: 1996–2001. *Los Alamos National Laboratory, USA.*

Song, G., Gu, H., & Mo, Y.-L. (2008). Smart aggregates: multi-functional sensors for concrete structures—a tutorial and a review. *Smart Materials and Structures*, *17*(3), 033001.

Stubbs, N., & Kim, J.-T. (1996). Damage localization in structures without baseline modal parameters. *AIAA Journal*, *34*(8), 1644–1649.

Sümer, Y., & Aktas, M. (2015). Defining parameters for concrete damage plasticity model. *CHALLENGE*, *1*(3), 149–155.

Szczecina, M., & Winnicki, A. (2017). Relaxation Time in CDP Model Used for Analyses of RC Structures. *Procedia Engineering*, *193*, 369–376.

Tan, C. M. (2003). *Nonlinear vibrations of cracked reinforced concrete beams* (Doctoral dissertation, University of Nottingham).

Tanigawa, Y., & Uchida, Y. (1979). Hysteretic characteristics of concrete in the domain of high compressive strain. In *Proceedings of Annual Architectural Institute of Japan (AIJ) Convention, Japan* (pp. 449–450).

Tao, X., & Phillips, D. V. (2005). A simplified isotropic damage model for concrete under bi-axial stress states. *Cement and Concrete Composites*, *27*(6), 716–726.

Ziad, N. T. (2008). *Elasto-plastic and damage modeling of reinforced concrete* (Doctoral dissertation, PhD thesis, Louisiana State University, Baton Rouge, LA).

Taqieddin, Z. N., & Voyiadjis, G. Z. (2009). Elastic plastic and damage model for concrete materials: Part II: Implementation and application to concrete and reinforced concrete. *Int. J. Struct Changes Solids--Mech. and App*, *1*(1), 187–209.

Teughels, A., & De Roeck, G. (2005). Damage detection and parameter identification by finite element model updating. *Archives of Computational Methods in Engineering*, *12*(2), 123–164.

Thompson, K. J., & Park, R. (1978). Stress-strain model for grade 275 reinforcing steel with cyclic loading. *Bull. New Zealand Nat. Soc. for Earthquake Engrg., Waikanae, New Zealand*, *11*(2), 101.

Transport and Main Roads. (2016). Structures Inspection Manual, 1–77. Retrieved from https://www.tmr.qld.gov.au/business-industry/Technical-standards-publications/Structures-Inspection-Manual

Tsyfansky, S. L., & Beresnevich, V. I. (2000). Non-linear vibration method for detection of fatigue cracks in aircraft wings. *Journal of Sound and Vibration*, *236*(1), 49–60.

Tudjono, S., Lie, H. A., & As'ad, S. (2016). Reinforced Concrete Finite Element Modeling based on the Discrete Crack Approach. *Civil Engineering Dimension*, *18*(2), 72–77.

Ubertini, F., Materazzi, A. L., D'Alessandro, A., & Laflamme, S. (2014). Natural frequencies identification of a reinforced concrete beam using carbon nanotube cement-based sensors. *Engineering Structures*, *60*, 265–275.

Ulfkjær, J. P., Krenk, S., & Brincker, R. (1995). Analytical Model for Fictitious Crack Propagation in Concrete Beams. *Journal of Engineering Mechanics*, *121*(1), 7–15.

Van Den Abeele, K., & De Visscher, J. (2000). Damage assessment in reinforced concrete using spectral and temporal nonlinear vibration techniques. *Cement and Concrete Research*, *30*(9), 1453–1464.

Vermeer, P. A., & De Borst, R. (1984). Non-associated plasticity for soils, concrete and rock. *HERON, 29 (3), 1984*.

Voyiadjis, G. Z., & Taqieddin, Z. N. (2009). Elastic plastic and damage model for concrete materials: Part I-theoretical formulation. *The International Journal of Structural Changes in Solids*, *1*(1), 31–59.

Voyiadjis, G. Z., Taqieddin, Z. N., & Kattan, P. I. (2008). Anisotropic damage-plasticity model for concrete. *International Journal of Plasticity*, *24*(10), 1946–1965.

Wahab, M. A., & De Roeck, G. (1997). Effect of temperature on dynamic system parameters of a highway bridge. *Structural Engineering International*, *7*(4), 266–270.

Wahab, M. A., & De Roeck, G. (1999). Damage detection in bridges using modal curvatures: application to a real damage scenario. *Journal of Sound and vibration, 226*(2), 217-235.

Wahab, M., Maeck, J., & De Roeck, G. (1999). Numerical simulation of damage scenarios of bridge Z 24. In *Society for Experimental Mechanics, Inc, 17 th International Modal Analysis Conference.* (Vol. 2, pp. 1276–1282).

Waltering, M., Bungard, V., Waldmann, D., Zürbes, A., Maas, S., & De Roeck, G. (2007). Damage Assessment of Civil Engineering Structures by the Observation of Non-linear Dynamic Behaviour. *Proceedings of the International Conference on Experimental Vibration Analysis for Civil Engineering Structures*.

Wang, T., & Hsu, T. T. . (2001). Nonlinear finite element analysis of concrete structures using new constitutive models. *Computers & Structures*, *79*(32), 2781–2791.

Wischers, G. (1978). Application of effects of compressive loads on concrete. *Betontechnische Berichte*, (2).

Worden, K., & Dulieu-Barton, J. M. (2004). An Overview of Intelligent Fault Detection in Systems and Structures. *Structural Health Monitoring*, *3*(1), 85–98.

Worden, K., Farrar, C. R., Manson, G., & Park, G. (2007). The fundamental axioms of structural health monitoring. In *Proceedings of the Royal Society of London A: Mathematical, Physical and Engineering Sciences* (Vol. 463, pp. 1639–1664).

Worden, K., & Tomlinson, G. R. (2000). *Nonlinearity in structural dynamics: detection, identification and modelling*. CRC Press.

Wu, Y., & Crawford, J. E. (2015). Numerical Modeling of Concrete Using a Partially Associative Plasticity Model. *Journal of Engineering Mechanics*, *141*(12), 04015051.

Xenos, D., & Grassl, P. (2016). Modelling the failure of reinforced concrete with nonlocal and crack band approaches using the damage-plasticity model CDPM2. *Finite Elements in Analysis and Design*.

Xia, Y., Weng, S., Xu, J. Z., & Xu, Y.-L. (2011). Temperature effect on variation of structural frequencies: from laboratory testing to field monitoring. Proceedings of the *6th International Workshop on Advanced Smart Materials and Smart Structures Technology, ANCRiSST 2011, Dalian, China, 25-26 July 2011*.

Xu, B., & Xia, H. (2018). Effect of Damage on Natural Vibration Characteristics of Large Semi-cushion Spiral Case Structure. *Arabian Journal for Science and Engineering*, 1–12.

Yousefianmoghadam, S., Behmanesh, I., Stavridis, A., Moaveni, B., Nozari, A., & Sacco, A. (2018). System identification and modeling of a dynamically tested and gradually damaged 10-story reinforced concrete building. *Earthquake Engineering and Structural Dynamics*, *47*(1), 25–47.

Yuchuan, L., Shaoqian, X., & Xuechao, G. (2011). An Energy-based Damage Model for Concrete Structures under Cyclic Loading. *Procedia Engineering*, *14*, 460–469.

Yun, C.-B., Lee, J.-J., Kim, S.-K., & Kim, J.-W. (2003). Recent R&D activities on structural health monitoring for civil infra-structures in Korea. *KSCE Journal of Civil Engineering*, *7*(6), 637–651.

Zait, Y., Zolotarevsky, V., Kligerman, Y., & Etsion, I. (2010). Multiple Normal Loading-Unloading Cycles of a Spherical Contact Under Stick Contact Condition. *Journal of Tribology*, *132*(4), 041401.

Zaitsev, V., Nazarov, V., Gusev, V., & Castagnede, B. (2006). Novel nonlinear-modulation acoustic technique for crack detection. *NDT & E International*, *39*(3), 184–194.

Zanardo, G., Hao, H., Xia, Y., & Deeks, A. J. (2006). Stiffness assessment through modal analysis of an RC slab bridge before and after strengthening. *Journal of Bridge Engineering, 11*(5), 590-601.

Zhu, Y., Kang, G., & Yu, C. (2017). A finite cyclic elasto-plastic constitutive model to improve the description of cyclic stress-strain hysteresis loops. *International Journal of Plasticity*, *95*, 191–215.

Ziegler, H. (1959). A modification of Prager's hardening rule. *Quarterly of Applied Mathematics*, *17*(1), 55–65.

# LIST OF PUBLICATIONS AND PAPERS PRESENTED

## Publications

**Hanif, M. U.**, Ibrahim, Z., Jameel, M., Ghaedi, K., & Aslam, M. (2016). A new approach to estimate damage in concrete beams using non-linearity. *Construction and Building Materials*, 124, 1081-1089. **(IF: 3.49)**.

**Hanif, M. U.**, Ibrahim, Z., Ghaedi, K., Hashim, H., & Javanmardi, A. (2018). Damage Assessment of Reinforced Concrete Structures using a Model-based Nonlinear Approach – A Comprehensive Review. *Construction and Building Materials*, 192, 846-865. **(IF: 3.49)**.

**Hanif, M. U.**, Ibrahim, Z., Jameel, M., & Ghaedi, K. (2018). Simulation-based nonlinear vibration model for damage detection of RC beams. *European Journal of Environmental and Civil Engineering*. **(IF: 1.29) - (Revision submitted)**.

**Hanif, M. U.**, Ibrahim, Z., Sutan, N. M., Ghaedi, K. & Javanmardi, A. (2018). Calibration of CDPM Parameters for Constitutive Modeling of Concrete. International Journal of Concrete Structures and Materials. **(IF: 2.36) - (Under Review)**.

## International Conferences

**Hanif, M. U.**, Ibrahim, Z., Jameel, M., Ghaedi, K., Javanmardi, A., Rehman, S. K., (2016). Finite Element Simulation of Damage in Reinforced Concrete Beams. 13th *International Conference on Concrete Engineering and Technology 2016 CONCET2016.* May 31-June 2, 2016, Universiti Teknologi Mara, Shah Alam, Selangor, Malaysia. **(Published in Journal of Civil Engineering, Science and Technology)**.

**Hanif, M. U.**, Ibrahim, Z., Lim, H. X., Hang, Y. X., (2017). Effect of incremental static damage on modal frequencies of reinforced concrete beams. *4th International Conference on Civil and Environmental Engineering for Sustainability 2017 IConCEES2017*. December 4 – December 5, 2017, Langkawi, Malaysia. **(Published in Scopus Indexed International Journal of Integrated Engineering).**